THESIS FOR THE DEGREE OF DOCTOR OF PHILOSOPHY (PHD)

In vitro investigation of the clearance of anoikic and autophagy-associated dying retinal pigment epithelial cells – implications for age-related macular degeneration

by Mária Szatmári-Tóth

Supervisor: Prof. Dr. Goran Petrovski MD, PhD

UNIVERSITY OF DEBRECEN

DOCTORAL SCHOOL OF MOLECULAR CELL AND IMMUNE BIOLOGY

DEBRECEN, 2016

Table of Contents

List of Abbreviations

2-MEA	2-mercaptoethanol
3-MA	3-methyladenine
ADORA3	adenosine A3 receptor
AMD	age-related macular degeneration
AnxV	Annexin-V
ARPE-19	adult retinal pigment epithelium-19
AV	autophagic vacuole
AXL	AXL receptor tyrosine kinase
CFDA	carboxyfluorescein diacetate, succinimidyl ester
CMTMR	5-(and-6)-(((4-chloromethyl)benzoyl)amino)tetramethylrhodamine
CNV	choroideal neovascularization
CQ	chloroquine
DAPI	4',6'-diamidino-2-phenylindole
DC	dendritic cells
DMEM	Dulbecco's modified Eagle's medium
DNA	deoxyribonucleic acid
ECM	extracellular matrix
EDTA	ethylenediaminetetraacetic acid
ELISA	enzyme-linked immunosorbent assay
FACS	fluorescence-activated cell sorter
FAK	focal adhesion kinase
FCS	fetal calf serum
FITC	fluorescein isothio-cyanate
FSC	forward light scattering
GAPDH	glycerinaldehyde-3-phosphate dehydrogenase
GFP	green fluorescent protein
Gas6	growth-arrest-specific 6
GM-CSF	granulocyte-macrophage colony-stimulating factor
H_2O_2	hydrogen peroxide
HRP	horseradish-peroxidase
hESC-RPE	human embryonic stem cell-derived RPE

hRPE	human retinal pigment epithelium
iDC	immature dendritic cell
IL	interleukin
IMDM	Iscove's Modified Dulbecco's Medium
LC3	light-chain-3
MCSF	macrophage colony stimulating factor
mDC	mature dendritic cells
MerTK	c-Mer proto-oncogene tyrosine kinase
MFG-8	milk fat globule-8
MΦ	macrophage
PBS	phosphate-buffered saline
PEI	polyethylenimine
PFA	paraformaldehyde
PGE_2	prosztaglandin E2
PI	propidium iodide
poly-HEMA	poly(2-hydroxyethylmethacrylate)
POS	photoreceptor outer segment
PS	phosphatidyl serine
SD	standard deviation
siRNA	small interfering ribonucleic acid
SSC	side light scattering
TAM kinase	TYRO3, AXL, Mer kinase
TBS-T	tris buffered saline containing 0.05 % tween-20
TC	triamcinolone
TEM	transmission electron microscopy
THBS1	thrombospondin 1
TGFβ	tumor growth factor beta
TLDA	TaqMan low-density array
TNF-α	tumor necrosis factor-α
VEGF	vascular endothelial growth fact

1. Introduction

The eye is considered as one of the most complex and important sensory organs in the human body. It provides the ability to process visual details by receiving light stimuli from the environment and transfers it to the brain where they are converted into visual images (Hoar, 1982). The light-sensitive retina is located in the posterior segment of the eye and consists of two distinct layers: a complex network of sensory cells (neuroretina) and a monolayer of retinal pigment epithelial (RPE) cells. The neuroretina serves to convert light into neural signals, the RPE play an essential role in maintaining retinal homeostasis (Kolb, 1995).

Dysfunction or death of the RPE and photoreceptor cells can initiate a cascade of events that may result in the impairment or even loss of vision. Degenerative diseases of the retina, such as age-related macular degeneration (AMD), are the leading cause of blindness in the elderly population in the Western world; two types of AMD – dry and wet/exudative, can be distinguished clinically based upon absence or presence of neovascularizations, respectively AMD currently affects an estimated 50 million people worldwide, and this number is continuously increasing (Kaarniranta et al., 2013, KInnunen et al., 2012).

The visual acuity is dramatically affected by advanced forms of AMD due to the disease causing disruptions in the macula – the part of the retina responsible for central vision. These patients lose their ability to perform daily activities, such as reading, writing, driving and face recognition. The impairment of these functions can have a considerably deleterious effect on patient' quality of life (Kaarniranta et al., 2013, Klettner et al., 2013).

The pathogenesis of this common disease in the elderly is multi-factorial. Environmental, genetic and inflammatory factors play a role in the development of AMD (Armstrong and Mousavi, 2015). Current treatments are limited due to our inadequate understanding of the pathogenic events leading to AMD. *In vitro* RPE cell models can help better understand the pathophysiological and molecular mechanisms of this disease, and may contribute to discovery of novel AMD therapeutic targets.

2. Theoretical background

2.1. The retina

The wall of the human eye is composed of three main concentric layers: the outermost layer (opaque white sclera and transparent cornea), the middle vascularized layer (iris anteriorly, intermediate ciliary body and choroid posteriorly) and the innermost layer (retina) (Hoar, 1982). The highly vascularized connective tissue - choroid, is responsible for support and nourishment of the retina. The latter can be found in the posterior chamber of the eye, which comprises multiple layers of different cell types (Hoon et al., 2014). The neuroretina and the outermost RPE layer (***see section 2.2***) form the retina (Strauss, 2005). The neuroretina is further divided into nine anatomical layers from posterior to anterior: photoreceptors, external limiting membrane, outer nuclear layer, outer plexiform layer, inner nuclear layer, inner plexiform layer, ganglion cell layer, nerve fiber layer and internal limiting membrane (Kolb, 1995; Nguyen-Ba-Charvet and Chedotal, 2014).

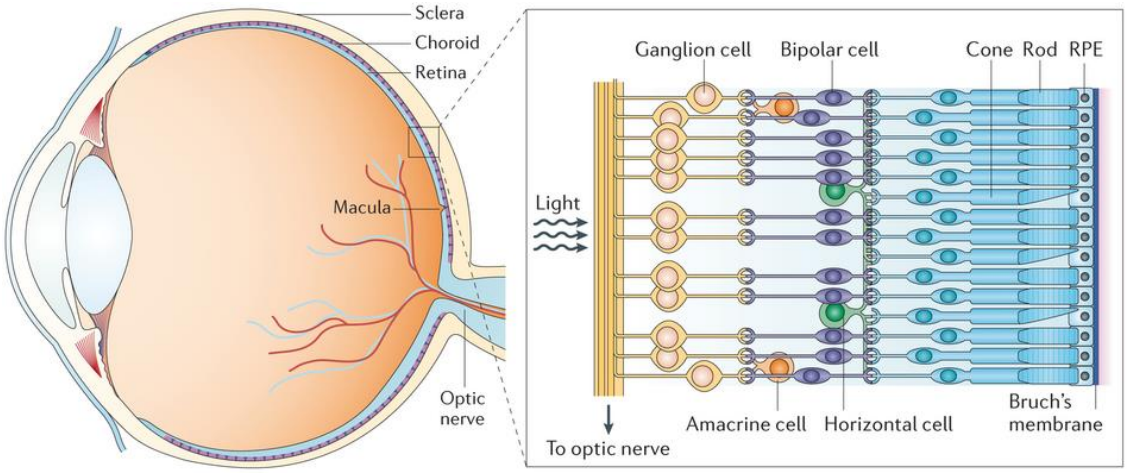

Figure 1. The layers of the eye and cell types of the retina. *A simplified cross-section schematic of the human eye (left panel), with a schematic enlargement of the retina (right panel). The wall of the eye is formed by three layers: sclera, choroid and retina. The RPE layer is located in the outermost region of the retina, which is attached to the Bruch's membrane. The photoreceptors (consisting of cones and rods), the connecting neurons (amacrine, bipolar and horizontal cells) and the ganglion cells represent layers of neurons in the interior of the eye.*

Figure adapted from (Kimbrel and Lanza, 2015)

Two types of photoreceptors can be distinguished: the rods for vision in dim light, and the cones for daylight and for color vision (Lamb, 2013). The neuronal networks in the retina comprise the photoreceptors, a middle layer of connecting neurons such as bipolar, amacrine and horizontal cells, which modify the visual stimulus, and the innermost layer of retinal ganglion cells, that are responsible for transferring the signals from the retina through the optic nerve and finally to the brain (Kimbrel and Lanza, 2015) (**Figure 1**).

The synapses between photoreceptor terminals and bipolar, horizontal and amacrine cells occur in the outer plexiform layer. The photoreceptor cell bodies are found in the outer nuclear layer, and the inner nuclear layer contains the cell bodies of bipolar, amacrine and horizontal cells (Grossniklaus et al., 2015). The synaptic contacts of ganglion cells with the amacrine and bipolar cells are detectable in the inner plexiform layer (Masland, 2012b). The nerve fiber layer involves the ganglion cell axons that continue towards the optic nerve. The innermost layer of the retina is the internal limiting membrane, which is located between the nerve fiber layer and the vitreous (Masland, 2012a). The Müller cells act as specialized glial cells to form the internal limiting membrane and have an essential role in the homeostatic and metabolic support of retinal neurons (Giannelli et al., 2011). The macula is the small, central area of the retina that is responsible for central and fine detail vision needed to do daily tasks such as reading or driving (Parmeggiani et al., 2012).

2.2. The retinal pigment epithelium (RPE)

The RPE layer is composed of single highly pigmented, polarized, hexagonal cells. It is the outermost layer of the retina, laying at the interface between the neuroretina and the vascular choriocapillaris (Strauss, 2005).

The RPE is attached to the underlying Bruch's membrane, an extracellular matrix (ECM) structure, and forms an important physiological barrier, namely the outer blood-retinal barrier (BRB). The BRB has an essential role to maintain the eye as a privileged site, and required for the retinal homeostasis and the normal visual function. Alterations of the BRB contribute to the development of wide number of retinal diseases, such as diabetic retinopathy and age-related macular degeneration (AMD); these are directly related to the breakdown of BRB (Cunha-Vaz et al., 2011; Rizzolo, 2014).

Moreover, the RPE has a crucial and multifunctional role in supporting the overall health of the retina, and the homeostasis of overlaying photoreceptors by regulating the rate of phagocytosis of photoreceptor outer segments (POS) (Simo et al., 2010; Strauss, 2005), as well as transporting nutrients, such as glucose, retinol and fatty acids from the blood and back to the photoreceptors (Reichhart and Strauss, 2014). The RPEs are responsible for absorbing scattered light to improve the optical quality by forming the pigmented cell layer which covers the inner wall of the bulbus, and accumulates high amount of antioxidants in order to protect against photo-oxidative damage (Plafker et al., 2012). Another function of the RPEs is the secretion of growth factors, as well as factors that are critical for the structural integrity of the retina and choriocapillaris, for example pigement epithelium- or vascular endothelium- derived growth factors (PEDF or VEGF, respectively); in addition, the RPEs secrete immunosuppressive factors that contribute to the maintenance of the immune privileged status of the eye (Stein-Streilein, 2013).

Increasing the knowledge of the multiple functions of the RPEs contributes to better understanding of the pathogenesis of different forms of degenerative diseases and facilitates development of new therapeutic strategies against diseases that lead to blindness. To date, there are some well-established model systems available for investigating RPE homeostasis and pathology *in vitro*.

2.3. *In vitro* RPE cell models

2.3.1. ARPE-19 cell line

During the last decade, ARPE-19 cells have become the most commonly used immortalized cell line to evaluate RPE function. Originally the cells were extracted from the eye of a 19-year old male donor (Dunn et al., 1996). It was then spontaneously transformed into continuous cell line with normal karyotype, which forms polarized epithelial monolayers (Dunn et al., 1998). This commercially available cell line is capable of expressing RPE-specific markers, such as RPE65 or CRALBP. The properties of the ARPE-19 cells depend on the culturing conditions and the duration of maintenance. The typical cobblestone morphology of the uniform epithelial monolayer is detectable at passages 15 to 20 of ARPE-19 cells cultivated in tissue culture flasks. Further passage of these cells results in a heterogeneous mixture of elongated and

polygonal cells, and they can easily lose some of their important features of the original RPEs (Luo et al., 2006). The cells have been widely used to investigate retinal pathogenesis, signaling pathways or the response of RPEs to oxidative stress, as well as in drug and toxicity related studies (Kuznetsova et al., 2014; Turowski et al., 2004).

2.3.2. Primary human RPE (hRPE) cells

The hRPE cells are obtained from human adult cadaver eyes obtained as an unused tissue from Eye Banks. In countries where no human Eye Banks exist, other primary RPE cell sources have been used, including bovine (Hernandez et al., 1995), pig (Maenpaa et al., 2002), rabbit (Stanzel et al., 2005) or rat (Chang et al., 1997). Primary hRPE cells are commercially available as well: ScienCell Research Laboratories (CA, USA) offers these cells at passage 1 or Lonza Walkersville Inc. (NJ, USA) offers them at passage 2. Researchers in different laboratories have used essentially the same protocol on how to isolate RPE cells from human adult eyes (***see section 4.3.1***). It has been demonstrated that the primary cells can polarize and form cell layer with barrier properties (Hornof et al., 2005). Usually, the melanosomes can be detected after the extraction of primary cells, but they disappear during the sub-culturing process (Kanuga et al., 2002). Primary cells may preserve the typical properties of the original tissue, which may be lost over several passages. The primary hRPEs show a relatively heterogeneous morphology and exhibit donor-to-donor variability in contrast to the immortalized cell lines. Generally speaking, all primary cells can be expanded only for few passages, whereas virally or spontaneously immortalized cell lines can be maintained for several passages.

2.3.3. Human embryonic stem cell-derived RPE (hESC-RPE) cells

It is well-known that human pluripotent stem cells can be characterized by unlimited, self-renewal properties and potential to differentiate into any cell type of the body (Takahashi et al., 2007; Yu et al., 2007). In recent years, developments in embryonic stem cell technologies have generated novel ways to establish RPE cells (Kamao et al., 2014; Schwartz et al., 2012; Schwartz et al., 2015). Our collaborating partner, Skottman et al., has previously created a xeno-free culture and differentiation protocol without the use of any animal-derived components, to develop functional RPE-like cells from

pluripotent hESC lines, which were derived from pre-implantation blastocyst stage embryos (Vaajasaari et al., 2011). *In vitro,* it was shown that these cells have hexagonal, cobblestone-like morphology with high pigmentation rate, and form a highly polarised epithelial cell layer. In addition, the expression of RPE cell-specific markers were detected in hESC-RPE cells, such as *MITF, RPE65,* bestrophin, *OTX2v1*, *PMEL*, *PEDF*, tyrosinase at gene level, and MITF, CRALBP, RPE65, and ZO-1 at protein level (Vaajasaari et al., 2011). The integrity and barrier function of these cells (Onnela et al., 2012; Savolainen et al., 2011), as well as their ability to transport different types of drugs have also been demonstrated (Juuti-Uusitalo et al., 2012). Altogether, the functional properties of the hESC-derived RPE-like cells appeared to be very similar to the native RPE, and these data suggest that these cells can serve as an additional *in vitro* model for investigating the pathogenesis of RPE-associated diseases.

2.4. AMD, a degenerative eye disease

AMD is one of the most common irreversible causes of legal blindness, manifested in the elderly people mostly in Western or developed countries. It is considered to be a neurodegenerative macular disorder, with its prevalence increasing in parallel with aging. AMD affects the most sensitive area of the fundus, the macula. A global survey demonstrates that approximately 50 million people suffer from the symptoms of AMD-worldwide, and hundreds of thousands of new cases are diagnosed each year, suggesting that AMD represents a growing public health problem (Gordois et al., 2012; Klein and Klein, 2013).

Typical symptoms of AMD patients include drastically decreasing visual acuity, contrast sensitivity defects, distortion of straight lines, abnormal dark adaptation, progressive impairment of central vision, scotomas and color vision impairment. The loss of central vision in AMD can interfere with simple daily activities, such as reading, driving, or recognising faces (Gehrs et al., 2006; Kaarniranta et al., 2013) (**Figure 2A**).

The pathophysiology of AMD is not yet fully understood, the internal and the environmental risk factors together contribute to the clinical manifestations of this complex multifactorial disease dependent on aging, genetic background, smoking, low antioxidant content, unhealthy/nutrient poor diet, obesity, high blood pressure, hypercholesterolemia or arteriosclerosis (Armstrong and Mousavi, 2015; Kaarniranta et al., 2011) (**Figure 2B**).

AMD can be classified on broad terms as either dry or wet type; these two major forms can be subdivided into early and late stage. Dry AMD is the most common, slowly progressing, chronic form of the disease, which is characterized by intact Bruch's membrane; it usually leads to some degree of visual impairment (but may cause severe blindness in some of the patients) (Bowes Rickman et al., 2013). In contrast, the wet type of AMD occurs only in about 10-15% of the total AMD population; it emerges abruptly and its progression is relatively rapid, with a possibility for causing acute loss of vision as well. The development of wet AMD is strongly associated with the excessive expression of VEGF by RPE cells, which results in the formation of new vessels and breakdown of the BRB (Kulkarni and Kuppermann, 2005; Smith and Kaiser, 2014).

Phenotypically, in the early stage of dry AMD, pigment mottling, accumulation of intracellular lysosomal lipofuscin and extracellular drusen deposits can be observed. The gradual degradation of the confluent areas of RPE cells and the overlying photoreceptor cells lead to late stage of dry AMD, also known as geographic atrophy. The early stage of wet AMD is characterized by choroidal neovascularization (CNV), a process in which abnormal blood vessel growth occurs from the choroid and into the retina via penetration of the Bruch's membrane; it usually results in hemorrhage formation, lipid exudation and retinal edema. In wet AMD, late stage fibrosis and permanent visual loss may develop in absence of treatment (Kinnunen et al., 2012; Yonekawa et al., 2015) (**Figure 2B**).

In the retina, the substantial oxygen consumption, the high mitochondrial activity and the almost constant light exposure can evoke chronic oxidative stress to the RPE cells, which plays a significant role in the pathogenesis of AMD. The increased oxidative stress is closely linked to the increased accumulation of auto-oxidative lipofuscin in the lysosomes of RPE cells as well as extracellular drusen formation between the space of RPE and Bruch's membrane, which frequency rises with aging (Blasiak et al., 2014; Chiras et al., 2015; Mao et al., 2014) (**Figure 2C**). In addition to the oxidative stress and protein aggregation, dysfunction and death of RPE cells (*see section 2.5*), chronic inflammation (*see section 2.6*), as well as failure of dead RPE cells' clearance (*see section 2.7*) have been associated with AMD progression.

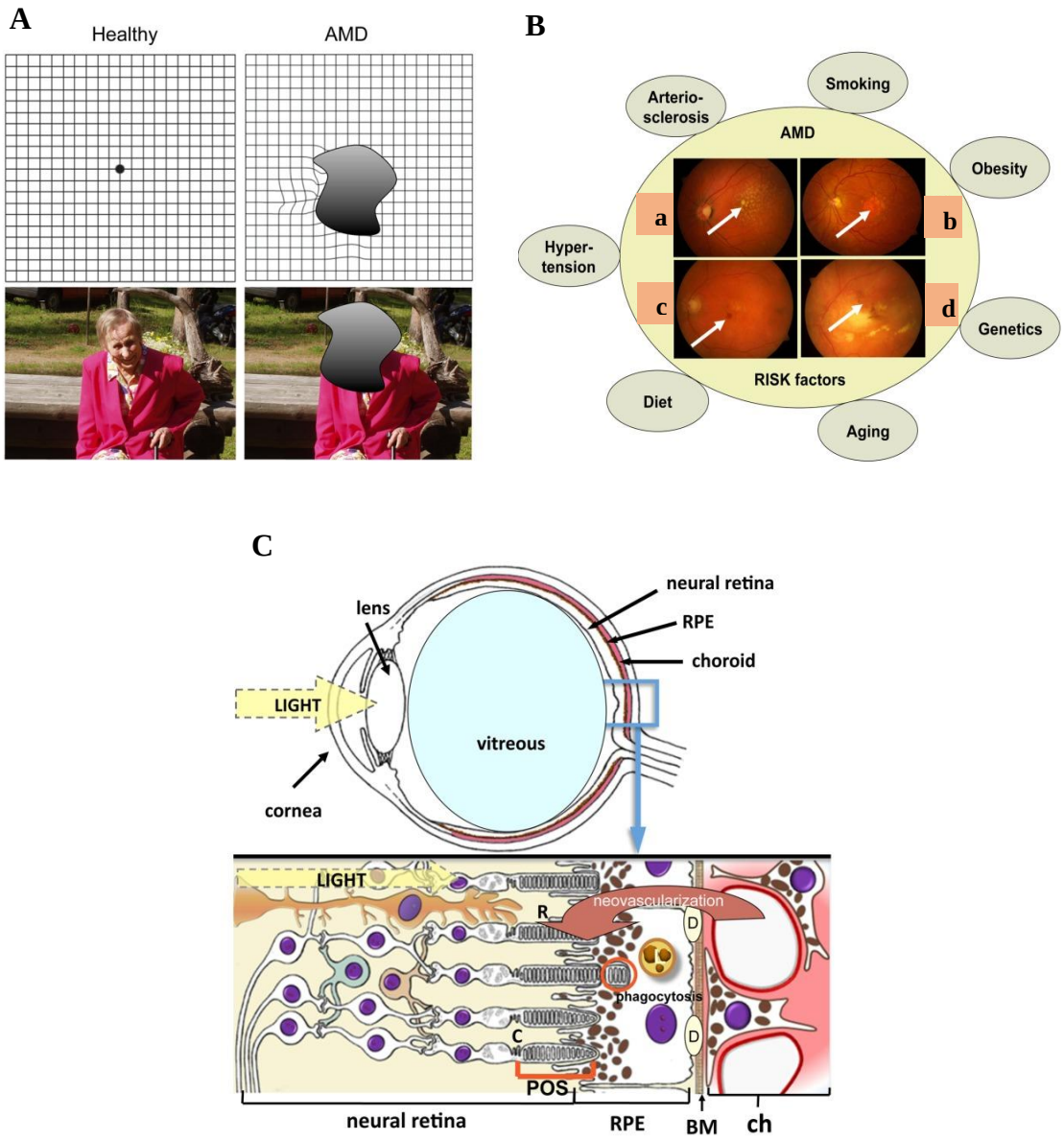

Figure 2. Clinical symptoms, risk factors and pathomechanism of age-related macular degeneration (AMD). ***(A)*** *Symptoms of AMD.* ***(B)*** *Risk factors of AMD associated with different phenotypes of macular degeneration:* ***(a)*** *the early stage of dry AMD,* ***(b)*** *the late stage of dry AMD,* ***(c)*** *the early stage of wet AMD, and* ***(d)*** *the late stage of wet AMD.* ***(C)*** *Cross-sectional illustration of the eye and retina. Light projects via the cornea and the lens to the retina. Abbreviations used: R, rods; C, cones; RPE, retinal pigment epithelium; POS, photoreceptor outer segments; BM, Bruch's membrane; L, lipofuscin; D, drusen; ch, choroid. Red arrow indicates choroidal neovascularization in the wet AMD process. Red circle shows the shed POS vesicle.*

Figure adapted from (Kaarniranta et al., 2013)

2.5. Cell death types in AMD pathogenesis

The dysfunction and death of RPE cells play an important role in the development and progression of AMD. Until recently, a wide range of cell death modalities have been identified in the retina of AMD patients, including apoptosis, anoikis, or autophagy-associated (Dunaief et al., 2002; Kaarniranta et al., 2013).

2.5.1. Anoikic cell death

Anoikis is a form of programmed cell death, which is derived from the ancient Greek word for “homelessness”. The process was first described in epithelial and endothelial cells by Frisch and Francis two decades ago as a unique phenomenon reflecting a specific mode of apoptosis (Frisch and Francis, 1994; Frisch and Screaton, 2001). Induction of anoikic cell death occurs when cells lose the attachment to ECM, or due to inappropriate cell adhesion (Gilmore, 2005). Anoikis is a physiologically relevant process, which is essential for ensuring development and tissue homeostasis, and functions as a major defense mechanism for the organism by preventing adherent-independent cell growth and attachment to an inappropriate matrix (Paoli et al., 2013).
Cellular attachment to the ECM is mediated by the integrin class of heterodimeric transmembrane receptors, which provide physical links with the intracellular actin cytoskeleton. The integrins modulate cell viability via their contact with the ECM and they 'sense' mechanical forces arising from such interactions and modify accordingly these stimuli into intracellular signals (Miranti and Brugge, 2002). It has been demonstrated that integrins can suppress anoikis in attached cells by activating focal adhesion kinase (FAK) (Frisch et al., 1996).
The initiation and execution of anoikis is mediated by different pathways, all of which terminally converge into the activation of caspases, DNA fragmentation and cell death. In accordance with classical apoptosis, the anoikis program can be mediated by both the extrinsic pathway, triggered by cell surface death receptors, and the intrinsic pathway driven by mitochondria. In the extrinsic pathway, caspase-8 is considered to be a key factor, activated through engagement of death receptors, such as Fas or tumor necrosis factor receptor 1 (TNFR1), which results in the cleavage and activation of 'executioner caspases'. Anoikis due to the intrinsic pathway is mainly initiated by pro-apoptotic

members of the Bcl-2 family, in particular, the protein Bim and mitochondrial cytochrome C (Taddei et al., 2012).

Anoikis has been shown in many cell types, including keratinocytes, thyroid cells or osteoblasts. In addition, it has also been observed *in vivo* to occur in normal skin or intestinal epithelial tissues (Zhan et al., 2004). Moreover, anoikic cell death can be induced in the photoreceptors, RPE cells, and possibly in the choriocapillary endothelial cells by accumulation of drusen in the space between the Bruch's membrane and the RPEs, which can result in decreased cell adhesion and elevation of the RPE cells from this membrane (de Jong, 2006). Recently, our research group reported an *in vitro* model for triggering of anoikic cell death in ARPE-19 cell line which was cultured on poly-2-hydroxyethylmethacrylate (poly-HEMA)-covered culture dishes for 24h to block cell attachment (Petrovski et al., 2011b).

2.5.2. Autophagy and autophagy-associated cell death

Autophagy is an evolutionarily conserved mechanism in eukaryotic cells used for lysosomal degradation of cytosolic constituents, including long-lived macromolecules, damaged organelles or intracellular pathogens, as well as recycling of the breakdown products (Eskelinen and Saftig, 2009). The eye, as an organ, shows the highest dead cell turnover in the human body. The role of autophagy in the different segments of the eye is not well documented (Ferguson and Laurie, 2016).

In mammals, three different types of autophagy have been described: macroautophagy, chaperon-mediated autophagy and microautophagy (Parzych and Klionsky, 2014). In chaperone-mediated autophagy, substrate proteins containing a KFERQ-like pentapeptide sequence are selectively recognized by chaperones and then translocated into the lysosomal lumen after binding with lysosomal LAMP-2A (lysosomal-associated membrane protein 2A) (Li et al., 2011). Microautophagy as a non-selective lysosomal degradative process, involves direct lysosomal invagination of small pieces of the cytoplasm (Mijaljica et al., 2011). In macroautophagy, double-membrane vesicles are responsible for sequestering and transporting cytoplasmic materials, such as protein aggregates and organelles to the lysosomes to be degraded (He and Klionsky, 2009).

The main topic here will be on the macroautophagy pathway (referred further in the text as autophagy), which is considered to be a highly dynamic and complex process and regulated at multiple steps (Parzych and Klionsky, 2014). The mammalian target of

rapamycin (mTOR) is a highly conserved nutrient-sensing Ser/Thr kinase that negatively regulates the autophagy process. The mTOR pathway consists of two distinct functional complexes: mTORC1 (mTOR complex 1) and mTORC2. The active mTORC1 interacts with ULK (unc-51-like kinase) complex which includes the following proteins: ULK1, Atg13, RB1CC1 (Rb1-inducible coined-coil 1, also known as FIP200) and Atg101 (Alers et al., 2012). Under nutrient-rich conditions, the active mTORC1 inhibits the autophagy process via phosphorylation of the ULK1 and hyperphosphorylation of the Atg13, thereby inactivating the kinase complex. Conversely, under nutrient deprivation or rapamycin treatment, the mTORC1 is inactivated, the phosphorylation status of ULK1 and Atg13 is changed, which finally leads to the enhancement of ULK1 kinase activity and triggering of autophagy (Chen and Klionsky, 2011).

In the autophagy process, the next step is the formation of isolation membrane called phagophore, which expands and encloses its cargo to form double-membrane vesicles termed autophagosomes. The formation of an autophagosome is mediated by around 20 highly conserved autophagy-related (ATG) proteins. The vesicle nucleation step begins with the recruitment of Atg proteins to the mammalian autophagosome formation site (Fullgrabe et al., 2014; Itakura and Mizushima, 2010; Maiuri et al., 2007). During this step, the activation of a phosphatidylinositol 3-kinase (PtdIns3K) complex is essential, which can be classified into three types (class I, II and III) in higher eukaryotes (Burman and Ktistakis, 2010). The core components of mammalian class III PtdIns3K complex is beclin 1, phosphoinositide 3-kinase (PI3K) (Vps34) and phosphoinositide-3-kinase, regulatory subunit 4 (Vps15) and this complex contains interacting proteins, such as UV radiation resistance-associated gene (UVRAG) protein, activating molecule in beclin-1-regulated autophagy (AMBRA1), Atg14L (yeast Atg14-like), Bax-interacting factor 1 (Bif-1) (Mizushima et al., 2011). Two ubiquitin-like-conjugation systems are required for the expansion of the phagophore and the maturation of the autophagosomes, namely the Atg12-Atg5-Atg16 complex and the microtubule-associated protein 1 light chain 3 (LC3) conjugation system (Geng and Klionsky, 2008). The cytosolic form of LC3, named LC3-I, covalently conjugated to the lipid phosphatidyl-ethanolamine (PE) forms the LC3-II, which is then inserted into the phagophore membrane (Tanida et al., 2004). p62, also known as sequestosome 1 (SQSTM1) protein, functions as a link between LC3 and ubiquitilated proteins, and facilitates the degradation of ubiquitilated substrates (Lippai and Low, 2014; Pankiv et

al., 2007). Finally, the outer membrane of the autophagosome fuses with the primary lysosomes, forming autophagolysosomes, where their sequestered contents are degraded by lysosomal hydrolases. After degradation, the resulting molecules are exported to the cytosol through membrane permeases, where they can be reused to synthesize proteins (Chen and Klionsky, 2011; Mizushima, 2007) (**Figure 3**).

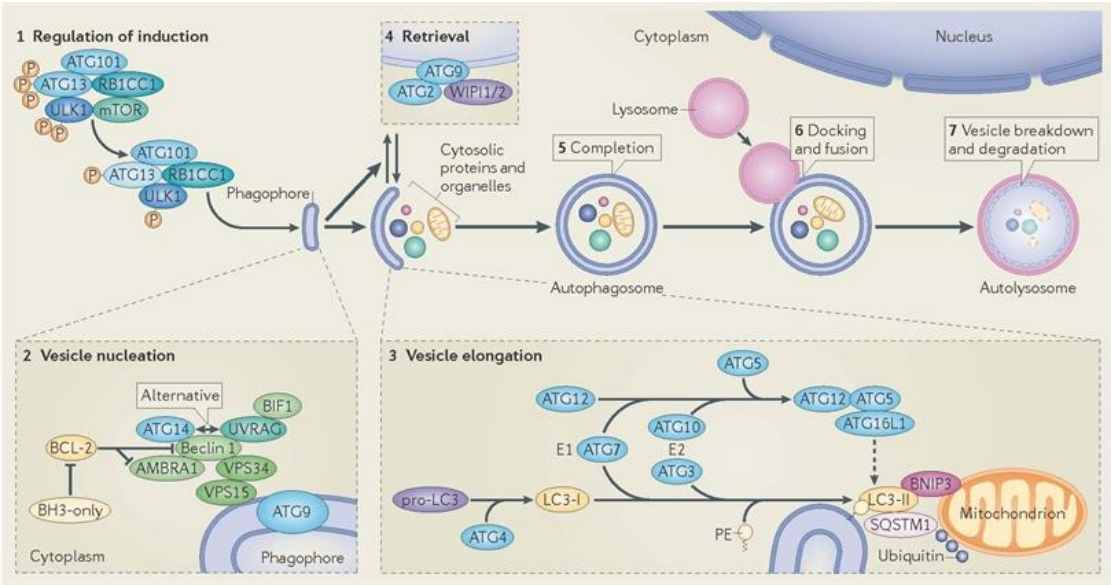

Figure 3. Overview of the autophagy pathway. *The repression of mTOR kinase initiates the formation of the phagophore (isolation membrane), which starts to elongate to enclose cytosolic proteins and organelles. The phagophore expands and matures into double-membraned vesicle, known as autophagosome. Subsequently, this process is followed by the fusion of autophagosomes with lysosomes to generate the autolysosome, which promotes the degradation of the sequestered material inside the autolysosome by lysosomal enzymes and released into the cytoplasm for recycling.*

Figure adapted from (Fullgrabe et al., 2014)

Autophagy activators and inhibitors have been commonly used to investigate autophagy-related processes. A low basal rate of autophagy occurs under normal physiological conditions in most eukaryotic cells, and can be induced to higher levels by various compounds or strategies, including starvation by deprivation of serum and amino acids, endoplasmic reticulum stress inducers (brefeldin A), rapamycin, small molecule enhancers of rapamycin, trehalose, IMPase inhibitors (carbamazepine) or Class I PI3K inhibitors (C2-ceramide) (Yang et al., 2013).

Autophagy can potentially be blocked at any phase of the autophagy process**.** To date, many chemical inhibitors have been described acting at different stages, e.g. PI3K

inhibitors (3-methyladenine: 3-MA; LY294002; wortmannin), protein synthesis inhibitor (cycloheximide), vacuolar-type H (+) ATPase inhibitor (bafilomycin A1), lysosomal lumen alkalizers (chloroquine: CQ; NH_4Cl) or acid protease inhibitors (leupeptin; E64d; pepstatin A). Recent studies suggest that genetic intervention serves as a potent approach to inhibit autophagy, such as ATG gene deletions or inactivations, functional knockdowns (Atg5; Atg7; Beclin 1) or microRNAs (miR-101; miR-30a) (Yang et al., 2013).

Till now, a wide range of methods have been made available to monitor autophagy activation (Klionsky et al., 2016), the most commonly used is the detection of the conversion from endogenous LC3-I to LC3-II by immunoblotting with antibodies against LC3 (Mizushima and Yoshimori, 2007). The amount of LC3-II generally correlates with the number of autophagosomes, which is a good marker of the autophagosome formation, and can be assessed, besides to a Western blot analysis, by fluorescence and electron microscopy (Kabeya et al., 2000). Autophagy is a highly dynamic, multi-step process, and the accumulation of autophagosomes does not in all cases represent induction of autophagy; on the contrary, it may indicate a blockage of further steps in the autophagy pathway, including failed fusion or decreased lysosomal degradation. The determination of autophagic flux is therefore considered to be a more reliable marker for monitoring autophagic activity. Autophagic flux indicates the whole dynamism of autophagy, including autophagosome synthesis, maturation and fusion with lysosomes, delivery of autophagic substrate to the lysosomes as well as its degradation inside the lysosomes and the release of molecules back into the cytosol (Ju et al., 2010; Zhang et al., 2013). The autophagic flux can be monitored based on the turnover of LC3-II using Western blot analysis in the presence or absence of an autophagy inhibitor, such as chloroquine, which can suppress autophagy via inhibition of lysosomal protein degradation by neutralizing the lysosomal pH. If autophagic flux is actually occurring, the transit of LC3-II through the autophagic pathway will thus be inhibited upon CQ-treatment, which leads to increased level of LC3-II formation (Mizushima et al., 2010).

Autophagy has been considered primarily as a cell survival process that delivers cytoplasmic materials to the lysosomes for degradation and subsequently produces amino acids and fatty acids that can be used to synthesize new proteins. If autophagy occurs at excessive levels, it can promote cell death (Chen and Klionsky, 2011). The autophagic cell death was firstly described as type II programmed cell death that is

accompanied by the accumulation of autophagosomes in the dying cells. This morphology-based definition did not imply any functional role of autophagy in the cell death process (Cecconi and Levine, 2008; Kroemer and Levine, 2008).

To avoid confusion, recently, the Nomenclature Committee on Cell Death has published the recommendations for definition of autophagic cell death that proposed biochemical and functional considerations, to indicate a type of cell death that is mediated by autophagy and that can be limited or delayed by chemical inhibition or genetic manipulations of the autophagic pathway (Galluzzi et al., 2012).

2.6. Inflammation in AMD pathogenesis

The retina is considered as an immune privileged tissue; this phenomenon allows for immune protection of the eye. Multiple factors and mechanisms are responsible for maintaining the immune privilege, such as the presence of BRB and the absence of lymphatic drainage, the inhibitory ocular microenvironment with cell-bound and soluble immunosuppressive factors, as well as the regulation of systemic immune responses within the eye (Zhou and Caspi, 2010). The wet type of AMD can be characterized by a breakdown of BRB, which results in CNV formation, infiltration of macrophages from the peripheral circulation, accumulation of immune cells and generation of a highly immunogenic environment (Shaw et al., 2016).

Two subtypes of macrophages have been demonstrated in wet AMD, the pro-inflammatory M1 macrophages, which play a role in the increased levels of inflammatory cytokines and chemokines in the retina, and the relatively anti-inflammatory M2 macrophages, which have inflammation suppressing phenotype and involved in debris scavenging and tissue remodeling (Ding et al., 2009). The exact ratio of the two types of macrophages in AMD is not known yet, however, a disbalance towards the pro-inflammatory type has been speculated.

Furthermore, several histochemical studies have confirmed that soft drusen contains a variety of inflammation-related proteins, such as C-reactive protein (CRP), immunoglobulins, acute phase molecules as well as many complement-related proteins (C3a, C5a, C5, C5b-9, CFH, CD35 and CD46), suggesting that drusen can be considered as inflammatory nodes in the pathogenesis of AMD (Gemenetzi and Lotery, 2016; Kauppinen et al., 2016).

Nowadays, an increasing number of studies focus on identification of reliable biomarkers for AMD. These selective markers would help in the diagnosis of early AMD, even before symptoms would appear. In addition, biomarkers may contribute to clarify the pathogenesis of AMD as well as to detect the response to therapy. Several molecules involved in immune mechanisms and inflammatory mediators have been proposed as biomarkers of AMD, because of their elevated levels have been determined at the site of AMD lesions, such as C-reactive protein (CRP) or interleukin-6 (IL-6).However**,** to date, there is no accepted, specific blood marker that meets the requirements of initial AMD detection (Ross et al., 2007; Stanton and Wright, 2014).

2.7. Clearance of dying cells by professional and non-professional phagocytes

In healthy human adults, billions of cells that are harmful, useless, or senescent die each day in many tissues throughout the body. The rapid elimination of these dying cells is essential for development and for maintaining tissue homeostasis and innate immune balance. The phagocytic clearance is mediated either by professional phagocytes such as macrophages or immature dendritic cells (iDCs), and non-professional "neighbouring" phagocytes such as fibroblasts and epithelial cells (Nagata et al., 2010).
Recently, Parnaik et al. reported that the steps of the clearance of dying cells are similar in professional and non-professional phagocytes, although they have demonstrated a major kinetics difference. The professional phagocytes are characterized by high motility, immediate ingestion of apoptotic cells, and fast digestion, which leads to high phagocytic rate and capacity. Contrarily, non-professional phagocytes are sessile, show lengthy palpating movements, and delay ingestion of dying cells for hours after the first recognition (Parnaik et al., 2000).
The removal of apoptotic cells is a very complex process, regulated by several molecules and signalling pathways and it can be generally divided into four major steps. The first step begins with the release of soluble chemoattractants, so called "find-me" signals by dying cells to recruit phagocytes to the site of death. Several molecules serve as such "find-me" signal, including triphosphate nucleotides (ATP and UTP), the chemokine fractalkine (CX3CL1), the lipids lysophosphatidylcholine and sphingosine 1-phosphate (Hochreiter-Hufford and Ravichandran, 2013; Ravichandran, 2010).
The next step is characterized by the specific recognition of "eat-me" signals on the dying cell surface by engulfment receptors on the phagocytes. To date, the most

extensively studied “eat-me” marker has been the phosphatidylserine (PS), which is an essential factor in efficient phagocytosis. In viable cells, PS is confined to the inner leaflet of the plasma membrane, and it is actively and rapidly exposed on the outer leaflet of the plasma membrane during apoptosis (Green et al., 2016). Two different ways have been described for PS recognition by phagocytes, either via direct-binding receptors or via soluble bridging molecules. Multiple direct-binding PS receptors have been identified, including members of the TIM family (TIM-4, TIM-1 and TIM-3), the seven transmembrane brain angiogenesis inhibitor 1 (BAI1) as well as the atypical EGF-motif containing membrane protein Stabilin-2 (Elliott and Ravichandran, 2010). The members of the TAM family of receptor tyrosine-kinases, such as Tyro3, Axl, Mer, cannot engage PS on the apoptotic cells directly, but use bridging molecules that bind PS on the apoptotic cells. Growth arrest-specific 6 (Gas6) is a well-characterized PS binding bridging molecule, which physically links to the TAM receptors with different affinities: AXL ≥ Tyro3 >> MerTK, and contributes to the enhancement of the clearance of apoptotic cells (Erwig and Henson, 2008; van der Meer et al., 2014).

The third step of the phagocytic clearance process is the engulfment of the cellular corpse by the phagocytes. Several important events are required for the uptake of apoptotic cells such as, the reorganization of actin filaments, the formation of phagocytic cuparound the dying cell corpse and subsequent internalization, as well as the series of phagosome maturation steps. Two evolutionary conserved signalling pathways are responsible for the regulation of these processes, both mediating the activation of Rac-1 (Nagata et al., 2010). The first pathway is initiated by MerTK, $\alpha_v\beta_3/\alpha_v\beta_5$ integrins or BAI1 phagocytic receptors that contributes to the formation of CrkII-Dock180-ELMO complex and promotes the activation of small GTPase Rac1, which results in actin polymerization and cytoskeletal rearrangement (Nakaya et al., 2006). In the other signalling pathway, LRP1 or stabilin-2 engulfment receptors interact with the adaptor protein GULP to activate Rac1 (Park et al., 2010).

The uptake and internalization of dying cells is accompanied by the formation of membrane-bound intracellular vacuoles, termed phagosome structure, which contain the phagocytic target. During the phagosome maturation process, the phagosomal lumen becomes increasingly acidic, eventually leading to the fusion with an acidic lysosome structure and efficient degradation of dying cells into their basic cellular building blocks (Zhou and Yu, 2008).

The fourth step of the clearance of apoptotic cells involves the immune response to the engulfed corpses by the phagocytes. In contrast to the phagocytosis of necrotic cell (Poon et al., 2010), apoptotic cells' clearance, in principle, does not result in an inflammatory response. This is an immunologically silent process, which can be characterized by the release of anti-inflammatory cytokines, such as IL-10 or TGF-β, as well as the inhibition of pro-inflammatory cytokine production, such as TNF-α, IL-1β, IL-12 by phagocytes (Gregory and Devitt, 2004; Savill et al., 2002; Savill and Fadok, 2000). However, if the apoptotic cells are not cleared properly and occasionaly, the loss of membrane integrity of the remained cells can induce necrotic cell death, which leads to secretion of pro-inflammatory cytokines and inflammatory response (Fernandez-Boyanapalli et al., 2010; Medina and Ravichandran, 2016; Poon et al., 2014).

In the eye, the atrophy of RPE cells contributes to the accumulation of dead cells and the formation of debris. This is a potentially dangerous material which must be cleared on a daily basis to maintain the retinal homeostasis. If the removal of dying retinal cells is inefficient, degeneration and inflammation may occur (Kinnunen et al., 2012).

In the wet type of AMD, the proliferation of new blood vessels and their penetration through the Bruch's membrane contribute to the infiltration of macrophages and DCs into the subretinal space, and these professional phagocytes are able to eliminate the apoptotic cells from there (Kohno et al., 2013). However, in the dry form of AMD, the BRB is intact, therefore the professional phagocytes cannot reach the dead cells, and in that case, the non-professional phagocytes (neighbouring live RPE cells) are responsible for the uptake of dying RPE cells (Bowes Rickman et al., 2013).

The phagocytic synapse has been investigated by several research groups in the retina. **Figure 4** summarizes the molecules which have been identified as contributors in the phagocytosis of dying RPE cells or POS by macrophages and/or RPE cells (Szabo et al., 2014).

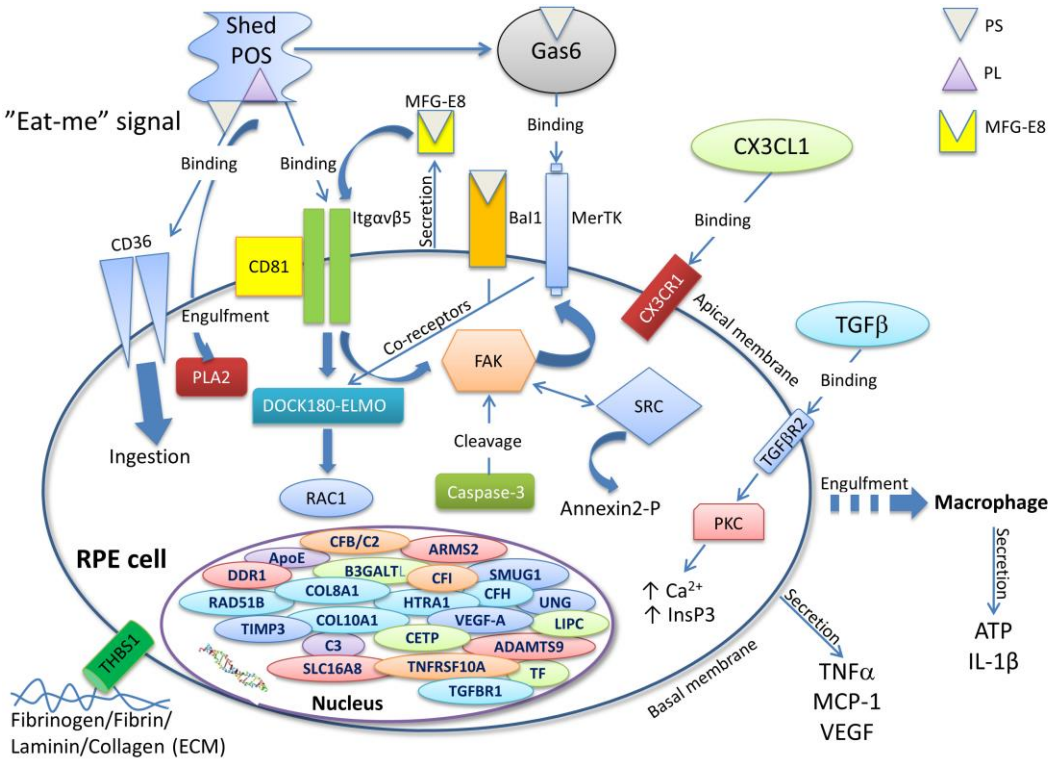

Figure 4. Molecules involved at the phagocytic synapse in the retina. *Blue font indicates genes in which SNPs have been related to AMD. Abbreviations: DOCK180-ELMO, dedicator of cytokinesis-engulfment and cell motility protein; ECM, extracellular matrix; FAK, focal adhesion kinase; Gas6, Growth arrest-specific 6; MFG-8, milk fat globule-8; POS, photoreceptor outer segment; PS, phosphatydil serine; RAC1, Ras-related C3 botulinum substrate 1; RPE, retinal pigment epithelium; TAM kinase, TYRO3, AXL, Mer kinase; THBS1, thrombospondin 1; TGFβ, tumor growth factor beta; VEGF-A, vascular endothelial growth factor-A.*

Figure adapted from (Szabo et al., 2014)

2.8. Treatment of AMD

The number of AMD patients is expected to be doubled over the next 20 years, suggesting that AMD will become a major public health problem. Therefore, it is very important to identify potential therapeutic targets and to establish an effective therapy against AMD (Gehrs et al., 2006; Gordois et al., 2012). To date, only palliative forms of treatments are available, which relieve the symptoms of AMD, but they are not causal treatments.

There is currently no approved treatment for dry type of AMD, which represents the majority of the AMD cases. However, the beneficial effect of antioxidants and omega-fatty acids on the pathogenesis of this disease has been demonstrated. The dietary

supplement-based treatment, including antioxidant vitamin C and E, trace element zinc and carotenoids, lutein and zeaxanthin, as well as omega-3 fatty acids, has been associated with the protection of the retinal tissues and the prevention or the delay of progression to the late wet form of AMD. Various formulations of micronutrients that are currently available on the market alone or as mixtures, have been proposed by ophthalmologists to AMD patients and to people being at risk of developing the disease (Buschini et al., 2015; Damico et al., 2012).

In the case of wet type of AMD, the traditional treatment forms, such as laser photocoagulation or photodynamic therapy (PDT) may help in slowing or preventing the further proliferation of CNVs (Gaynes and Fiscella, 2004; Michels et al., 2006). However, the intravitreal injection of anti-VEGF agents (e.g. bevacizumab, ranibizumab or aflibercept), has been the mainstay of treatment in the clinics, by blocking the growth of new blood vessels in the wet type of AMD. These drugs can bind to the VEGF receptors, which are well-known promoters of angiogenesis and these contribute to the pathogenesis of wet AMD (Amoaku et al., 2015).

Corticosteroids (CS) have also been widely used in the treatment of numerous medical conditions, such as in retinal disorders for their rapid and delayed effects on physiological and pathological functions. The CS exerts their effects through cytosolic CS receptors, which move into the nucleus to regulate gene expression or upon ligand binding to membrane-bound CS receptors. Triamcinolone (TC) is a conventional corticosteroid, which has been used as an intravitreal injection for the treatment of neovascular ocular diseases, particularly exudative AMD (Danis et al., 1996). TC can exert anti-inflammatory, anti-permeability, anti-fibrotic and anti-angiogenic properties (Jonas et al., 2004; Jonas et al., 2003). Combined therapies are currently used in the ophthalmology practice, to increase the efficiency of primary treatments, for example CS in combination with PDT or anti-VEGF (Lim et al., 2015).

On the other hand, tissue engineering strategies have been developed based on the development and transplantation of scaffolds, which mimic the Bruch's membrane and serve for cell engraftment (Fernandez-Robredo et al., 2014; Nowak, 2014). Recent studies have demonstrated that several microRNAs, such as miR-21, miR-23, miR-27, miR-31 and miR-150, can play a crucial role in the regulation of AMD-associated processes, suggesting that miRNAs may represent novel therapeutic targets for AMD (Wang et al., 2012).

Moreover, many new emerging therapeutic approaches for AMD have shown promising results. One of them is a cell-based transplantation therapy that focuses on the replacement or regeneration of damaged RPEs *in vivo*, using retinal and iris pigment epithelium cells as well as stem cells (Zarbin, 2016).

Exploring previously unknown AMD associated molecular mechanisms can contribute to the characterization of new therapeutic targets, thereby, possibly help block the accumulation of drusen deposits, reduce inflammation and retinal oxidative stress, as well as repair choroidal perfusion.

3. Aims of the studies

- To induce autophagy-associated cell death in ARPE-19, hRPE and hESC-RPE cells by serum deprivation and oxidative stress using hydrogen-peroxide (H_2O_2).

- To establish an *in vitro* detection model for studying autophagy in H_2O_2-treated ARPE-19, hRPE and hESC-RPE cells.

- To study and quantify the clearance of anoikic and autophagy-associated dying RPE cells by non-professional phagocytes, macrophages or dendritic cells using FACS analysis as a model for AMD pathogenesis.

- To examine the effect of TC-treatment on the phagocytic capacity of professional and non-professional phagocytes during the engulfment of autophagy-associated dying RPEs.

- To investigate the role of MerTK receptor in the TC-enhanced phagocytosis of anoikic dying RPE cell by professional and non-professional phagocytes.

- To determine the released pro-inflammatory cytokines during phagocytosis of anoikic and autophagy-associated dying RPE cells by macrophages.

4. Materials and methods

4.1. Ethics statements

All protocol of human cell isolation experiments complied with the Guidelines of the Declaration of Helsinki.

The isolation of primary hRPE cells from human cadaver eyes was undertaken in strict accordance and approval of the National Ethical Committee in Hungary.

The establishment of hESC lines was approved of the National Authority for Medicolegal Affairs Finland (Dnro 1426/32/300/05). These cell lines were derived from surplus or poor quality pre-implantation embryos, which could not be used for *in vitro* fertilization treatment. The derivation, characterization, and differentiation of hESC lines were performed according to the approval of the Ethics Committee of Pirkanmaa Hospital District, Finland (Skottman/R05116).

Human monocytes were obtained from buffy coats of anonymous healthy blood donors by the Hungarian National Blood Service and Finnish Red Cross Blood Service, all volunteers had given their informed consent in writing. The Ethics Committee of the Medical and Health Science Center, University of Debrecen, Hungary (DEOEC RKEB/IKEB Prot. No. 2745 -2008 and 3093 - 2010) and Kuopio University Hospital, Finland (42/2014) approved this consent procedure for these studies.

4.2. Materials

4.2.1. Cell culture media

- AIM V medium (Gibco)
- Antibiotic/antimycotic solution (HyClone, Logan, Utah, USA)
- Dulbecco's modified Eagle's medium (DMEM) (Sigma-Aldrich, St. Louis Missouri, USA)
- DMEM Nutrient mixture F-12 (DMEM-F12) (Sigma- Aldrich)
- Fetal calf serum (FCS) (Gibco, Paisley, UK)
- Glutamax (Thermo Fisher Scientific)
- Granulocyte macrophage colony-stimulating factor (GMCSF) (Peprotech EC)

- Human AB serum (Sigma)
- human basic fibroblast growth factor (bFGF) (Pepro-Tech, NJ, USA)
- IL-1β (Peprotech EC)
- IL-4 (Peprotech EC)
- IL-6 (Peprotech EC)
- Iscove's Modified Dulbecco's Medium (IMDM) (Gibco)
- Knock-OutTM Dulbecco's Modified Eagle Medium (KO-DMEM) (Thermo Fisher Scientific)
- KnockOutTM Serum Replacement (KO-SR) (Thermo Fisher Scientific)
- L-glutamine (Sigma-Aldrich)
- macrophage colony-stimulating factor (M-CSF) (Pepro-Tech EC, London, UK)
- non-essential amino acids (Lonza, Basel, Switzerland)
- penicillin-streptomycin (Sigma-Aldrich)
- prostaglandin E_2 (PGE_2) (Sigma-Aldrich)
- TNF-α (Peprotech EC)

4.2.2. Cell dyes used during the staining procedures

- Annexin-V-FITC/Propidium iodide Apoptosis Detection Kit (MBL, Woburn, MA, USA)
- Carboxyfluorescein-diacetate-succinimidyl ester (CFDA) (Molecular Probes, Eugene, Oregon, USA)
- 2-(4-amidinophenyl)-6-indolecarbamidine dihydrochloride (DAPI) (Sigma-Aldrich)
- 5-(and-6)-(((4-chloromethyl)benzoyl) amino)tetramethylrhodamine (CMTMR) (Molecular Probes)

4.2.3. Antibodies

- anti-β-actin monoclonal antibody, produced in mouse (Sigma-Aldrich)
- anti–GAPDH monoclonal antibody, produced in mouse (Covalab, Villeurbanne, France)

- anti-LC3 polyclonal antibody, produced in rat (Novus Biologicals, Littleton, Colorado, USA)
- anti-MerTk monoclonal antibody, produced in mouse (R&D systems, Minneapolis, USA)
- anti-p62 monoclonal antibody, produced in mouse (Santa Cruz Biotechnology, Dallas, Texas, USA)
- anti–tubulin monoclonal antibody, produced in mouse (Sigma-Aldrich)
- Human IL-6 and IL-8 ELISA OptEIA^{TM} kits
- horseradish-peroxidase (HRP)-conjugated anti-mouse antibody (Sigma-Aldrich)
- horseradish-peroxidase (HRP)-conjugated anti-rat secondary antibody (Sigma-Aldrich)
- NL-493 anti-mouse secondary antibody (R&D systems)

4.2.4. Reagents

- 2-mercaptoethanol (2-MEA) (Sigma-Aldrich)
- 3-methyladenine (3-MA) (Sigma-Aldrich)
- Bradford reagent (Sigma-Aldrich)
- chloroquine (CQ) (Sigma-Aldrich)
- EDTA (Sigma-Aldrich)
- Ficoll–Paque Plus (Amersham Biosciences, Uppsala, Sweden)
- hydrogen-peroxide (H_2O_2) (Sigma-Aldrich)
- Immobilon Western chemiluminescent substrate (Millipore-Merck)
- paraformaldehyde (PFA) (Sigma-Aldrich)
- poly-2-hydroxyethylmethacrylate (poly-HEMA) (Sigma-Aldrich)
- polyethylenimine (PEI) reagent (Sigma-Aldrich)
- TaqMan reverse transcription reagent kit (Applied Biosystems)
- triamcinolone (TC) (Sigma-Aldrich)
- Triton X-100 (Sigma-Aldrich)
- TRIzol Reagent (Invitrogen Life Technologies)
- trypsin (Sigma-Aldrich)
- Tween-20 (Sigma-Aldrich)
- protease inhibitor (Sigma-Aldrich)

4.3. Methods

4.3.1. Cell preparation and culturing

Adult retinal pigment epithelium-19 (ARPE-19) – human RPE cell line, was kindly provided by Prof. Stephen Moss, (UCL, London, UK). It was cultured in DMEM (Sigma-Aldrich, St. Louis Missouri, USA) supplemented with 10% fetal calf serum (FCS) (Gibco, Paisley, UK), 200 mM L-glutamine (Sigma-Aldrich) and 1% Antibiotic/antimycotic solution (HyClone, Logan, Utah, USA) at 37^{o}C, 5% $CO_{2.}$ Cells were detached from the cell culture flasks and plates using trypsin-EDTA (Sigma-Aldrich). ARPE-19 cells were used at passages 10-15 for all experiments.

The primary hRPE cells were obtained from adult cadaver human eyes (age range: 64-92) without any known ocular diseases. The isolation protocol was started with the removal of the anterior segment (corneo-scleral ring) and the lens, then paper sponges and forceps were used to remove the vitreous and neuroretina, respectively. Consequently, the RPE layer were gently scraped without damaging the Bruch's membrane using half-spherically bent-end Pasteur glass pipettes and the collected cell suspension was placed in PBS (Sigma-Aldrich) for centrifugation (10 min, 1000 rpm) (Johnen et al., 2012), then cultured in DMEM Nutrient mixture F12 medium (Sigma-Aldrich) supplemented with 10% FCS (Gibco), 200 mM L-glutamine (Sigma-Aldrich) and 1% Antibiotic/antimycotic solution (HyClone). The cells were passaged by incubation in trypsin-EDTA (Sigma-Aldrich) for 2-4- minutes. All experiments were performed on passage 2-5 hRPE cells.

The pluripotent hESC line Regea08/017 (46, XX) was derived from blastocyst stage embryos, as published by Skottman (Skottman, 2010), and was cultured on inactivated human foreskin fibroblast (hFF) (ATCC, Manassas, VA, USA) at 37 ºC, 5% CO_2 in hESC culture medium comprising KnockOut™ DMEM (KO-DMEM), 20% KnockOut^{TM} Serum Replacement (KO-SR), 2 mM Glutamax, 0.1 mM 2-mercaptoethanol (all from Thermo Fisher Scientific, Waltham, MA, USA), 1% Minimum Essential Medium non-essential amino acids, 50 U/ml penicillin-streptomycin (both from Lonza, Basel, Switzerland), and 8 ng/ml human basic fibroblast growth factor (bFGF) (Pepro-Tech, NJ, USA). The culture medium was changed 3 times a week. The RPE differentiation and the enrichment process from pluripotent hESCs was performed as previously described (Ilmarinen et al., 2015;

Vaajasaari et al., 2011). Cell growth and pigmentation were monitored weekly by Nikon Eclipse TE2000-S phase contrast microscope (Nikon Instruments Europe B.V. Amstelveen, The Netherlands). The confluent, pigmented hESC-RPE cell cultures were seeded on collagen IV-coated (5 μg/cm^2, Sigma-Aldrich) well plates for 6 weeks in RPE basic medium (Vaajasaari et al., 2011), after which the cells were detached from the cell culture plates using trypsin-EDTA (Sigma-Aldrich).

Human monocytes from 'buffy coats' of healthy blood donors were isolated by density gradient centrifugation using Ficoll–Paque Plus (Amersham Biosciences, New Jersey, USA), then CD14 human MicroBeads (Miltenyi Biotec, Bergisch Gladbach, Germany) were used for magnetic separation. Human macrophages were obtained through a 5-day differentiation using 5 ng/ml macrophage colony-stimulating factor (M-CSF) (Pepro-Tech) at 37°C in IMDM (Gibco) supplemented with 10% human AB serum (Sigma-Aldrich) and 10000 U/mL penicillin- 10 mg/mL streptomycin in a 5 % CO2 atmosphere. (Sigma-Aldrich) (Petrovski et al., 2007a).

To generate iDCs, freshly isolated monocytes were seeded into 6-well plates at a density of 2x10^6 cells/mL and cultured for 5 days in serum-free AIM V medium (Gibco) containing 80 ng/ml GMCSF (Pepro-Tech) and 100 ng/ml IL-4 (Pepro-Tech). Medium was supplemented with the same amounts of GMCSF and IL-4 on day 0 and 3 (Hodrea et al., 2012; Majai et al., 2010). Inflammatory cytokine mixture was used for the activation of resting DCs on day 5, which containing 10 ng/ml TNF-α (Pepro-Tech), 5 ng/ml IL-1β (Pepro-Tech), 20 ng/ml IL-6 (Pepro-Tech), 75 ng/ml GMCSF (Pepro-Tech), and 1 mg/ml PGE_2 (Sigma-Aldrich) and the cells were harvested on day 6 (Kis-Toth et al., 2013).

4.3.2. Induction of anoikic and autophagy-associated cell death

ARPE-19, primary hRPE or hESC-RPE cells were plated on poly-HEMA (Sigma-Aldrich) coated culture dishes for 24h to induce anokic cell death through ECM detachment (Petrovski et al., 2011b; Petrovski et al., 2007a).

For triggering of autophagy-associated cell death, ARPE-19 and primary hRPE cells were plated over a 24h period and cultured until they formed confluent (80-90%) monolayers, then co-treated by serum deprivation and 0.4-1 mM H_2O_2 (Sigma-Aldrich) for 2-4h before harvesting. In the case of hESC-RPE cells, the autophagy-associated

cell death was induced by the deprivation of serum and simultaneously the cells were treated by 1mM H_2O_2 for 2h.

4.3.3. Assay for cell death analysis

Anoikic and autophagic-associated cell death (in ARPE-19, primary hRPE and hESC-RPE cells) was determined by the Annexin-V-fluorescein isothio-cyanate Apoptosis Detection Kit (MBL, Woburn, Massachusetts, USA) according to the manufacturer's recommendations. Annexin V-FITC staining was used to detect that PS translocates from the intracellular plasma membrane to the cell surface during apoptosis and then fluorochrome-labeled Annexin V can be specifically bound to this. In parallel, necrotic cell death can assess by Propidium Iodide (PI) staining, which can permeate through the disturbed cell membranes and binds to DNA. The percentage of Annexin-V and/or PI positive cells was determined by relative fluorescence intensity using a BD FACS Calibur or BD Accuri C6 flow cytometer (BD Biosciences, San Jose, California USA) and data was analyzed using WinMDI 2.8. software (Joseph Trotter, La Jolla, CA, USA) (Petrovski et al., 2007a; Vermes et al., 1995).

4.3.4. Antibodies and immunoblotting

Cells were collected and washed with PBS, homogenized either in ice-cold lysis buffer containing 50 mM Tris–HCl; 0.1% Triton X-100 (Sigma-Aldrich), 1 mM EDTA (Sigma-Aldrich), 15 mM 2-mercaptoethanol (2-MEA) (Sigma-Aldrich) and protease inhibitor (Sigma-Aldrich) or in M-PER cell lysis reagent (mammalian protein extraction reagent) (Thermo Scientific). Insoluble cellular material was removed by centrifugation and the protein concentration was determined by using Bradford reagent (Sigma-Aldrich) and then the lysates were mixed with 5x Laemmli loading buffer, boiled for 10 min. Equal amounts of protein (20 μg) were separated on 8% SDS- polyacrylamide gel for MerTk or on 10% SDS- polyacrylamide gel for p62 or on 15% SDS-polyacrylamide gel for LC3. Proteins were transferred onto a PVDF Immobilon-P Transfer Membrane (Merck-Millipore, Darmstadt, Germany; pore size 0.45 μm) and followed by blocking in Tris-buffered saline containing 0.05% Tween-20 (Sigma-Aldrich) (TBS-T) and 5% skimmed milk (AppliChem, Darmstadt, Germany) for 1h. The membranes were then probed overnight at 4ºC with anti–LC3 (1:2000) rat

polyclonal antibody (Novus Biologicals, Littleton, Colorado, USA), which recognizes both LC3-I and LC3-II, with anti–p62 (1:2000) mouse monoclonal antibody (Santa Cruz Biotechnology, Dallas, Texas, USA) or with anti-MerTk (1:1000) mouse monoclonal antibody (R&D systems), all of them in TBS-T containing 1% skimmed milk, and followed by incubation with horseradish-peroxidase (HRP)-conjugated species corresponding secondary antibodies (Sigma-Aldrich) for 1h at room temperature. For loading control mouse monoclonal antibodies against GAPDH (1:5000) (Covalab, Villeurbanne, France), tubulin (1:5000) (Sigma-Aldrich) or β-actin (1:5000) (Sigma-Aldrich) was used overnight at 4°C in TBS-T containing 1% skimmed milk. Immunoreactive products were visualized using Immobilon Western chemiluminescent substrate (Merck-Millipore). Densitometry analysis of western blots was performed using Image J software (National Institutes of health, USA).

4.3.5. Electron microscopy

For transmission electron microscopy (TEM) analysis, H_2O_2-treated (1mM, 2h) ARPE-19 cells were fixed in 0.1 M sodium cacodylate-buffered, pH 7.4 and 2.5% glutaraldehyde solution for 2h and then rinsed (three times, 10 min) in 0.1 M sodium cacodylate buffer, pH 7.4 and 7.5% saccharose and followed by post-fixation with 1% osmium tetroxide (OsO_4) solution for 1h. Then the samples were dehydrated through an ethanol gradient (70% ethanol (20 min), 96% ethanol (20 min), 100% ethanol (two times, 20 min), and embedded in Durcupan ACM. To stain ultrathin sections, uranyl acetate and lead citrate were used. Sections were examined in a Philips CM-10 transmission electron microscope (Philips Electronic Instruments, Mahwah, NJ, USA) at 80 kV (Petrovski et al., 2011b).

4.3.6. Quantification of LC3 positive cells by FACS analysis and fluorescence microscopy

Autophagy was assessed by detection of autophagic vacuoles (AVs) in GFP-LC3 transfected ARPE-19 cells. The GFP-LC3 expression plasmid was kindly provided by Prof. Noboru Mizushima (Tokyo Medical and Dental University, Tokyo, Japan). ARPE-19 cells were seeded on adherent glass coverslips and the confluent cells were transiently transfected with the GFP-LC3 expression plasmid using polyethylenimine

(PEI) reagent (Sigma-Aldrich) (PEI:DNA ratio=4:1, 1µg DNA/well) to analyzed by fluorescent microscopy. Transfected ARPE-19 cells were pre-treated with CQ (25 µM, 1h) (Sigma-Aldrich) and then incubated with H_2O_2 (1mM, 2h) in serum-free condition. After treatments, cells were fixed with 4% paraformaldehyde (PFA) (Sigma-Aldrich) for 10 min and stained with 4',6'-diamidino-2-phenylindole (DAPI) (0.3 µg/ml) (Sigma-Aldrich) to visualize cell nuclei. Fluorescent images were taken using an Axiovert-200 Zeiss microscope (Carl Zeiss MicroImaging GmbH, Göttingen, Germany). The number of GFP-LC3 positive cells were counted manually based on the fluorescent images at least ten different visual fields on microscopy from three independent experiments in each condition. In parallel, the percentage of GFP-LC3 positive cells was quantified by flow cytometry using a BD FACS Aria III (BD Biosciences).

Moreover, the GFP-LC3-positive ARPE-19 cells were sorted out on the basis of their GFP fluorescence using a BD FACS Aria III. The samples were prepared the following way, the GFP-LC3 transfected cells were harvested by trypsinization, washed, centrifuged and resuspended in PBS to a final density of $2x10^6$ cells/mL, and filtered through a nylon filter (Merck-Millipore) to remove cell aggregates. Data acquisition and analysis were performed using BD FACS Diva 6.2 software. GFP signals were detected with a 530/30-nm bandpass filter. The green fluorescent cell population of interest was gated based on relative fluorescence intensity. The GFP-LC3 positive, AV-containing cells and parallelly the GFP-LC3 negative were selected by gates and the fluorescence intensity of events within the gated regions was quantified. Data were collected from 10000–20000 events for each sample. Control-sort was performed to prove a greater than 98% sorting efficiency (Kovala et al., 2000).

To detect AVs and cell death simultaneously, ARPE-19 cells were transiently transfected with mCherry-LC3 plasmid, which was kindly provided by Dr. Gian Maria Fimia (University of Salento, Lecce, Italy), treated with H_2O_2 (1mM 2h) and then Annexin V-FITC labelling was used to determine the PS externalization, (which reflects upon apoptotic cell death). Cells containing LC3-positive AVs and/or cells exposing PS on their surface were quantified using a BD FACS Calibur flow cytometer.

4.3.7. Phagocytosis assay

Pre-treatment of phagocytes with 1μM TC (Sigma-Aldrich) was performed 48h prior to the phagocytosis assay. Living RPE cells acting as phagocytes were plated in serum-free medium 24h before phagocytosis. The phagocytes were stained with 7.5μM CMTMR (5-(and-6)-(((4-chloromethyl)benzoyl)amino)tetramethylrhodamine) (Molecular Probes, Eugene, Oregon, USA) for 16h. ECM detachment-induced anoikic and H_2O_2-induced (2h, 1mM) autophagy-associated dying RPE cells were stained for 2h with 12.5mM CFDA (carboxyfluorescein diacetate, succinimidyl ester) (Molecular Probes). Before the assay the labelled phagocytes and dying cells were washed twice with PBS. Phagocytes were co-cultured with anoikic or autophagy-associated dying RPE cells for 4, 8, 12 or 24h at a ratio of 1:3 or at 1:2 or 1:5, where specifically indicated at 37°C, 5% CO_2 atmosphere in IMDM medium the absence of human 10% AB serum. After co-culture, the phagocytic cell mixture was collected by trypsinization to remove bound but not engulfed dying cells, centrifuged, washed twice with PBS and fixed with 1% PBS-buffered PFA (pH 7.4). The phagocytosis rate was determined by FACS Calibur BD flow cytometer as percent phagocytic cells (CMTMR positive) that have engulfed dying cells (positive for both CMTMR and CFDA). WinMDI 2.8. software was used for data analysis (Petrovski et al., 2011b).

ARPE-19 cells were pre-treated with 10 mM 3-MA for 24h for inhibition of autophagy-associated cell death (Petrovski et al., 2011a; Petrovski et al., 2007a). To investigate the subsequent impact of 3-MA pre-treatment on phagocytosis, the 3-MA pre-treated (10mM, 24h) and then H_2O_2-exposed (1mM, 2h) ARPE-19 cells were co-incubated with macrophages for 4, 8, 12, 24h at a ratio of 1:3.

The GFP-LC3-positive as well as the negative sorted ARPE-19 cells were resuspended in IMDM medium and added to the macrophages. The rate of phagocytosis was analyzed after 8h co-incubation.

For the blocking experiments, macrophages were pre-incubated with 10 μg/mL anti-MerTk antibody (R&D systems) for 10 min before co-incubation with dying cells. For testing the effect of Gas6 on phagocytosis, macrophages were treated with 200ng/mL Gas6 (R&D systems) for 24h before adding the dying cells.

4.3.8. Time-lapse imaging microscopy

For *in vitro* phagocytosis assay, the macrophages were seeded on 24 well cell culture plates, stained with CMTMR (7.5μM, 16 h) and co-incubated with the CFDA-stained (12.5 mM, 2h) or GFP-LC3 transfected dying RPE cells in a ratio of 1:2. For the time-lapse microscopy of the co-cultures, an incubation chamber system (Solent Scientific, Segensworth, United Kingdom) attached to a motorized Olympus IX-81 inverted microscope (Olympus Europa Holding, Hamburg, Germany) equipped with a cooled high-speed Hamamatsu ORCA-R2 camera (Hamamatsu Photonics, Hamamatsu City, Japan) was used. The incubation chamber system consisted of a temperature logging controller (consistent 37°C), a sterile airflow and humidity circulator and an inner CO_2 enrichment multi well plate holder. Cells were monitored for 24h and in every 5 min per channel and per well an image was taken automatically through a PlasDIC filter with the help of a motorized cubic filter. To generate time-lapse videos from the digital images, the XCE-RT xCellence Real Time software with 24 fps (Olympus) was used (Sarvari et al., 2015).

4.3.9. RNA preparation and TaqMan real-time RT-PCR

For total cellular RNA isolation, the untreated and TC-treated macrophages were collected in TRIzol Reagent (Invitrogen Life Technologies). After DNase treatment (Sigma-Aldrich), the concentration and purity of total RNA were determined by means of NanoDrop spectrophotometer (Thermos Scientific). Total RNA (1μg/sample) was reverse transcribed into cDNA using TaqMan reverse transcription reagent kit (Applied Biosystems, Foster City, CA, USA) according to manufacturer's guidelines. To determine the expression level of genes, which previously listed (Zahuczky et al., 2011), a predesigned, factory-loaded 384-well TaqMan Low-Density Array (TLDA) (Applied Biosystems,) was used, with two technical replicates per targeted gene and three biological parallels. Expression levels of target genes were normalized to human cyclophyllin (hCYC) as endogenous control.

An ABI Prism 7700 sequence detection system (Applied Biosystems) was used to determine relative gene expression analyzing knock-down effect in macrophage. Gene primers and probes were designed and supplied by Applied Biosystems. All samples were measured in 3 technical parallels. Human cyclophyllin was used as endogenous

control. Gene expression values were calculated based on the $\Delta\Delta C_t$ method, where one sample was designated as calibrator, through which all other samples were analyzed. ΔC_t represents the threshold cycle (C_t) of the target minus that of hCYC and $\Delta\Delta C_t$ represents the ΔC_t of each target minus that of the calibrator. Relative quantities (or fold changes) were determined using the equation, where relative quantity equals $2^{-\Delta\Delta Ct}$ (average of three replicated experiments) (Zahuczky et al., 2011).

4.3.10. siRNAs and electroporation of macrophages

In order to knock-down each investigated gene, small interfering ribonucleic acid (siRNA) constructs were obtained from Ambion (Life Technologies), targeting adenosine A3 receptor (ADORA3) [3′-CGUCUAUGCCUAUAAAAUAtt (sense) and 5′-UAUUUUAUAGGCAUAGACGtt (antisense)], AXL receptor tyrosine kinase [3′-GGAACUGCAUGCUGAAUGAtt (sense) and 5′-UCAUUCAGCAUGCAGUUCCtg (antisense)], c-mer proto-oncogene tyrosine kinase (MERTK) [3′-GAACUUACCUUACAUAGCUtt (sense) and 5′-AGCUAUGUAAGGUAAGUUCaa (antisense)] and thrombospondin-1 (THBS1) [3′-GGACUGCGUUGGUGAUGUAtt (sense) and 5′- UACAUCACCAACGCAGUCCtt (antisense)]. Non-targeting siRNA negative control (scrambled) was obtained from Sigma-Genosys (3781976-F/112). Living ARPE-19 cells and macrophages, three days after isolation, were harvested from the 24 well plates and washed once with DMEM or IMDM accordingly and once with PBS (all at room temperature). The cells were resuspended in OptiMEM without phenol red (Invitrogen Life Technologies) at a concentration of 4×10^7/mL. siRNA was transferred to a 4-mm cuvette (3 μM final concentration or as indicated). A volume of 100 μL of cell suspension was added and incubated for 3 min before being pulsed in a Genepulser Xcell (Bio-Rad). Pulse conditions were square-wave pulse, 500 V, 0.5 ms for macrophages (Zahuczky et al., 2011) and 250 V, 10ms for non-dying ARPE-19 cells (Fujimoto et al., 2010). Immediately after electroporation, the cells were transferred to human AB serum supplemented IMDM with the previously indicated concentrations of M-CSF and TC or FBS supplemented DMEM, accordingly.

4.3.11. Immunofluorescent staining and confocal microscopy

Macrophages were seeded on the surface of 12 mm glass coverslips (1.5×10^6/well) and cultured as previously described. After co-culturing of the macrophages with the anoikic dying cells for 4h, the cells were washed and incubated with anti-MerTk primary antibody (R&D systems) for 1h on ice. As secondary antibody, anti-mouse NL-493 (R&D systems) was used before being washed and fixed in 4% PFA for 10min on ice. Confocal fluorescent images were taken by a Zeiss LSM 510 or Olympus FV1000 confocal laser scanning microscope. For visualizing the distribution of MerTk, overview images and three-dimensional stacks were acquired at 1-µm optical thickness. Three-dimensional reconstructions and x-y-z projections were created with the LSM 4.0 software. Images were processed and protein accumulation was analyzed by Fiji software as for positive events at least 20% of the total investigated protein exposed by a macrophage was clustered to the connecting points between phagocytes and dying ARPE-19 cells.

4.3.12. Quantification of IL-6 and IL-8 release by ELISA

The released pro-inflammatory cytokines by the macrophages was investigated during phagocytosis of dying RPE cells. Differentiated macrophages were co-cultured with anoikic or H_2O_2-induced (2h, 1mM) autophagy associated dying RPE cells at a ratio of 1:3 for 4 and 8h, respectively, at 37°C, 5% CO_2 atmosphere in IMDM medium the absence of human 10% AB serum. The culture supernatants were harvested and stored for cytokine measurements. Macrophages were either treated with 1µM TC for 48h or left untreated prior to starting the phagocytosis assays. The concentration of released IL-6 (pg/ml) and IL-8 (pg/ml) cytokines was measured from the collected cell culture media using Human IL-6 ELISA OptEIA™ and Human IL-8 ELISA OptEIA™ kits (BD Biosciences) according to the manufacturer's specifications (Petrovski et al., 2011a). The measurement was performed in each case with two technical replicates and three biological parallels. Statistically significant differences were determined by the paired Student's t-test.

4.3.13. Statistical analysis

All the data are representative of at least three independent experiments and each sample was tested in triplicate (exception were marked accordingly). Results are expressed as the mean ± SD or mean ± SEM. For multiple comparisons of groups, statistical significance was calculated and evaluated by one-way ANOVA followed by Tukey post-hoc test. Statistically significant difference between the two groups was determined with paired Student's t-test (two tailed) and values of $p<0.05$ were considered significant.

5. Results

5.1. Cell death induction and morphological analysis of RPE cells

5.1.1. ARPE-19 and primary hRPE cells die in a time- and concentration-dependent manner due to serum deprivation and H_2O_2 co-treatment

H_2O_2 administration is a commonly used *in vitro* model for the induction of oxidative stress. After serum deprivation and increasing time intervals (2h, 4h) and concentrations (0.4mM, 0.8mM, 1mM) of H_2O_2 co-treatment in ARPE-19 and hRPE cells, we assessed the cell viability and death rate using Annexin V-FITC/PI double staining (Petrovski et al., 2007a; Vermes et al., 1995). Representative dot plots show the viable cells, which are both Annexin-V (AnxV) and PI negative, the cells that are $AnxV^+$ and PI^-, $AnxV^-$ and PI^+ as the mark of early apoptosis and necrosis, respectively. Furthermore, AnxV/PI double positivity is a sign of late apoptosis or secondary necrosis. Time- and concentration-dependent cell death was observed with a mixture of viable, early or late apoptotic and necrotic cell populations by a high-throughput flow cytometry based method). We could determine that most of the cells die in parallel with PS externalization, especially after 2h, 1mM H_2O_2-treatment. The ratio of viable ARPE-19 cells significantly decreased from 91.4±1.7% to 28.6±14.2%, and parallelly the percentage of only $AnxV^+$ ARPE-19 cells significantly increased from 2.1±2% to 41±10.8% upon 2h of 1mM H_2O_2-treatment, compared to the untreated control ones (**Figure 5A**). In the case of primary hRPE cells, similar trend was observed, the percentage of viable cells also changed from 87.1±4.9% to 51.6±3.6% as a result of 2h 1mM H_2O_2-treatment, and 17.7±12.7% of the hRPE cells became $AnxV^+$, while the untreated control contained only 3.2±2.8% of these early apoptotic cells (**Figure 5B**). Sodium-azide administration (4h, 1mM) was used as positive control for the induction of necrotic cell death (Sato et al., 2008; Shiloach et al., 2014). As it was shown in **Figure 5**, this treatment mostly resulted in PI single positive cells, it was 67.92±3.32% in ARPE-19 and 42.59±12.80% in hRPE cells, this pattern markedly differed compared to the H_2O_2-administration, which resulted in only (10-30%) of PI positive cells. These results suggest that, however, the minority of cells might suffer a stress that leads to primary or secondary necrosis, most of the cells die with PS externalization. Altogether,

the H_2O_2-administration causes RPE cells to undergo a mixture of different cell death modalities over the tested time.

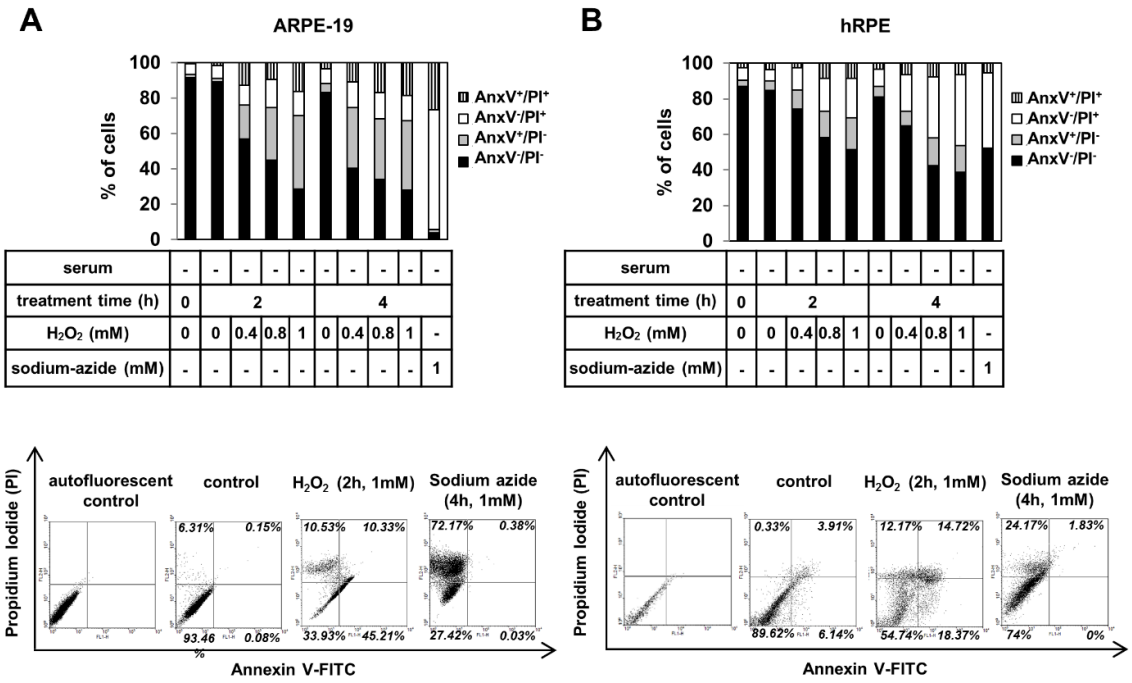

Figure 5. Quantification of the cell death rate after H_2O_2-treatment in the absence of serum in RPE cells by flow cytometry. *Induction of cell death by increasing time intervals (2h, 4h) and concentrations (0.4mM, 0.8mM, 1mM) of H_2O_2-treatment in the absence of serum in ARPE-19 (**A**) and hRPE (**B**) cells was determined by Annexin (Anx)V-FITC/PI assay. Sodium-azide-treatment (4h, 1mM) served as positive control to induce necrotic cell death. The bar charts represent the average percentage of $AnxV^-/PI^-$ (viable; black bars), $AnxV^+/PI^-$ (early apoptotic; grey bars), $AnxV^-/PI^+$ (necrotic; white bars) and $AnxV^+/PI^+$ (late apoptotic; striped bars) cells from 3 and 4 independent experiments for ARPE-19 and hRPE, respectively. Representative dot plots of AnxV/PI double staining of dying ARPE-19 and hRPE cells are also shown. The horizontal axis indicates the intensity of staining for Annexin V (logarithmic scale) and the vertical axis shows intensity of staining for PI (logarithmic scale). The percentage of different cell populations is marked in the quadrants. Cells in the lower left quadrant ($AnxV^-/PI^-$) are viable, those in the lower right quadrant ($AnxV^+/PI^-$) are early apoptotic, those in the upper left ($AnxV^-/PI^+$) are necrotic and those in the upper right ($AnxV^+/PI^+$) are late apoptotic cells. Data are representative of 3 independent experiments.*

5.1.2. The impact of serum deprivation and H_2O_2 co-treatment on the morphology and cell viability of hESC-RPE cells

Along with the ARPE-19 cell line and the primary hRPE cells, we examined a novel hESC derived RPE-like *in vitro* cell model. Our collaborator, Skottman et al. has previously confirmed that hESC-RPE cells are very similar to the native RPE cells,

based in their functional characteristics (Juuti-Uusitalo et al., 2012; Onnela et al., 2012; Savolainen et al., 2011; Vaajasaari et al., 2011). However, to the best of our knowledge, the death modalities of hESC-RPEs have not yet been investigated. Therefore, we studied the effect of serum deprivation and H_2O_2 co-treatment on the morphology and cell viability of hESC-RPE cells. We applied 1mM H_2O_2-treatment for 2h, based on the results of ARPE-19 and hRPE cells (**see Figure 5**). The typical RPE cell morphology (Marmorstein et al., 1998; Stern and Temple, 2015), such as the high degree of pigmentation and the cobblestone morphology have been observed in untreated hESC-RPE cells in the presence of serum by phase-contrast microscopy, but the serum deprivation (2h) led to the disruption of the monolayer. Swelling and detachment of hESC-RPE cells have been detected after H_2O_2-treatment (2h, 1mM) in the presence of serum. In addition, H_2O_2 (2h, 1mM) and serum deprivation co-treatment further enhanced the rate of detached, dead cell aggregates (**Figure 6A**). For the cell viability analysis, Annexin V-FITC/PI assay was used and detected by BD Accuri C6 flow cytometer (BD Biosciences). The homogeneous cell populations were gated based on their size (forward light scattering, FSC; X axis) and granularity (side light scattering, SSC; Y axis), which was enclosed in the P1 regions using red frame, as shown in the representative dot plots. Numbers indicate the percentage of cells within the P1 regions compared to the total cell population.(**Figure 6B, top dot plots**). Cells from region P1 were further analysed according to the AnxV/PI staining. Quadrant gates were used to distinguish the different cell populations: viable ($AnxV^-/PI^-$), early apoptotic ($AnxV^+/PI^-$), necrotic ($AnxV^-/PI^+$) and late apoptotic ($AnxV^+/PI^+$) cells upon different conditions (**Figure 6B, bottom dot plots**). The percentage of viable cells significantly decreased from 88.35±0.88% to 55.22±13.12%, as a result of serum deprivation and H_2O_2 co-treatment in hESC-RPE cells, compared to the untreated control ones. Simultaneously, we detected the significantly increased rate of AnxV single positive hESC-RPE cells upon the co-treatment, compared to the untreated control ones: it increased from 9.85 ±1.13% to 39.86±11.73% (**Figure 6C**). The response to the co-treatment was similar in hESC-RPE and ARPE-19 cells, approximately 40% of single positive AnxV, PS externalize cells were observed in both cases.

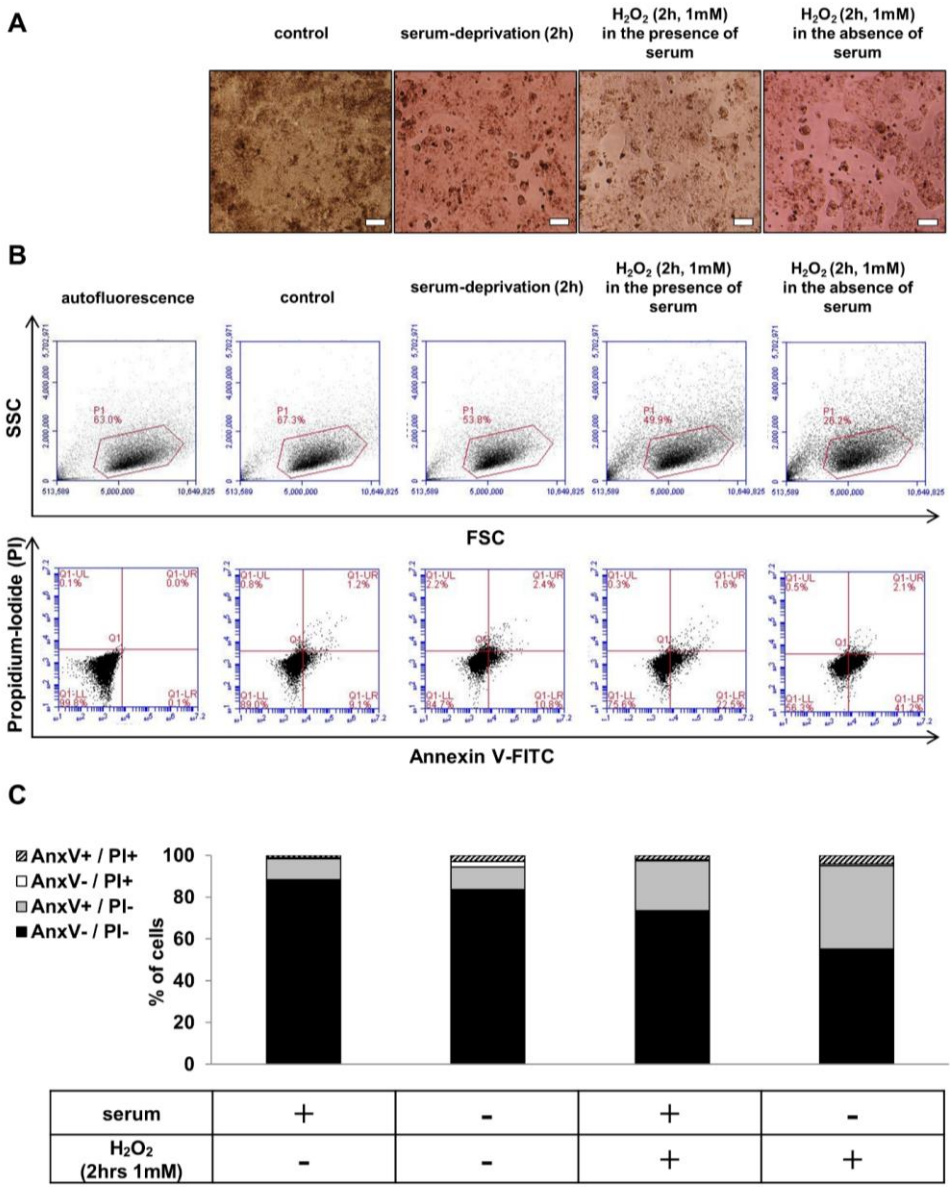

Figure 6. The induction of cell death as a result of serum deprivation and H_2O_2 co-treatment in hESC-RPE cells. *(**A**) Nikon Eclipse TE2000-S phase contrast microscope (Nikon Instruments Europe B.V. Amstelveen, The Netherlands) was used to capture images (10x) of untreated control, serum-deprived (2h) and H_2O_2-treated (2h, 1mM) hESC-RPE cells in the presence or absence of serum. Scale bar represents 20 µm. (**B**) AnxV-FITC/PI double staining assay was used to determine the cell death rate due to H_2O_2-treatment (2h, 1mM) in the absence of serum in hESC-RPE cells. Representative dot plots of AnxV/PI assay shown: (**top**) the measurements of FSC (X axis) vs. SSC (Y axis) and (**bottom**) the intensity of staining for AnxV (log scale; X axis) vs. the intensity of staining for PI (log scale; Y axis). The numbers in the quadrants represent the percentage of different cell populations: viable (lower left), apoptotic (lower right), necrotic (upper left), late apoptotic cells (upper right). Data are representative of 3 independent experiments. (**C**) The bar charts indicate the average percentage of $AnxV^-/PI^-$ (viable; black bars), $AnxV^+/PI^-$ (early apoptotic; grey bars), $AnxV^-/PI^+$ (necrotic; white bars) and $AnxV^+/PI^+$ (late apoptotic; striped bars) cells from 3 independent experiments*

5.1.3. ECM-detachment induced anoikis cell death in hESC-RPE cells

Anoikic cell death has an essential role in maintaining of tissue homeostasis. We used the protocol of Petrovski et al. for anoikis induction in hESC-RPE cells (Petrovski et al., 2011b). The representative phase contrast image of untreated (control) hESC-RPE cells shows a confluent, highly pigmented cobblestone monolayer. In contrast, we determined floating aggregate formations in anoikic hESC-RPE cells (**Figure 7A**). Annexin V-FITC/PI staining was used to evaluate the rate of PS^+ cells and plasma membrane permeability as a result of ECM-detachment, using a BD Accuri C6 flow cytometer. ECM detachment resulted in significantly decreased proportion of viable hESC-RPE cells, compared to the control; it changed from 88.35±0.88% to 64.36±1.84%. Simultaneously, we determined significantly increased rate of only annexin V single positive cells in anoikis-induced hESC-RPE (27.86±3.58%) than in the case of untreated controls (9.85±1.13%). Moreover, the anoikic cells contained 7.10±3.30% of double positive, late apoptotic cells; in contrast, only 1.14±0.11% of the control cells were double positive (**Figure 7B-C**). The anoikic hESC-RPE cells showed similar rate of early apoptosis (27%) than ARPE-19 cells, which was previously demonstrated (19%) (Petrovski et al., 2011b).

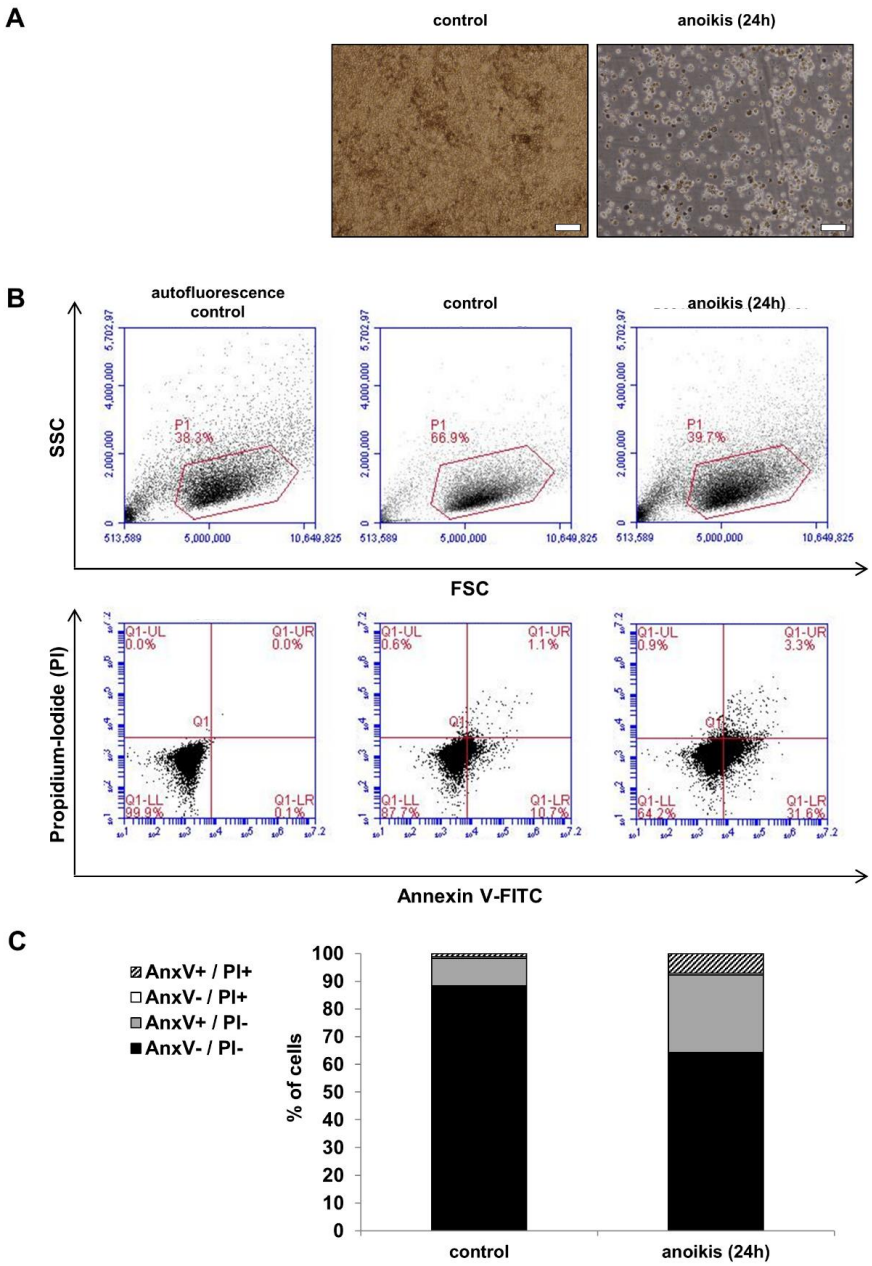

Figure 7. The effect of ECM-detachment of hESC-RPE cells on the morphology and cell viability. *(**A**) The hESC-RPE cells were cultured on poly-HEMA coated culture dishes for 24h to induce cell death by detachment from the ECM. The images (10x) of untreated control hESC-RPE cells and anoikic dying hESC-RPE cells were taken by a Nikon Eclipse TE2000-S phase contrast microscope. Scale bar represents 20 µm.* ***B****) AnxV-FITC/PI double staining assay was used to determine the induction of cell death through anoikis. Representative dot plots of AnxV/PI assay of anoikic dying hESC-RPE cells are shown. Top: the measurements of FSC (X axis) vs. SSC (Y axis). Numbers indicate the percentage of cells within the P1 regions compared to the total cell population. Bottom: the intensity of staining for Annexin V (log scale; X axis) vs. the intensity of staining for PI (log scale; Y axis). The percentage of different cell populations was marked in the quadrants: viable (lower left), apoptotic (lower right), necrotic (upper left), late apoptotic cells (upper right). Data are representative of 3 independent experiments. (**C**) The bar charts represent the average percentage of $AnxV^-/PI^-$ (viable; black bars), $AnxV^+/PI^-$ (early apoptotic; grey bars), $AnxV^-/PI^+$ (necrotic; white bars) and $AnxV^+/PI^+$ (late apoptotic; striped bars) cells from 3 independent experiments*

5.2. The induction of autophagy in RPE cells

5.2.1. Time- and concentration-dependent induction of autophagy in ARPE-19 and hRPE cells

Numerous studies have shown that H_2O_2-exposure resulted in oxidative stress in association with increased autophagic activity in RPE cells (Chang et al., 2015; Kunchithapautham and Rohrer, 2007; Li et al., 2014) and in other cell types (Ashabi et al., 2013; Essick et al., 2013; Ha et al., 2012). In addition, autophagy pathway can be stimulated by various forms of cellular stress, including starvation, nutrient deprivation, protein aggregates or damaged organelles. The accumulation of the major autophagic markers were investigated as a result of increasing concentrations (0.4mM, 0.8mM, 1mM) and time intervals (2h, 4h) of H_2O_2-exposure in the absence of serum in ARPE-19 and hRPE cells using Western blot analysis. The ratio of the free cytosolic LC3-I and the lipidated, autophagosome-membrane-bound LC3-II increased in a time-and concentration-dependent manner in both cell types upon this treatment, compared to the untreated control, which was considered to be the basal level of autophagy. In hRPE cells, the highest autophagic activity was observed at 2h of 1mM H_2O_2-treatment in serum-free condition, and in the case of ARPE-19 cells also an increased conversion of LC3-I into LC3-II was detected under the same treatment (**Figure 8A**). Parallelly, we monitored the expression level of another commonly used autophagy marker, SQSTM1/p62, which protein is specifically degraded through autophagy pathway. Decreasing trend of p62 level was detected in response to the serum deprivation and H_2O_2 co-treatment in ARPE-19 cells, compared to the untreated control (**Figure 8B**). This level over longer periods of treatment can change due to the constant recycling of p62, as well as LC3 during the auto-phago-lysosomal processing. Moreover, the double-membraned AVs with cytosolic components (black arrow) as well as the fusion of AV with the lysosomes (white arrow) could be determined as a result of H_2O_2-treatment (2h, 1mM) by TEM (**Figure 8C**). Taken together, these data suggest that 1mM H_2O_2-treatment for 2h lead to a significant induction of autophagy in ARPE-19 and hRPE cells.

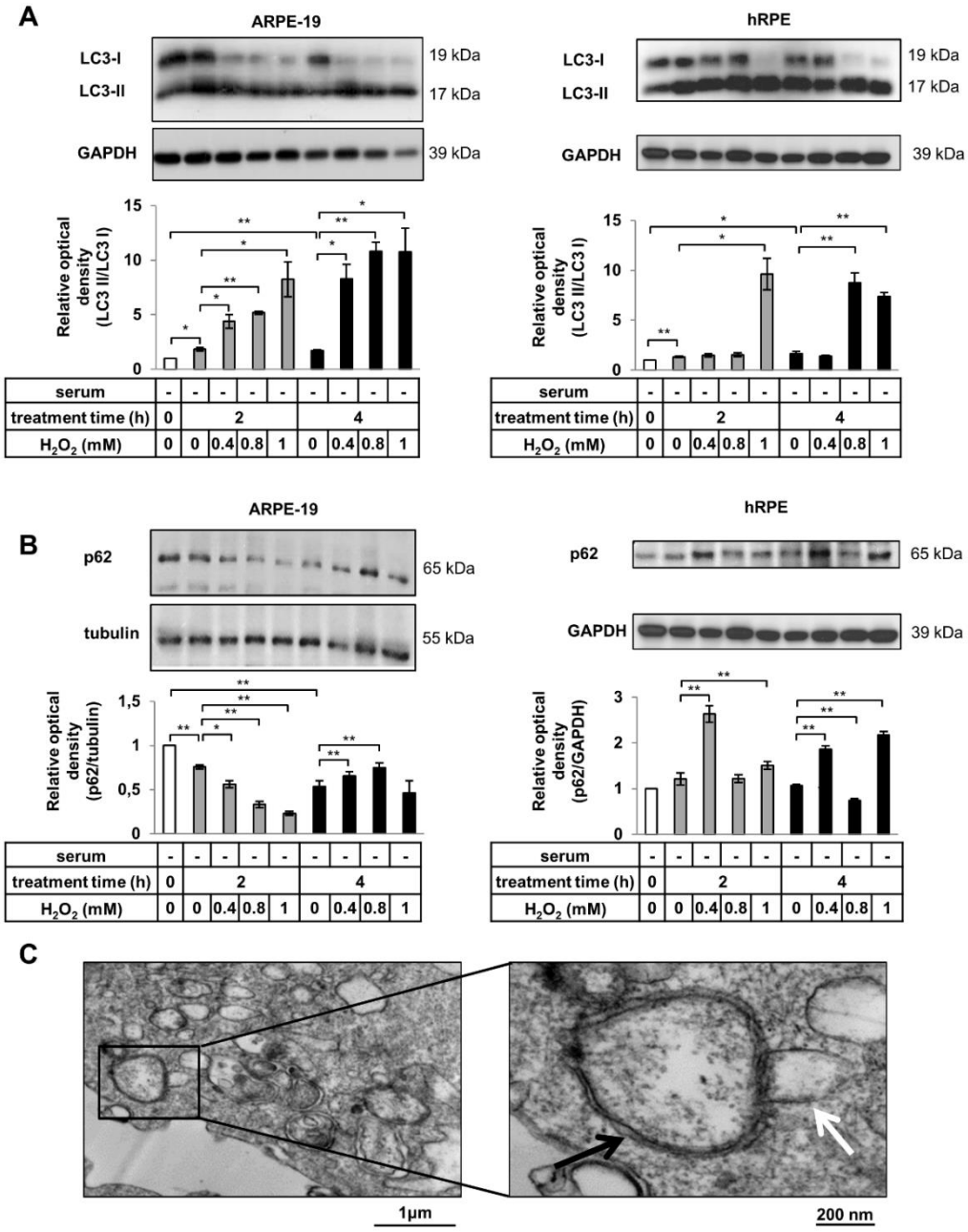

Figure 8. The induction of autophagy due to serum deprivation and H_2O_2 co-treatment in ARPE-19 and hRPE cells. *To detect the LC3-II/LC3-I ratio (**A**) and p62 expression (**B**) in ARPE-19 (left panels) and primary hRPE cells (right panels) after increasing time (2h, 4h) and concentrations (0.4mM, 0.8mM, 1mM) of H_2O_2-treatment in the absence of serum, Western blot analysis was used. Relative optical density was determined by densitometry, compared to the control group using the ImageJ software (white bars show the untreated controls, grey and black bars represent 2h and 4h long treatments, respectively). GAPDH and tubulin served as loading controls. Data are mean ± SEM of 3 independent measurements, *p<0.05, **p<0.01. (**C**) Double-membraned autophagic vesicles (black arrow) were detected in H_2O_2-treated (2h, 1mM) ARPE-19 cells using TEM (Philips CM 10 microscope). Fusion of autophagosomes and lysosomes (white arrow) was determined (the TEM images were acquired by Prof. Saeed Akhtar). Scale bars indicate 1µm (left panel) or 200nm (right panel). Data are representative of 3 independent experiments.*

5.2.2. Serum deprivation and H_2O_2 co-treatment result in induced autophagy in hESC-RPE cells

In the next experiment, we intended to investigate whether the autophagic activity is stimulated by serum deprivation and H_2O_2 (2h, 1mM) co-treatment also in hESC-RPE cells. The expression level of LC3 protein was determined using Western blot analysis and the quantification of LC3-II/LC3-I ratio was performed by densitometry. In the case of untreated control cells, basal autophagic activity was observed, which was increased as a result of serum deprivation for 2h and H_2O_2 (2h, 1mM) treatment in the presence of serum, separately. The LC3-II/LC3-I ratio was further enhanced in response to H_2O_2 (2h, 1mM) treatment in the absence of serum. These results suggest the autophagy process can be upregulated by serum deprivation and H_2O_2 (2h, 1mM) co-treatment in hESC-RPE cells (**Figure 9A-B**).

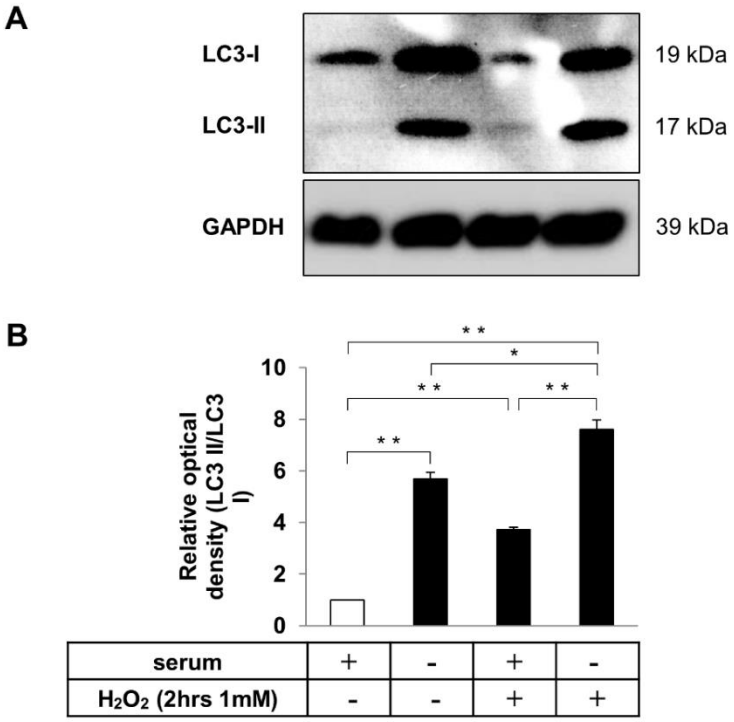

Figure 9. Autophagy triggering by serum deprivation and H_2O_2 co-treatment in hESC-RPE cells. *(**A**) The expression level of LC3 in H_2O_2-treated (2h, 1mM) hESC-RPE cells in the presence or absence of serum was detected using Western blot analysis. (**B**) Relative optical density was assessed by densitometry for quantification of the LC3-II/LC3-I ratio, compared to the untreated control, using the ImageJ software. The loading control was the GAPDH protein. Data are mean ± SEM of 3 independent measurements, *p<0.05, **p<0.01.*

5.2.3. Increased autophagic flux in ARPE-19 and hRPE cells

The increased number of autophagosomes may represent either the *bona fide* induction of autophagy or, alternatively, impairment in downstream steps of the autophagy pathway. The simple quantification of autophagosomes by measuring the levels of LC3-II using Western blot analysis is insufficient to distinguish between these two alternatives. However, the autophagic flux assays are more reliable for the estimation of autophagic activity, these methods indicate the dynamic process of autophagy, including the steps of autophagosomes synthesis, autolysosome formation and the degradation of autophagic substrate in the lysosome. Autophagic flux can be determined by monitoring of LC3-II turnover using immunoblot analysis in the presence and absence of lysosomal degradation inhibitors (Mizushima et al., 2010; Zhang et al., 2013).

To assess the autophagic flux as a result of H_2O_2-administration (2h, 1mM), we pre-treated the ARPE-19 and hRPE cells with a lysosomotropic reagent, namely CQ (0,5h, 12.5μM) before H_2O_2-exposure, to inhibit the degradation of LC3-II through blocking the autophagosome-lysosome fusion. In ARPE-19 cells, we could determine larger difference in the ratio of LC3-II/LC3-I in the presence and absence of CQ upon H_2O_2-treatment, both in serum-free or in serum-containing condition, which indicates that autophagic flux was increased during H_2O_2-exposure (**Figure 10A**). In the case of hRPE cells, CQ pre-treatment also led to the accumulation of LC3-II, the ratio of LC3-II/LC3-I was significantly increased in the presence of serum, which confirmed the increased autophagic flux (**Figure 10B**).

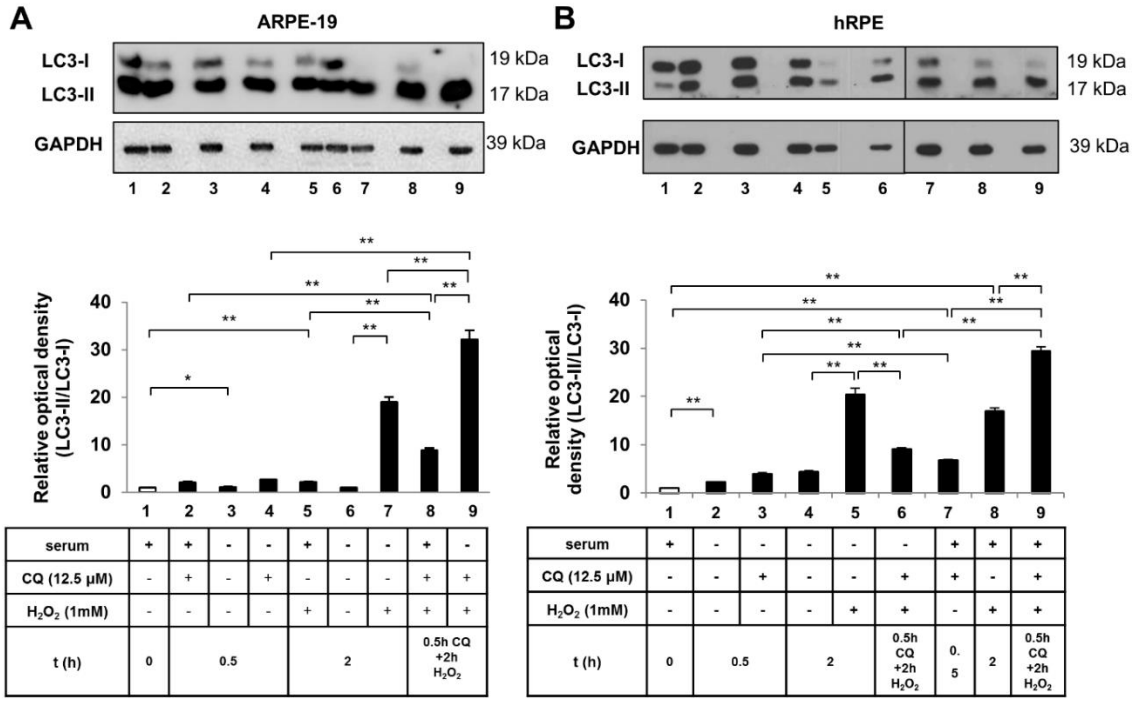

Figure 10. The analysis of autophagic flux in ARPE-19 and primary hRPE cells by LC3-II turnover using Western blotting. *(**A**) ARPE-19 and (**B**) primary hRPE cells were pre-treated with CQ (0.5h,12.5µM) and then treated with H_2O_2 (2h, 1mM) in the presence or absence of serum. The LC3-II/LC3-I ratio was detected by western blot analysis. The loading control was GAPDH protein. Relative optical density was determined by densitometry using the ImageJ software. Data are mean ±SEM of 3 independent experiments, *p<0.05, **p<0.01.*

5.3. Induction of autophagy-associated cell death in RPE cells

Next, we indirectly monitored the autophagy process by assessing the fluorescence of reporter protein GFP conjugated to LC3 through the use of fluorescent microscopy and flow cytometry. In order to determine autophagy induction as a result of H_2O_2-treatment, we transiently transfected ARPE-19 cells with GFP-LC3 plasmid and detected the fluorescent punctate distribution of GFP-LC3, which represents autophagosome formation. Due to serum-deprivation and H_2O_2 (2h, 1mM) co-treatment, accumulation of perinuclear GFP-LC3 positive aggregates or ring-shaped AVs were observed. The CQ-pre-treated (1h, 25μM) cells and then H_2O_2-exposed (2h, 1mM) cells showed more intense fluorescent punctuates and bigger GFP-LC3 positive AVs. 40.9±8.4% of the cells contained GFP-LC3-positive vacuoles upon H_2O_2 (2h, 1mM) treatment in serum-free medium, when counted manually the fluorescent images. Parallelly, 23.9±1.2 % of the cells were quantified as GFP-LC3-positive, based on their fluorescence using flow cytometry analysis (**Figure 11A**). These data also indicate that autophagy process can be triggered in ARPE-19 cells by H_2O_2-treatment in serum-deprived condition.

Depending on the level of activation, autophagy can promote cell death via an autophagy-associated pathway, which is distinguished from apoptosis. We proposed to investigate LC3-positive AVs and PS-externalization simultaneously in H_2O_2-treated ARPE-19 cells. Accordingly, ARPE-19 cells were transiently transfected with mCherry-LC3 plasmid, treated with H_2O_2 (2h, 1mM) and then Annexin V-FITC labelling was used. We found that 15.02% of the untreated cells were $LC3^+$ by FACS analysis, and it was increased to 28.76% as a result of H_2O_2-treatment; while the percentage of $AnxV^+$ cells increased from 3.4% to 17.5%. Furthermore, we observed 52.3% of $LC3^+$ cells were $AnxV^+$, meanwhile 83.88% of $AnxV^+$ cells were $LC3^+$ as well (**Figure 11B**). These results suggest that autophagy-associated process was activated in most of the dying ARPE-19 cells upon H_2O_2-treatment.

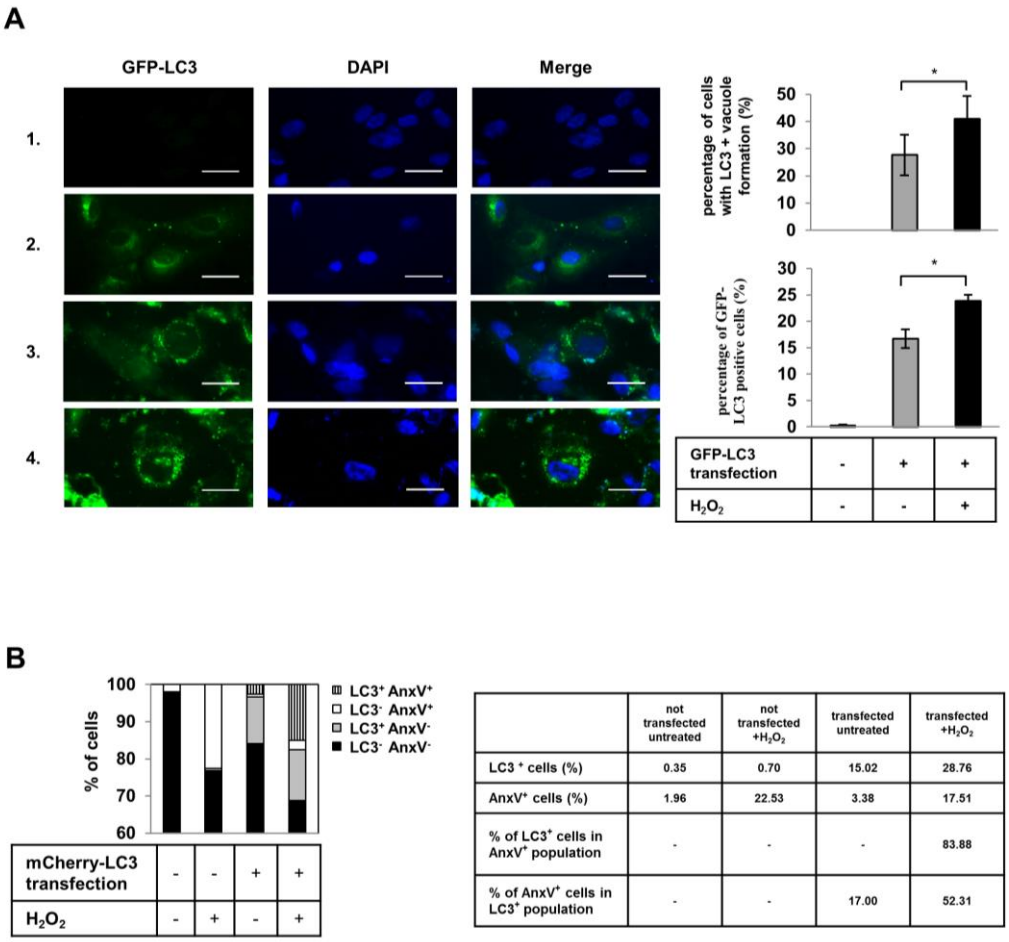

	not transfected untreated	not transfected +H_2O_2	transfected untreated	transfected +H_2O_2
$LC3^+$ cells (%)	0.35	0.70	15.02	28.76
$AnxV^+$ cells (%)	1.96	22.53	3.38	17.51
% of $LC3^+$ cells in $AnxV^+$ population	-	-	-	83.88
% of $AnxV^+$ cells in $LC3^+$ population	-	-	17.00	52.31

Figure 11. H_2O_2-induced autophagy-associated cell death in RPE cells. *(**A**) ARPE-19 cells were transiently transfected with a GFP-LC3 plasmid using PEI reagent. Representative immunofluorescence images are shown: non-transfected cells (**row 1**), GFP-LC3 transfected and untreated cells (**row 2**), GFP-LC3 transfected and H_2O_2 treated (2h, 1mM) cells (**row 3**), GFP-LC3 transfected, CQ pre-treated (1h, 25μM) and H_2O_2 treated (2h, 1mM) cells (**row 4**). Cell nuclei were labelled with DAPI. Scale bar indicates 20μm. Images are representative of 3 independent experiments. GFP-LC3-positive vacuoles containing cells were quantified by manual cell counting based on the fluorescent images (**top right bar chart**). The ratio of the number of GFP-LC3 positive cells to the total cell number in non-transfected cells, in transfected and untreated cells, in transfected and H_2O_2-treated (2h, 1mM) cells is shown as a percentage. Data are expressed as mean ±SD of at least 10 different visual fields on microscopy from 3 independent experiments in each condition (*$p<0.05$, by Student t-test). The percentage of GFP-LC3 positive cells was quantified using FACS analysis (**bottom right bar chart**). Data are expressed as mean ±SD of 3 independent experiments, *$p<0.05$ by Student t-test. (**B**) The rate of H_2O_2-induced cell death of ARPE-19 cells was detected, which containing LC3-positive AVs and expose PS on their surface, simultaneously. mCherry-LC3 plasmid was transiently transfected into ARPE-19 cells using PEI reagent, treated with H_2O_2 (2h, 1mM) and then Annexin V-FITC labelling was used. The bar charts indicate the average percentage of $LC3^-AnxV^-$ (black bars), $LC3^+AnxV^-$ (grey bars), $LC3^-AnxV^+$ (white bars) and $LC3^+AnxV^+$ (striped bars) cells. The table represents the average percentage of $LC3^+$ and $AnxV^+$ cells and the rate of $LC3^+AnxV^+/AnxV^+$ and $LC3^+AnxV^+/LC3^+$ untreated and H_2O_2-treated cells. Data are shown from 3 independent measurements.*

5.4. The clearance of dying RPE cells by professional and non-professional phagocytes and the effect of TC treatment on the phagocytic capacity

5.4.1. Anoikic dying RPE cells are efficiently phagocytosed by macrophages and non-dying RPE cells

Phagocytosis of apoptotic and necrotic cells has been widely examined in various organ systems. However, to date, only few studies have investigated the uptake of anoikic dying cells (Petrovski et al., 2011b).

To determine the clearance dynamics of anoikic dying ARPE-19 and primary hRPE cells by professional and non-professional phagocytes, the phagocytes were co-cultured with the dying cells for increasing time-intervals (4, 8, 12, 24h) and quantified by flow cytometer. Moreover, the effect of TC pre-treatment (48h, 1μM) on the phagocytosis capacity of phagocytes was examined.

We found that living RPE cells and macrophages were able to efficiently and increasingly engulf the anoikic dying RPE cells during the 24h period (**Figure 12A–C**). The average of phagocytosis percentage of anoikic dying ARPE-19 cells by non-professional living ARPE-19 cells was 3.16±0.91% (**Figure 12A**) at 4h of co-incubation. We observed higher phagocytosis rate during the engulfment of anoikic dying ARPE-19 cells by macrophages after 4h of co-incubation, it was 5.07±0.27 % (**Figure 12B**). The primary hRPE cells dying through anoikis were taken up by macrophages even more efficiently, the phagocytic capacity being 12.56±2.38% (**Figure 12C**) after 4h of co-incubation. These results show that TC treatment further enhanced the clearance process under most conditions (**Figure 12A-C**).

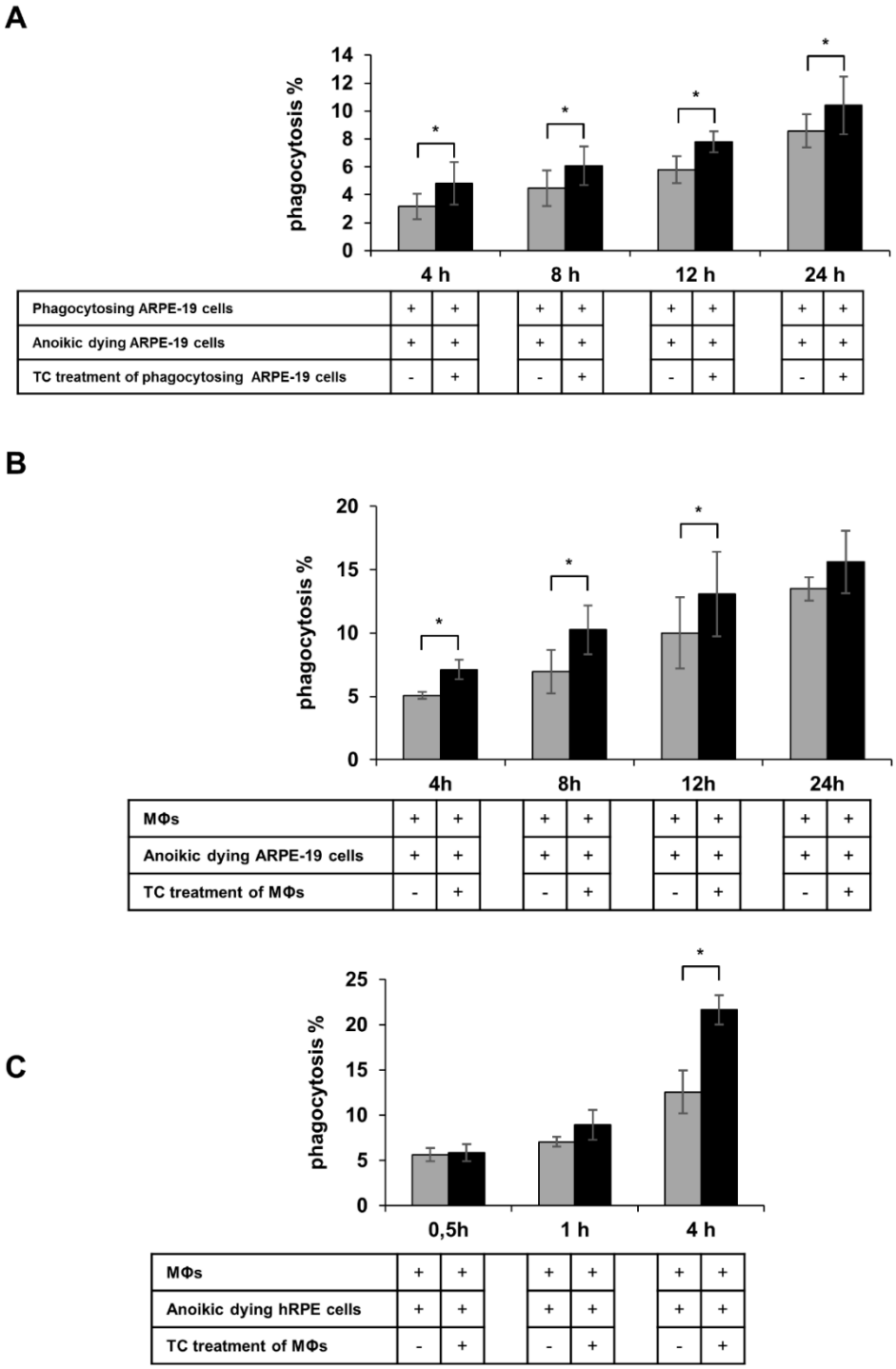

Figure 12. Non-professional and professional phagocytes are able to efficiently engulf anoikic dying RPE cells in vitro. *The clearance of anoikic dying ARPE-19 cells by living ARPE-19 cells (**A**) and macrophages (MΦ) (**B**) after increasing co-incubation periods (4h, 8h, 12h, 24h) is shown as determined by FACS analysis. Phagocytes pre-treated with TC (48h, 1μM) were labelled by black bars (grey bars indicate untreated phagocytes). (**C**) The rate of phagocytosis of anoikic dying primary hRPE cells by TC-treated (black bars) or untreated (grey bars) MΦs were measured after increasing co-incubation periods (0.5h, 1h, 4h) by FACS analysis. Bars represent the mean ±SD of 4 independent experiments. *p<0.05, **p<0.01.*

5.4.2. Macrophages and non-dying RPE cells are able to efficiently engulf autophagy-associated dying RPE cells

To date, no data exists about how efficiently autophagy-associated dying RPEs are removed by professional and non-professional phagocytes. The dynamics of the phagocytosis process of autophagy-associated dying (H_2O_2-treated, 2h, 1mM) ARPE-19 and primary hRPE cells by macrophages and living ARPE-19 cells after increasing time-intervals (4, 8, 12, 24h) of co-culturing was quantified by flow cytometry and demonstrated by time-lapse microscopy. Parallelly, we studied whether the TC pre-treatment (48h, 1μM) of phagocytes has an impact on the phagocytosis rate. In our study, ARPE-19 cells and macrophages could engulf autophagy-associated dying RPE cells with increasing capacity over 24h time (**Figure 13A–C; Supplementary Video 1 and 2**). As the result of flow cytometric analysis show, ARPE-19 cells took up the autophagy-associated dying ARPE-19 cells in an efficient manner; the average of the phagocytosis percentage was 3.8±1.1% at 8h of co-incubation (**Figure 13A**). We found similar phagocytosis rate during the engulfment of autophagy-associated dying ARPE-19 cells by macrophages after 8h of co- incubation - it was 6.9±1.7% (**Figure 13B**). The autophagy-associated dying primary hRPE cells were removed by macrophages even more efficiently, the phagocytic capacity being 21.2±3.3% (**Figure 13C**) after 8h of co-culturing. TC treatment of the phagocytes 48h prior the phagocytic assay, enhanced the engulfment capacity under most conditions (**Figure 13A-C; Supplementary Video 3 and 4**).

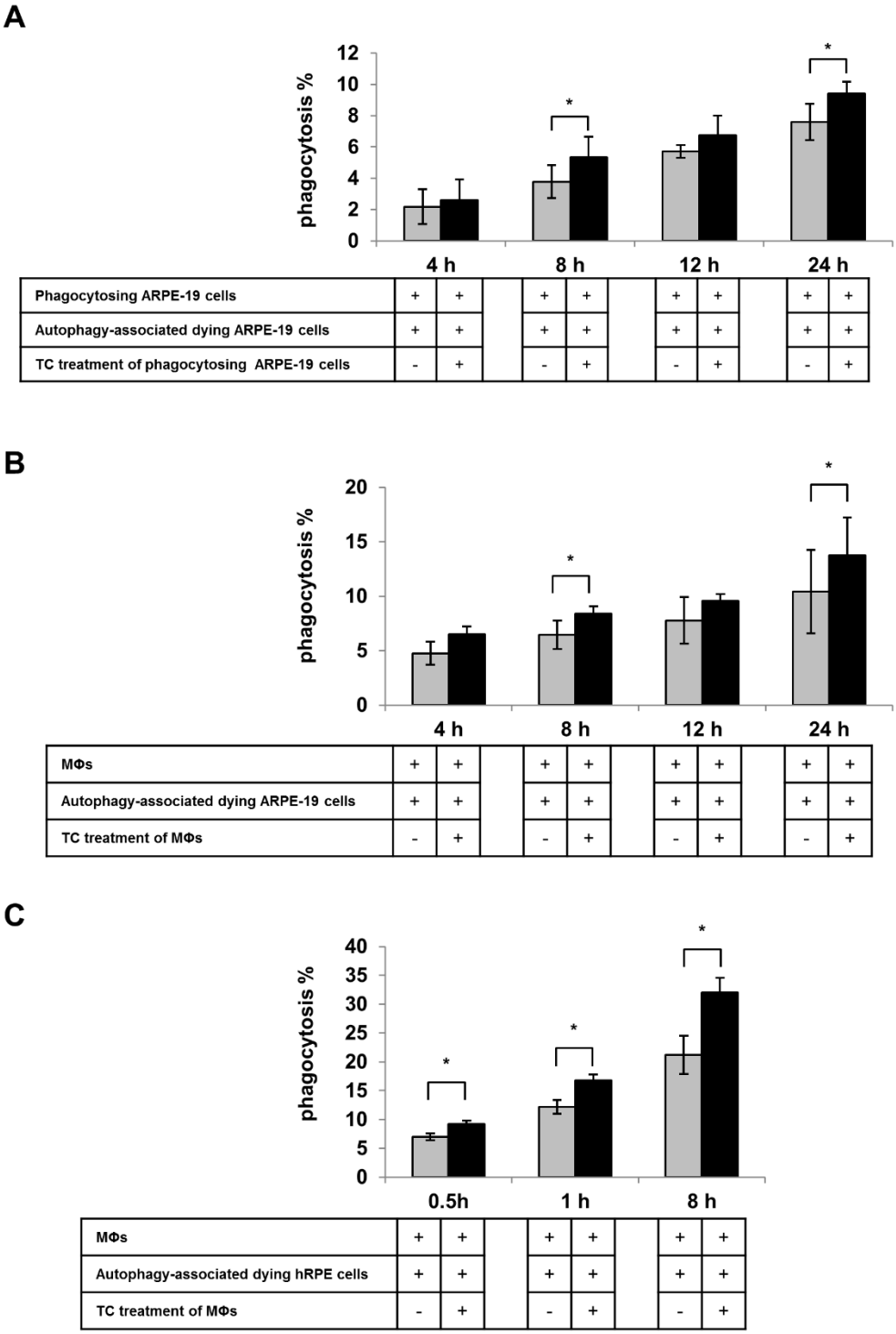

Figure 13. The clearance dynamics of autophagy-associated dying RPE cells by non-professional and professional phagocytes in vitro. *The phagocytic rate was determined by FACS analysis during the engulfment of autophagy-associated dying ARPE-19 cells by living ARPE-19 cells (**A**) and MΦ (**B**) after increasing co-incubation periods (4h, 8h, 12h, and 24h). The bar charts represent the phagocytic capacity of the TC pre-treated (48h, 1μM) (black bars) and the untreated phagocytes (grey bars). (**C**) The phagocytosis percentage of autophagy-associated dying primary hRPE cells by TC-treated (black bars) or untreated (grey bars) MΦs were quantified after increasing co-incubation periods (0.5h, 1h, 8h) by FACS analysis. Bars represent the mean ±SD of 4 independent experiments. *p<0.05, **p<0.01.*

5.4.3. The inhibitory effect of 3-MA on autophagy-associated cell death of ARPE-19 cells and subsequent impact on phagocytosis

To see the impact of 3-MA on the cell death and, consequently, the engulfment of 3-MA treated ARPE-19 cells, we used 10mM 3-MA-treatment 24h (Petrovski et al., 2011a; Petrovski et al., 2007a) prior to the H_2O_2-administration (2h, 1mM). Primarily, to confirm the inhibition of autophagy process as a result of 3-MA in H_2O_2-treated ARPE-19 cells, we determined the partially blocked conversion of LC3-I to LC3-II using Western blot analysis (**Figure 14A**). Then, we found that the number of living cells was significantly increased, while the number of $AnxV^+$ and PI^+, as well as double positive H_2O_2-treated ARPE-19 cells significantly decreased, when we used this inhibitor. Therefore, 3-MA pre-treatment inhibited the autophagy-associated cell death of ARPE-19 cells (**Figure 14B**). The inhibition of autophagy in ARPE-19 cells by 3-MA led to a significant change in phagocytosis rate of autophagy-associated dying cells, it was significantly decreased from 8.45±0.56% to 3.24±0.52% by untreated macrophages and from 10.49±1.01% to 5.90±2.89% by TC-treated macrophages after 8h co-incubation (**Figure 14C**).

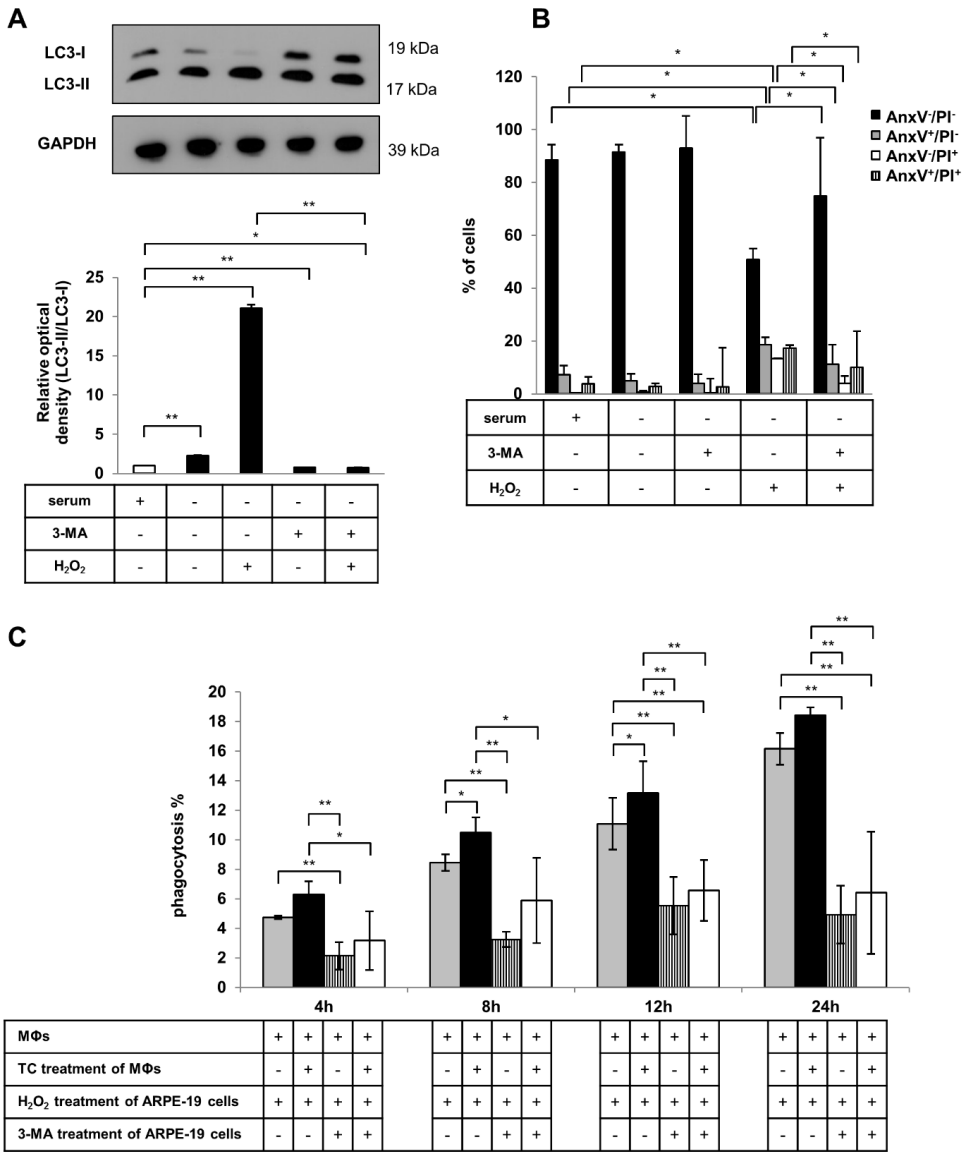

Figure 14. Inhibition of autophagy-associated cell death in ARPE-19 cells by 3-MA attenuates phagocytosis by macrophages. *(**A**) Autophagy inhibition was determined in 3-MA pre-treated (24h, 10mM) and H_2O_2-treated (2h, 1mM) ARPE-19 cells by quantification of LC3-II/LC3-I ratio using Western blot analysis. Relative optical density was shown by densitometry using the ImageJ software (white bars indicate the untreated controls; black bars represent the treated samples). GAPDH was used as a loading control. Data are mean ±SEM of 3 independent measurements, *p<0.05, **p<0.01. (**B**) The cell death rate was quantified in 3-MA pre-treated (24h, 10mM) and H_2O_2-treated (2h, 1mM) ARPE-19 cells by flow cytometry using Annexin V-FITC/PI assay. Data are expressed as mean ±SD of 4 independent experiments, *p<0.05 by Student t-test. (**C**) The clearance of 3-MA pre-treated (24h, 10mM) and H_2O_2-treated (2h, 1mM) ARPE-19 cells by untreated and TC-treated (48h, 1μM) MΦs after increasing co-incubation periods (4h, 8h, 12h, 24h) was measured by flow cytometry. Bars represent mean ±SD of 3 independent experiments, *p<0.05, **p<0.01*

5.4.4. The clearance of GFP-LC3 positive autophagy-associated dying ARPE-19 cells by macrophages

To study whether the phagocytosed cells were actually the autophagy-associated dying cells and not any other type of dying cells, the GFP-LC3 transfected, H_2O_2-treated ARPE-19 cells were co-cultured with macrophages for 8h and the phagocytic rate was quantified by flow cytometry. The macrophages were able to engulf the H_2O_2-treated, GFP-LC3 transfected ARPE-19 cells, the average of phagocytosis percentage being 9.3±3.7%, which was comparable to the clearance of vitally stained, H_2O_2-treated ARPE-19 cells by macrophages. Furthermore, the macrophages were co-cultured with the GFP-LC3 positive and negative ARPE-19 cells for 8h, which were sorted out by FACS Aria III. We observed that, negligible amount of GFP-LC3 negative, non-autophagic ARPE-19 cells were engulfed (0.6±0.2%). Meanwhile, in contrast, the phagocytic rate of the GFP-LC3 positive RPEs was the same (13.7±3.3%) **(Supplementary Video 7)** as in the case of the non-sorted autophagy-associated dying cells (**Figure 15A** and **Supplementary Video 5**), therefore we could prove their fate in the engulfment process. Moreover, significantly enhanced clearance of GFP-LC3 transfected, H_2O_2-treated ARPE-19 cells was found as a result of TC pre-treatment (**Figure 15B** and **Supplementary Video 6**).

A

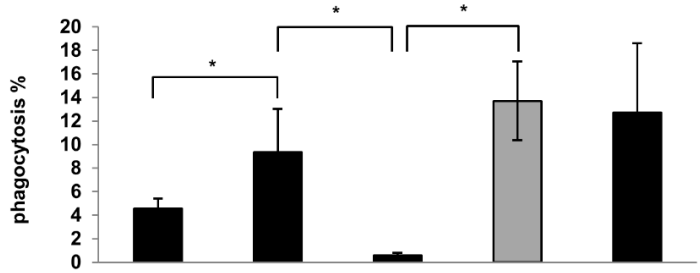

MΦs	+	+	+	+	+
GFP-LC3 transfection of ARPE-19 cells	+	+	+	+	-
CFDA labeling of ARPE-19 cells	-	-	-	-	+
H_2O_2 treatment of ARPE-19 cells	-	+	+	+	+
GFP-LC3 negative sorting of ARPE-19 cells	-	-	+	-	-
GFP-LC3 positive sorting of ARPE-19 cells	-	-	-	+	-

B

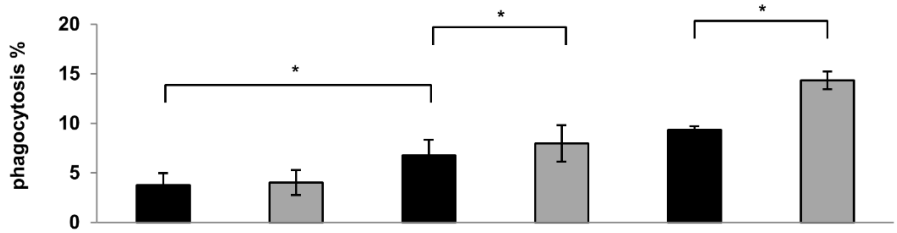

MΦs	+	+	+	+	+	+
TC treatment of MΦs	-	+	-	+	-	+
GFP-LC3 transfection of ARPE-19 cells	+	+	+	+	-	-
CFDA labeling of ARPE-19 cells	-	-	-	-	+	+
H_2O_2 treatment of ARPE-19 cells	-	-	+	+	+	+

Figure 15. The phagocytosis rate of GFP-LC3 transfected, H_2O_2-treated ARPE-19 cells by professional phagocytes. ***(A)*** *The phagocytic capacity of MΦs during the engulfment of GFP-LC3 transfected, untreated or H_2O_2-treated (2h, 1mM) and GFP-LC3 negative or positive sorted cells, and not transfected, H_2O_2-treated ARPE-19 cells after 8h co-incubation was quantified by flow cytometry.* ***(B)*** *The clearance of GFP-LC3 transfected, untreated or H_2O_2-treated and not transfected, H_2O_2-treated ARPE-19 cells by untreated (black bars) and TC-treated (48h, 1μM) (grey bars) MΦs after 8h co-incubation was measured by FACS Aria. Bars represent mean ±SD of 3 independent experiments, *p<0.05.*

5.4.5. The engulfment of anokic and autophagy-associated dying hESC-RPE cells by macrophages

To the best of our knowledge, no data exists about the clearance of dying hESC-RPEs by professional phagocytes to date. We quantified the phagocytosis rate of anoikic and autophagy-associated dying hESC-RPE cells by macrophages using flow cytometry, after 4h and 8h co-incubations, respectively. To determine whether TC is able to influence the phagocytic capacity of macrophages, we used 1μM TC treatment 48h prior to the phagocytosis assay. **Figure 16A** shows representative dot plots with the engulfed CFDA-labelled dying hESC-RPE cells (upper right quadrants of the dot plots) by CMTMR-labelled macrophages. The macrophages efficiently engulfed the anoikic dying hESC-RPE cells, the phagocytosis rate was 32.40±3.45% after 4h co-culturing. On the other hand, the uptake of autophagy-associated dying hESC-RPEs by macrophages after 8h of co-incubation, was more efficient, 50.72±2.98%. TC treatment resulted in moderately enhanced phagocytic capacity of macrophages during the engulfment of anoikic dying hESC-RPE cells (35.15±3.85%) and autophagy-associated dying hESC-RPEs (58.70±8.68%) (**Figure 16B**).

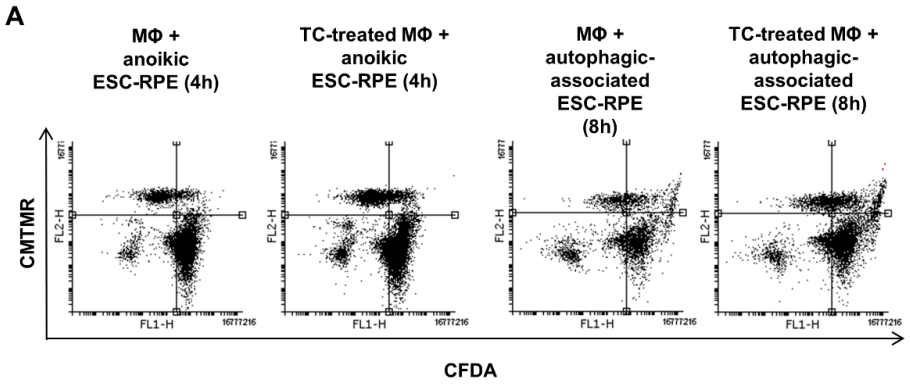

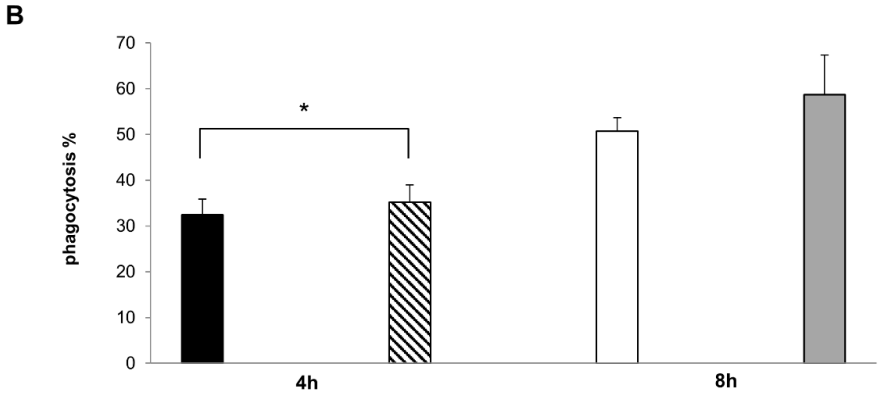

MΦ	+	+	+	+
TC	-	+	-	+
Anoikic dying ESC-RPE cells	+	+	-	-
Autophagy-associated dying ESC-RPE cells	-	-	+	+

Figure 16. Macrophages are able to efficiently taken up anoikic and autophagy-associated dying hESC-RPE cells. *The phagocytosis of anoikic and autophagy-associated dying hESC-RPE cells by TC-treated (48h, 1μM) and untreated MΦs after 4h and 8h co-incubation, was demonstrated by flow cytometry, respectively. (**A**) Representative dot plots are shown the intensity of staining for CFDA (log scale; X axis) and for CMTMR (log scale; Y axis). Cells in the upper right quadrant represent the engulfed hESC-RPE (CFDA-labelled) cells by MΦs (CMTMR-labelled). Data are representative of 3 independent experiments. (**B**) The bar chart indicates the mean ±SD from 3 independent phagocytosis assay, *p<0.05.*

5.4.6. Dendritic cells are able to efficiently take up the dying cells *in vitro*

DCs are considered to be professional phagocytes, which play an essential role in the defence mechanisms through elimination of debris and microorganisms. Immature DCs (iDC) are able to efficiently take up dead or dying cells in various tissues, such as bone marrow, spleen and the thymus (Albert et al., 1998; Hochreiter-Hufford and Ravichandran, 2013). Recently, the presence of DCs in drusen-associated changes in the retina has been reported in RPE cell injury (Hageman et al., 2001). However, to date, the phagocytosis of dying RPE cells by DCs has not yet been documented. Therefore, we decided to investigate the clearance of anoikic and autophagy-associated dying ARPE-19 cells by human monocyte-derived immature and mature DCs. We found a low phagocytosis percentage of anoikic dying ARPE-19 cells by immature (3.26±0.58%) as well mature DCs (2.88±1.14%), after 4h co-culturing. In contrast, the phagocytic capacity of DCs during the engulfment of autophagy-associated dying ARPE-19 cells was much higher, it was 26.7±10.8% in the case of immature DCs after 8h of co-incubation and 21.4±6.4% when we used a cocktail of inflammatory cytokine: IL- (5 ng/ml), IL-6 (100 ng/ml), TNFα (10 ng/ml), GMCSF (80 ng/ml) and PGE_2 (1 μg/ml), to stimulate the maturation of the DCs (**Figure 17**).

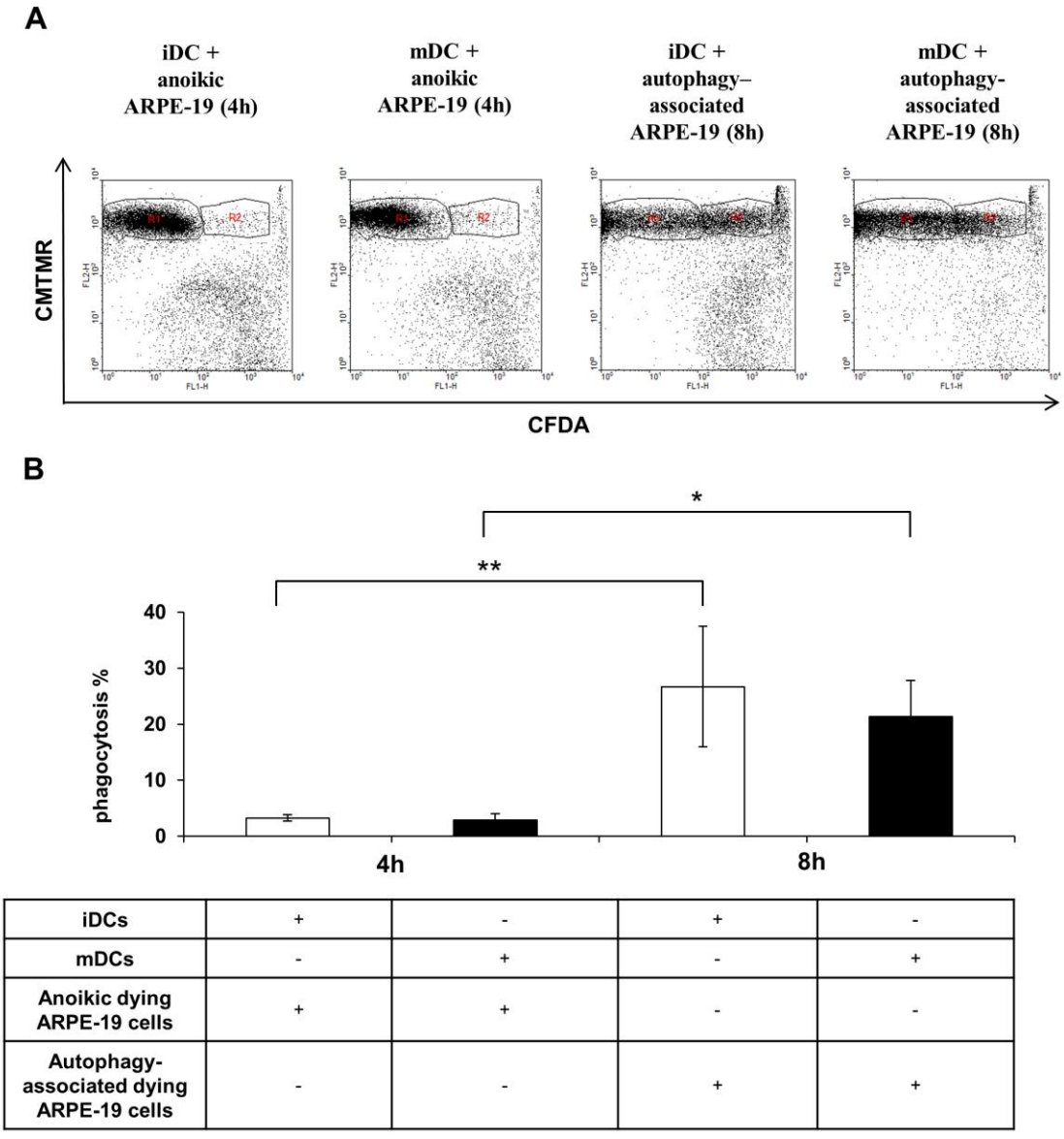

iDCs	+	-	+	-
mDCs	-	+	-	+
Anoikic dying ARPE-19 cells	+	+	-	-
Autophagy-associated dying ARPE-19 cells	-	-	+	+

Figure 17. The clearance of anoikic and autophagy-associated dying ARPE-19 cells by dendritic cells. *The phagocytic capacity of iDCs and mDCs during the engulfment of anoikic or autophagy-associated dying ARPE-19 cells after 4h and 8h co-incubation is shown, respectively. (**A**) Representative dot plots are shown the intensity of staining for CFDA (log scale; X axis) and for CMTMR (log scale; Y axis). The cells within the „R2" designated area represent the engulfed ARPE-19 (CFDA-labelled) cells by MΦs (CMTMR-labelled). „R1" area contains the phagocytes which did not engulf dying cells. Data are representative of 4 independent phagocytosis assay. (**B**) The bar chart indicates the mean ±SD of 4 independent measurements, *p<0.05, **p<0.01.*

5.5. A key role of MerTK receptor in the TC enhanced phagocytosis of dying RPE cells

5.5.1. The impact of knocking-down of TC upregulated genes on phagocytosis

Previously, our research group showed that during differentiation of human monocyte to macrophages the expression level of most of the apopto-phagocytic genes is highly up-regulated (Zahuczky et al., 2011). Moreover, we observed that glucocorticoid dexamethasone treatment of macrophages resulted in further up-regulation of six genes (MERTK, AXL, ADORA3, C1QA, MFGE8, THBS1) (Zahuczky et al., 2011).

Then we decided to examine how the apopto-phagocytic gene expression is changed in TC-treated phagocytes during the clearance of anoikic dying ARPE-19 cells. For these investigations, we used a self-designed TaqMan Low Density Array configuration containing TaqMan assays (Zahuczky et al., 2011). We found that significantly increased expression level of MFGE8, THSB1, ADORA3 and MERTK of the investigated 95 genes, in macrophages as a result of TC treatment (TC-treated MΦ vs. ctrl. MΦ). Furthermore, the expression level of 43 out of the analyzed 95 genes was significantly changed in the macrophages during the engulfment of anoikic ARPE-19 cells (ctrl assay vs. ctrl MΦ). On the other hand, we could determine that significantly altered expression level of 55 genes upon TC treatment during the phagocytosis of anoikic ARPE-19 cells as compared to TC-treated macrophages in the absence of dying cells (TC assay vs. TC MΦ) (Albert et al., 2014).

Next, we intended to show whether TC-induced upregulation of apopto-phagocytic genes had a direct impact on the enhanced phagocytic capacity of macrophages. For this purpose, siRNA transfection method was used to silence a selection of the upregulated genes: ADORA3, THBS1, AXL, MERTK or both AXL and MERTK simultaneously. The electroporation process did not result in significant loss of cell number and did not have a harmful effect on the phagocytic activity of macrophages (Kristof et al., 2013; Zahuczky et al., 2011). We observed that the silencing efficiency of the target genes show biological variance among different macrophage donors (**Table 1**) and varied among replicates of living ARPE-19 cells **(Table 2**). The members of TAM family represented the weakest silencing effect in macrophages (about 20-50%, **Table 1**) and significantly decreased phagocytosis was determined only in the TC-treated MERTK

and AXL knock-down macrophages (**Figure 18A**). The combination of MERTK silencing with siRNAs for AXL (**Figure 18A**) did not show a significant synergistic effect. Moreover, a significant decrease in non-professional engulfment of anoikic ARPE-19 cells was found as a result of silencing of MERTK and AXL in living TC-treated ARPE-19 cells (**Figure 18B, Table 2**).

Silenced gene expression%					
Gene name	Donor No. 1	Donor No. 2	Donor No. 3	Donor No. 4	Donor No. 5
AXL	20.96	16.84	1.89	-	-
MERTK	1.11	14.87	11.43	55.11	44.91

Table 1. Silenced gene expression level of TC upregulated apopto-phagocytic genes in macrophages showing the biological variance of different donors. *siRNA-mediated gene silencing efficiency in 5 different macrophage donors (in per cent as compared with TC treated Mock).*

Silenced gene expression%					
Gene name	ARPE-19 sample 1	ARPE-19 sample 2	ARPE-19 sample 3	ARPE-19 sample 4	ARPE-19 sample 5
ADORA 3	19.56	15.07	-	-	-
AXL	58.91	26.86	1.89	0.67	27.47
MERTK	27.64	56.80	4.41	28.15	60.54
THBS1	8.51	28.58	-	-	-

Table 2. Silenced gene expression level of AXL and MERTK genes in living ARPE-19 cells. *siRNA-mediated gene silencing efficiency in 5 different biological replicates (in per cent as compared with TC treated Mock).*

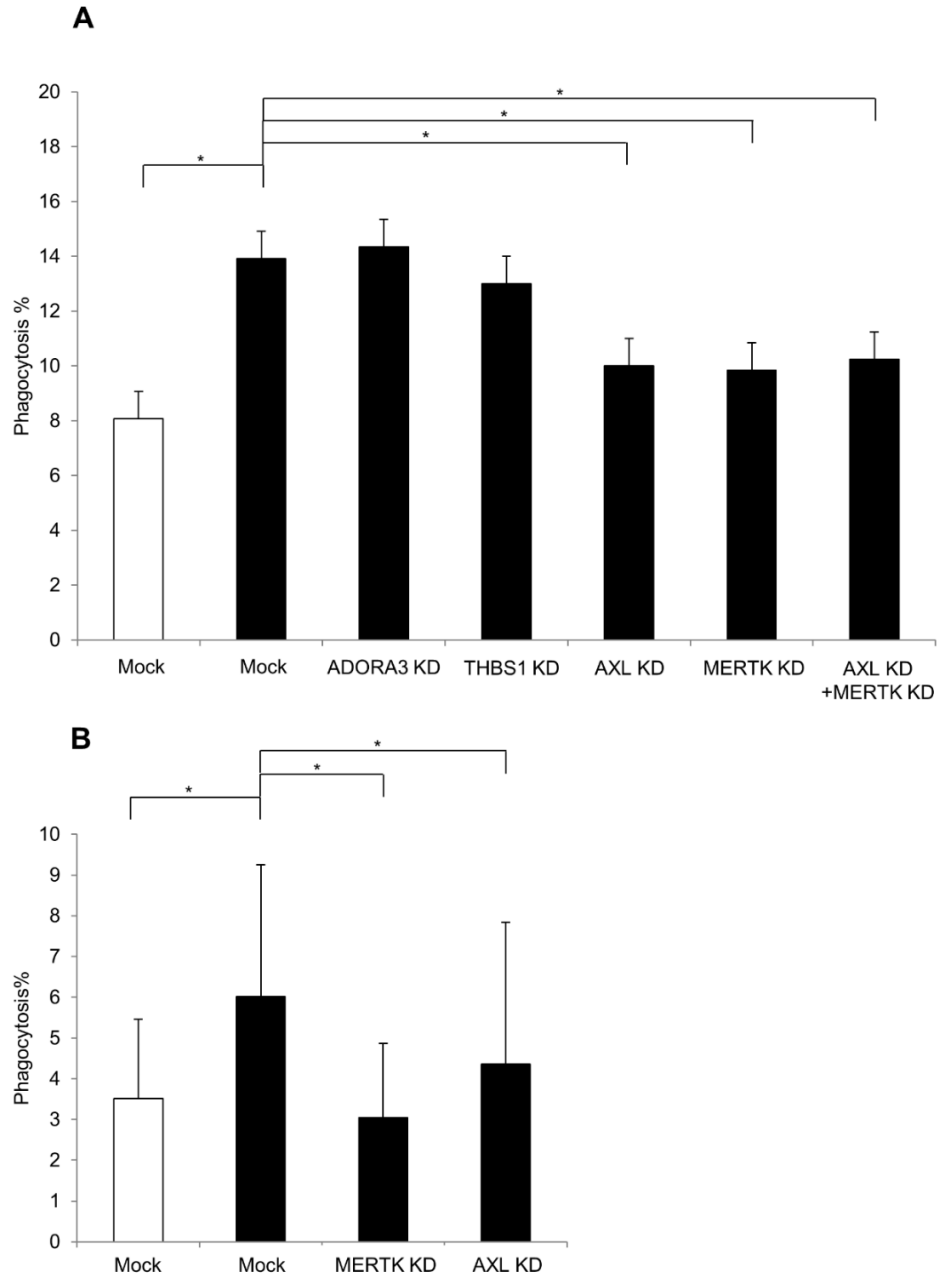

Figure 18. The effect of silencing of TC upregulated genes on phagocytic efficiency of professional and non-professional phagocytes. *(**A**) The clearance of anoikic dying ARPE-19 cells by macrophages after knocking down of TC upregulated apopto-phagocytic genes was determined by flow cytometer. The ratio of phagocytes and cells to be engulfed was set at 1:5 for the dying ARPE-19 cells. Genes were silenced using specific siRNA: ADORA3, THBS1, AXL, MERTK (n=5) or AXL and MERTK simultaneously (n=3). Black bars indicate TC-treated macrophages; *p<0.05. (**B**) The clearance of anoikic dying ARPE-19 cells by living ARPE-19 cells after knocking down of AXL and MERTK genes was quantified by FACS analysis. Black bars indicate TC treated phagocytes; *p<0.05, n=5.*

5.5.2. MerTk receptor has a pivotal role in the TC enhanced clearance of anoikic dying ARPE-19 cells by macrophages

The next question was whether MerTK receptor has a key role in the TC enhanced phagocytosis of dying RPE cells by macrophages. To check the direct role of MerTk, a specific antibody was used for blocking MerTk on the surface of macrophages prior to the phagocytosis assay. We observed that the phagocytic capacity of macrophages in the absence of TC was not inhibited as a result of MerTK blocking antibody, meanwhile the TC enhanced engulfment of anoikic dying ARPE-19 by macrophages could be prevented using this blocking antibody (**Figure 19A**). The distribution of the MerTk receptor at the engulfment portals of macrophages during the uptake of anoikic dying ARPE-19 cells in the presence or absence of TC was determined using immunofluorescent staining (**Figure 19B)**. We could detect MerTK in punctuated structures at the cell borders of macrophages and anoikic ARPE-19 cells, which was significantly accumulated at the connecting points between dying ARPE-19 cells and TC treated macrophages, it was observed in 30-50% of the engulfment gates of three different donors. Moreover, the MerTk protein expression was evaluated by Western blot analysis, both untreated cell types were shown lower expression level and TC treatment resulted in much more elevated expression in macrophages even during the engulfment of anoikic dying ARPE-19 cells (**Figure 19C**).

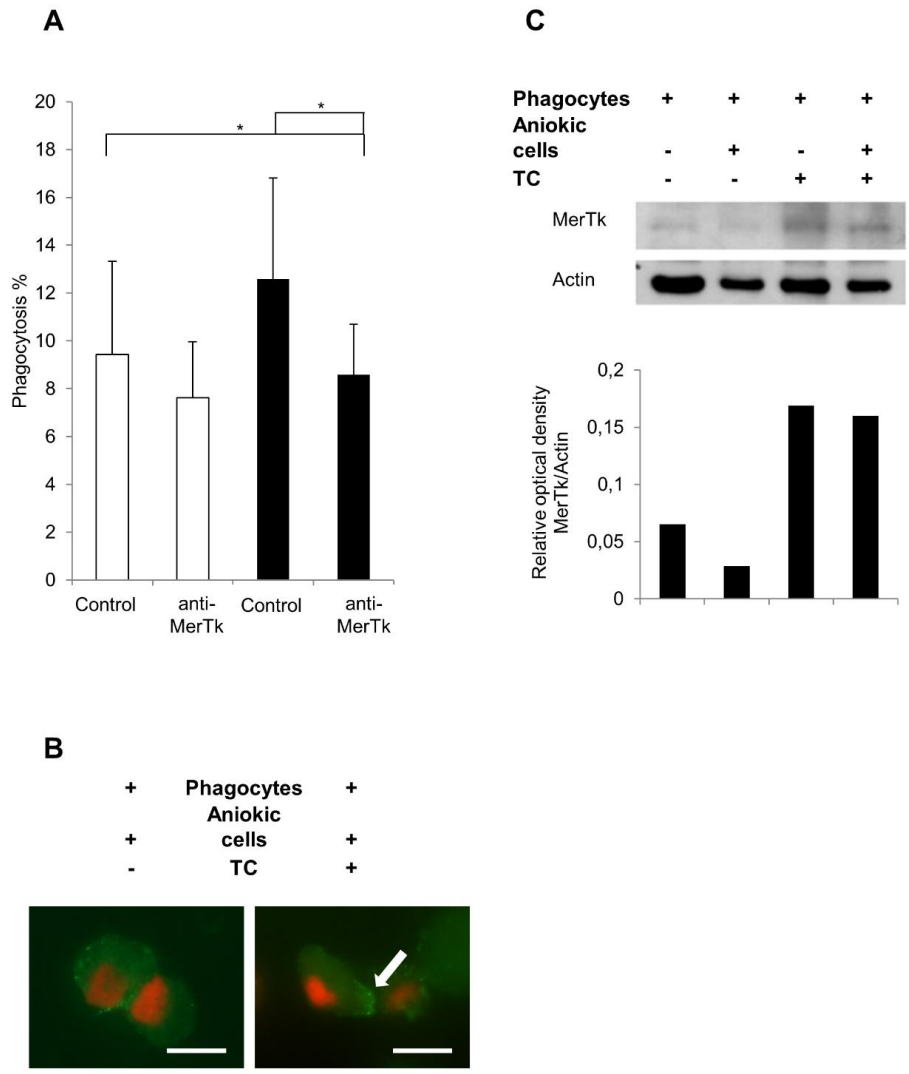

Figure 19. The effect of blocking of MerTK receptor on the phagocytosis of anoikic dying ARPE-19 cells by professional phagocytes. *(**A**) The clearance of anoikic dying ARPE-19 cells by macrophages was quantified by flow cytometer after blocking of Mertk on the surface of macrophages using specific antibody. The ratio of phagocytes and cells to be engulfed was set at 1:5 for the dying ARPE-19 cells. Black bars indicate TC treated macrophages; *p<0.05, n=4. (**B**) Immunofluorescent staining of MerTK during recognition of dying ARPE-19 cells by macrophages in the presence or absence of TC. Anti-MerTk primary antibody and anti-mouse NL-493 fluorescent secondary antibody was used. Cell nuclei were labelled with propidium-iodide (PI). Images were taken by a Zeiss LSM 510 fluorescent microscope. Bars indicate 5 μm. Arrow shows the clustering of Mertk at the engulfment portals of macrophages. (**C**) Western blot analysis of Mertk expression in one representative macrophage donor that engulf anoikic ARPE-19 cells in the presence or absence of TC. Relative optical density was determined by densitometry using ImageJ software.*

5.5.3. The effect of MerTk blocking on the TC enhanced clearance of dying RPE cells by non-professional phagocytes

In addition, we aimed to study the effect of blocking MerTk receptor on the TC enhanced engulfment of anoikic dying RPEs by non-professional phagocytes. We found that MerTk blocking antibody did not inhibit the phagocytic capacity of living ARPE-19 cells in the absence of TC, Contrarily, the TC-enhanced phagocytosis rate could be significantly decreased as a result of treatment with this blocking antibody either on the side of the phagocytes or to the anoikic ARPE-19 cells (**Figure 20A**). We could also determine MerTk in punctuated structures at the cell borders of non-professional phagocytes and anoikic dying ARPE-19 cells by immunofluorescent staining, which was significantly accumulated at the engulfment portals between TC-treated phagocytes and dying cells (**Figure 20B**); it was observed in 20-40% of the engulfment areas of three different replicates. Furthermore, the MerTk protein expression was investigated by Western blot analysis - lower expression was detected in TC untreated cells, and much more elevated expression during the engulfment process even as a result of TC treatment of the phagocytosing ARPE-19 cells (**Figure 20C**).

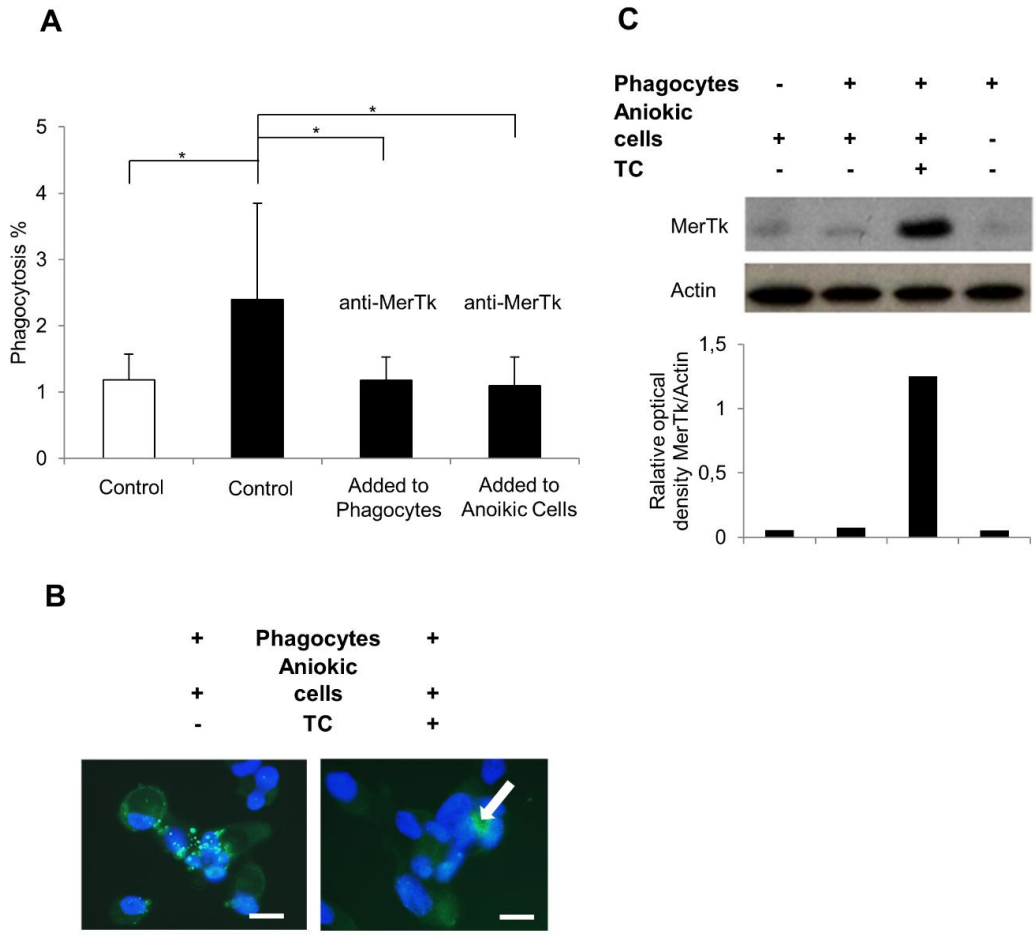

Figure 20. The effect of blocking of MerTK receptor on the phagocytosis of anoikic dying ARPE-19 cells by non-professional phagocytes. *(**A**) The clearance of anoikic dying ARPE-19 cells by living ARPE-19 cells was quantified by flow cytometer after blocking of Mertk on the surface of living and dying ARPE-19 cells using specific antibody. The ratio of phagocytes and cells to be engulfed was set at 1:5 for the dying ARPE-19 cells. Black bars indicate TC treated phagocytes; *p<0.05, n=4. (**B**) Immunofluorescent staining of MerTK during recognition of dying ARPE-19 cells by TC-treated and untreated living ARPE-19 cells. Anti-MerTk primary antibody and anti-mouse NL-493 fluorescent secondary antibody was used. Cell nuclei were labelled with DAPI. Images were taken by a Zeiss LSM 510 fluorescent microscope. Bars indicate 5 µm. Arrow shows clustering of Mertk at the engulfment portals of non-professional phagocytes. (**C**) Western blot analysis of Mertk expression in living and dying ARPE-19 cells and even during engulfment of anoikic ARPE-19 cells in the presence or absence of TC. Relative optical density was determined by densitometry using ImageJ software.*

5.5.4. The effect of blocking and augmentation of MerTk receptor on the phagocytosis of dying primary hRPE cells by macrophages

In the following experiments, we intended to study the effect of TC treatment on the clearance of anoikic dying hRPEs by macrophages; moreover, the role of MerTK receptor was investigated during this engulfment process. We found that TC treatment (48h, 1μM) significantly enhanced the phagocytic capacity of macrophages during the clearance of dying hRPE cells, about 1.5-2 times increase of phagocytic rate was observed at 4h of co-incubation (**Figure 21A**). Significantly reduced engulfment of dying hRPE cells was determined by TC treated macrophages upon administration of MerTk blocking antibody (**Figure 21B**), similarly to the *in vitro* phagocytosis model of anoikic dying ARPE-19 cells described previously (**Figure 19A**). Finally, we wanted to examine whether the augmentation of MerTk by its ligand, the bridging molecule Gas6 can affect the phagocytosis of anoikic ARPE-19 and hRPE cells. In the absence of TC, the phagocytic capacity of macrophages moderately increased upon Gas6 treatment, while parallelly, a remarkable clearance enhancing effect was found in a concentration-dependent manner in the case of TC treated macrophages (**Figure 21C, D**) in which MerTk was significantly overexpressed both, at mRNA (**Table 2**) and protein levels (**Figure 19C**).

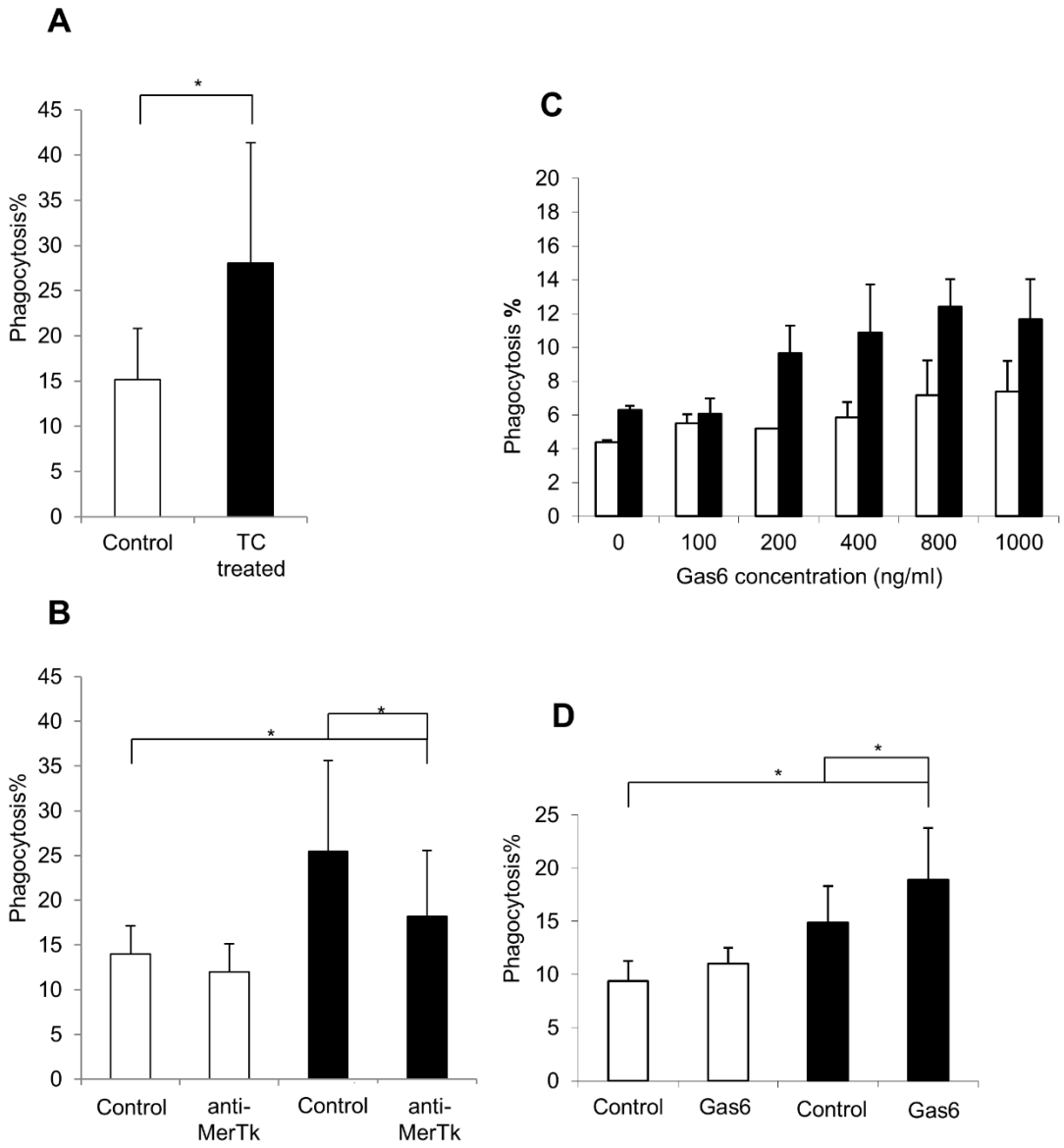

Figure 21. The effect of blocking and augmentation of Mertk receptor on the engulfment of dying human primary RPE cells by macrophages. *(**A**) Phagocytosis of anoikic hRPE cells by macrophages with or without TC treatment was determined by flow cytometry analysis. The ratio of phagocytes and cells to be engulfed was set at 1:2 for the dying hRPE cells. Black bar indicates TC treated macrophages; *p<0.05, n=7. (**B**) The engulfment of dying hRPE cells by macrophages was quantified by FACS analysis after blocking of Mertk on the surface of macrophages using specific antibody. Black bars indicate TC treated macrophages; *p<0.05, n=4. (**C**) Clearance of anoikic dying ARPE-19 cells by macrophages after augmentation of Mertk on the surface of macrophages by the bridging molecule Gas6. Black bars indicate TC treated macrophages. Results showing phagocytosis capacity of one representative macrophage donor. SD means the experimental error of the technical replicates. (**D**) Phagocytosis of anoikic dying hRPE cells by macrophages after augmentation of Mertk on the surface of macrophages by Gas6. Black bars indicate TC treated macrophages; *p<0.05, n=4.*

5.6. The phagocytosis of dying RPE cells by macrophages resulted in the release of pro-inflammatory cytokines

5.6.1. Release of IL-6 and IL-8 during the clearance of autophagy-associated dying RPE cells by professional phagocytes

Several studies have demonstrated that the clearance of apoptotic cells is an immunologically silent process (Gregory and Devitt, 2004; Savill et al., 2002; Savill and Fadok, 2000); in contrast, the engulfment of necrotic cells by macrophages has been shown to lead to a pro-inflammatory response (Fadok et al., 2001; Fadok et al., 1998; Poon et al., 2010). Previous reports from our laboratory have shown that phagocytosis of autophagic dying MCF-7 cells resulted in enhanced pro-inflammatory cytokine release (Petrovski et al., 2011a). Next by analogy, we wanted to know, whether the phagocytic uptake of the autophagy-associated (1mM H_2O_2-treatment for 2h) dying RPE cells induces an inflammatory effect in professional phagocytes. For this purpose, we investigated the release of IL-6 and IL-8 during the clearance of autophagy-associated dying ARPE-19 and hRPE cells by macrophages, after 8h co-incubation. Parallelly, we tested the effect of TC pre-treatment (1μM, 48 h) on the cytokine release. The level of IL-6 and IL-8 cytokines was measured from the collected cell culture media by ELISA. We observed a negligible amount of IL-6 and IL-8 secretion by TC-treated and untreated MΦs (in the absence dying cells). Autophagy-associated dying ARPE-19 and hRPE cells themselves released significantly higher amount of IL-8 compared to the amount of secreted IL-6. Co-culturing of macrophages with the dying ARPE-19 or hRPE cells resulted in increased concentration of IL-6 and IL-8, which indicated an induction of a pro-inflammatory response. Larger amount of IL-8 was detected upon macrophage-dying cell co-incubation as compared to the secreted amount of IL-6. We determined the decreased production of IL-6 and IL-8 cytokines during the phagocytosis of ARPE-19 and hRPE cells by TC-treated macrophages, due to the anti-inflammatory impact of the glucocorticoid TC (**Figure 22**). These observations indicate that the clearance of autophagy-associated dying RPE cells by macrophages leads to a pro-inflammatory response *in vitro*, which are in accordance with our previously published results. It should be noted that the minority of the dead cells interacting with the macrophages were primary or secondary necrotic cells. Based on this, we cannot

exclude the possibility that these cells play a role in the stimulation of inflammatory cytokine release by macrophages completely.

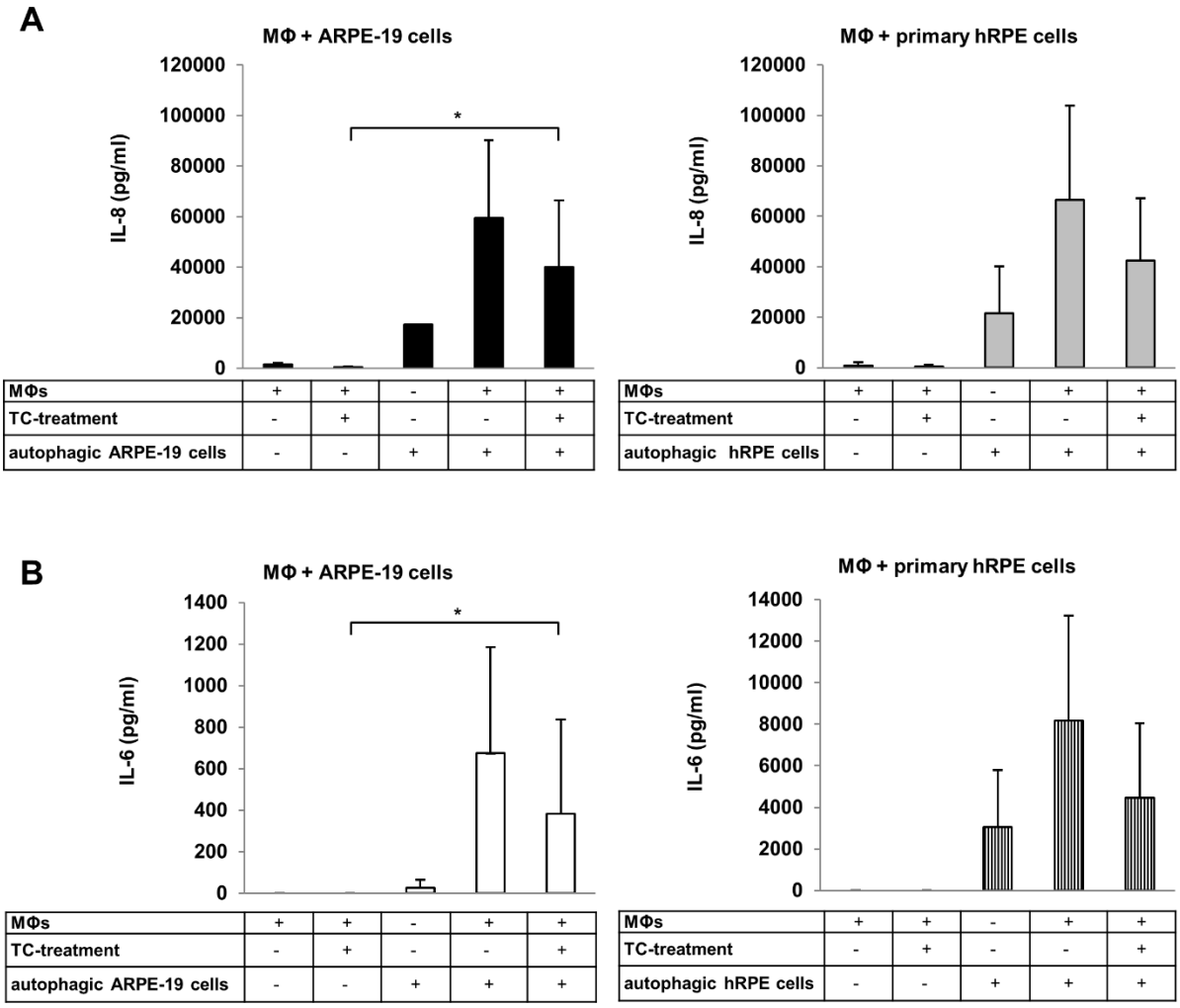

Figure 22. Detection of IL-6 and IL-8 release during the engulfment of autophagy-associated dying ARPE-19 and hRPE cells by macrophages using ELISA method. *H_2O_2-induced (2h, 1mM) autophagy-associated dying ARPE-19 (**left panels**) and hRPE cells (**right panels**) were co-cultured with untreated and TC-treated (48h, 1μM) MΦs for 8h, then the supernatants were collected, and the concentration of IL-8 (**A**) and IL-6 (**B**) measured by ELISA. Bars indicate the mean ±SD of 3 independent experiments, *p<0.05, **p<0.01.*

5.6.2. The engulfment of anoikic and autophagy-associated dying hESC-RPE cells by macrophages led to a release of IL-6 and IL-8 cytokines

In the following experiments, we wanted to examine whether the macrophages release pro-inflammatory cytokines during the uptake of dying hESC-RPE cells. Anoikic or autophagy-associated dying hESC-RPE cells induced by H_2O_2 (2h, 1mM) were added to the macrophages, and the cell culture media were collected after 4 or 8h, respectively, for cytokine measurements using ELISA method. Furthermore, we tested how the glucocorticoid TC (48h, 1μM) influenced the secretion of IL-6 and IL-8 cytokines during clearance of dying cells by macrophages. We found that macrophages by themselves (in the absence of dying cells) did not produce IL-6 (control state). The phagocytosis of anoikic hESC-RPE cells by macrophages led to a significantly increased IL-6 secretion (836.33±252.27 pg/ml), which decreased as a result of TC treatment (780.87± 279.18 pg/ml). In the case of autophagy-associated dying cells' uptake, significantly lower levels of IL-6 release (324.37±67.43 pg/ml) were observed compared to the clearance of anoikic dying cells. We found low amount of IL-8 secretion by TC-treated (120.92±1.90 pg/ml) and untreated (84.40±2.48 pg/ml) macrophages (in the absence of dying cells). Interestingly, macrophages responded to the uptake of anoikic cells with increased IL-8 production (1057.33±416.56 pg/ml), which significantly decreased upon TC-treatment (892.11±442.08 pg/ml). Lower amount of IL-8 was released during the engulfment of autophagy-associated dying cells (318.13±67.99 pg/ml) as compared to anoikic ones, even this secretion was significant as compared to the released background level of IL-8 by macrophages alone or in the presence of TC. No significant differences in the secretion of IL-6 and IL-8 during the co-incubation of autophagy-associated dying cells with macrophages were determined upon TC-treatment (**Figure 23**).

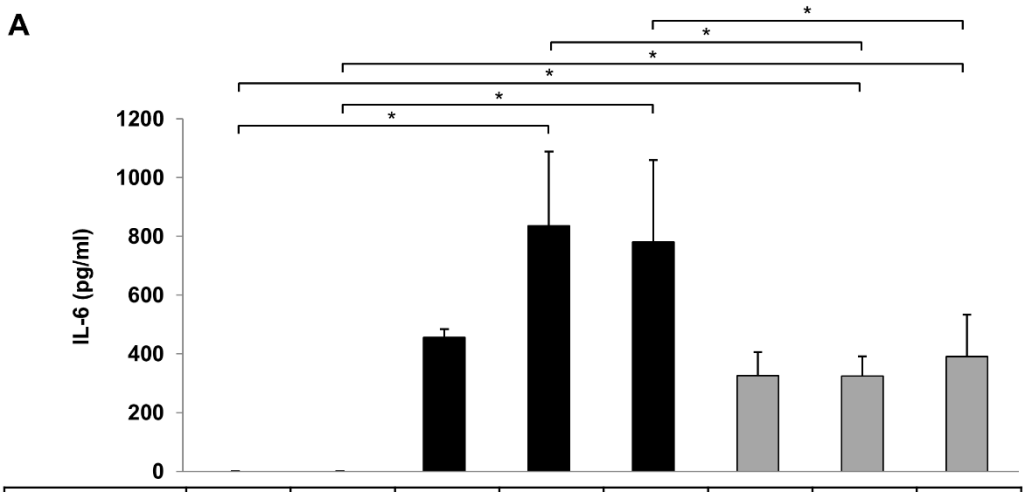

MΦ	+	+	-	+	+	-	+	+
TC-treatment	-	+	-	-	+	-	-	+
anoikic dying ESC-RPE cells	-	-	+	+	+	-	-	-
autophagic dying ESC-RPE cells	-	-	-	-	-	+	+	+

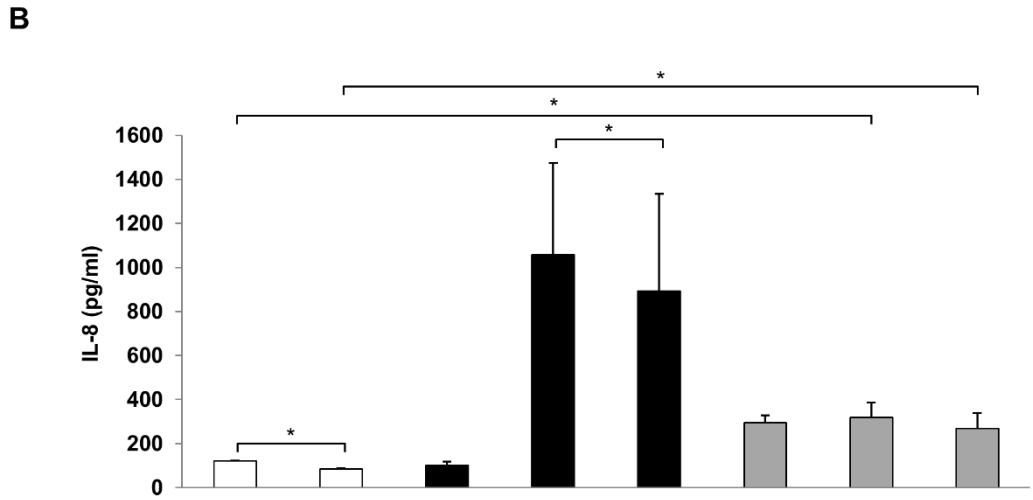

MΦ	+	+	-	+	+	-	+	+
TC-treatment	-	+	-	-	+	-	-	+
anoikic dying ESC-RPE cells	-	-	+	+	+	-	-	-
autophagic dying ESC-RPE cells	-	-	-	-	-	+	+	+

Figure 23. Release of IL-6 and IL-8 cytokines during the phagocytosis of anoikic and autophagy-associated dying hESC-RPE cells by macrophages. *Anoikic dying hESC-RPE cells (**left panels**) and H_2O_2-induced (2h, 1mM) autophagy-associated dying hESC-RPE cells (**right panels**) were added to the untreated and TC-treated (48h, 1μM) macrophages, co-cultured for 4h and 8h, respectively. After the collection of supernatants, the level of secreted IL-6 (**A**) and IL-8 (**B**) cytokines were measured by ELISA. Bars represent the mean ±SD of 3 independent experiments, *p<0.05.*

6. Discussion

AMD is a complex, neurodegenerative, multifactorial disease (Armstrong and Mousavi, 2015; Kaarniranta et al., 2011); the prevalence of which is increasing worldwide, thus becoming a significant global public health problem (Gordois et al., 2012; Klein and Klein, 2013). Dry AMD is the most common form of the disease and affects approximately 80% of the patients who suffer from AMD. There is no specific cure to date for dry AMD (Bowes Rickman et al., 2013). In the wet form of AMD, detrimental new blood vessels grow through the Bruch's membrane into the subretinal pigment epithelial space, where they can cause membrane disruption and blood or fluid leakage, trigger fibrogliosis, and eventually result in severe visual loss if not treated properly (Kulkarni and Kuppermann, 2005). To date, only some treatment options are available for wet AMD, the principal therapy target being the use of anti-VEGFs for blocking the neovascularization process. The use of intravitreal injections such as ranibizumab, bevacizumab or VEGF Trap to prevent severe vision loss or slow the progression of the disease has become a standard treatment modality, although it is an invasive procedure (Smith and Kaiser, 2014). This makes it necessary to create models for investigating AMD pathogenesis *in vitro* under conditions mimicking the disease pathogenesis *in vivo*. Such models can help generate new therapeutic approaches against AMD, and hopefully, some much needed non-invasive approaches for its prevention and treatment.

Nowadays, numerous studies focus on better understanding of the molecular background of the disease (Blasiak et al., 2014; Kaarniranta et al., 2013; Kinnunen et al., 2012). Various *in vitro* cell models are available for studying AMD, the most widely used is the immortalized ARPE-19 cell line (Dunn et al., 1996; Dunn et al., 1998), while another well-known model is the primary hRPE cells, which are isolated from adult cadaver human eyes (Johnen et al., 2012). Furthermore, in the recent years, the extreme development of the human embryonic stem cell (hESC) technologies (Idelson et al., 2009; Klimanskaya et al., 2004; Meyer et al., 2009; Vugler et al., 2008) has lead to the establishment of efficient RPE differentiation protocols from hESCs (Vaajasaari et al., 2011).

There is increasing evidence which suggest that many pathways interplay in the progression of AMD, including such as cell death, phagocytosis, inflammation and angiogenesis (Kinnunen et al., 2012; Yonekawa et al., 2015). Different types of retinal cell death may contribute to the development of AMD, including anoikis, apoptosis

(Dunaief et al., 2002), autophagy (Kaarniranta et al., 2013), or necrosis (Hanus et al., 2015). In the present study, we aimed to establish an *in vitro* detection model for investigating the anoikic and autophagy-associated cell death in all three types of RPE cells.

In the pathogenesis of dry type of AMD, the accumulation of drusen deposits can cause RPE detachment from the Bruch's membrane, which results in anoikic cell death (Bowes Rickman et al., 2013; de Jong, 2006). Recently, we could induce anoikic cell death in ARPE-19 cells *in vitro*, using poly-HEMA-covered dishes over a 24h cultivation to block the cell adhesion (Petrovski et al., 2011b). To the best of our knowledge, cell death analyses have not been performed in hESC-RPEs so far. Thus, we investigated whether anoikic cell death would be induced in hESC-RPE cells using the same protocol, and we quantified the cell death rate by Annexin V-FITC/PI double staining assay using flow cytometry analysis. The latter cells could not attach to the plate using phase contrast microscope, in addition they formed floating aggregates. A high rate of AnxV positivity (27%) was observed in the anoikic hESC-RPE cells, which was similar to the detected rate in ARPE-19 (19%) cells (Petrovski et al., 2011b).

The retina can be characterized by high oxygen consumption, constant light exposure and high mitochondrial activity, which results in constant subjection to high level of oxidative stress (Blasiak et al., 2014). Several studies confirm that the RPE cells are sensitive to oxidative stress (Hanneken et al., 2006; Wada et al., 2001). High rate of ROS can cause cellular or molecular damage and the accumulation of intracellular lipofuscin and extracellular drusen. It has been shown that the increased oxidative damage of RPE cells is implicated in the progression of AMD (Mao et al., 2014; Winkler et al., 1999). This is due to an imbalance between the generation of ROS and the expression of anti-oxidative enzymes, such as catalase or superoxide dismutase, which are serve as antioxidant protect responses (Rose et al., 1998). One of the main known ROS is the H_2O_2, which is accumulated in the human eyes under pathological conditions (Finkel, 2011). The most frequently used *in vitro* oxidative stress inducer is the H_2O_2 (Coyle et al., 2006; Scandalios, 2005). Moreover, it has been shown that oxidative stress is related to high autophagic activity (Ha et al., 2012; Levonen et al., 2014; Yang et al., 2014). Recently, autophagy-related proteins have been determined in the drusen of AMD patients, (Wang et al., 2009) which suggests the association of autophagy process with the pathogenesis of AMD (Kaarniranta et al., 2013; Klettner et al., 2013). In addition, increased levels of autophagy markers have been detected upon

H_2O_2-exposure in several cell types *in vitro* (Ashabi et al., 2013; Essick et al., 2013; Ha et al., 2012).

Based on these results, we applied H_2O_2-treatment as an oxidative stress model to induce and study autophagy and autophagy-associated cell death in RPE cells. The literature provides contradictory data about the concentration and time-intervals of H_2O_2-exposure for triggering increased autophagic activity in dying cells. Therefore, we used increasing concentration (0.4-1mM) and time-intervals (2-4h) of H_2O_2-treatment in ARPE-19 and hRPE cells to detect the most effective treatment for autophagy induction. Moreover, we combined the H_2O_2-treatment with serum deprivation, which is a well-known autophagy inducer, and tested the effect of this co-treatment on the cell death rate and the level of autophagy in RPEs. The co-treatment resulted in heterogeneous dying RPE cell populations to be present at the same time. The ratio of the PS positive or dying RPE cells increased in a time-and concentration dependent manner upon H_2O_2-treatment. The highest percentage of single positive AnxV cells was found upon 2h of 1mM H_2O_2.treatment, 41±10.8% of the ARPE-19 cells, 17.7±12.7% of the hRPE and approximately 40% of hESC-RPE cells became $AnxV^+$.

There are some limitations of the methods used for monitoring and quantifying autophagy due to an inconsistency in the internationally accepted markers for the autophagic process. In mammalian cells, the LC3 protein represents the main autophagic marker; its lipidated LC3-II form binds to the membrane of the autophagosomes (Kabeya et al., 2000; Tanida et al., 2004). In addition, the p62 protein also plays a role in this pathway, functioning as a link between LC3 and ubquitilated proteins and facilitating degradation of ubiquitilated substrates (Lippai and Low, 2014; Pankiv et al., 2007). The well-established approaches for investigation of the autophagic activity are the Western blot analysis to determine the level of LC3 or p62 protein**,** the immunofluorescent staining to visualize LC3 or p62 positive puncta using fluorescent microscopy, as well as the detection of autophagosomes by TEM (Klionsky et al., 2016). Furthermore, the autophagic activity can be followed by transfection of GFP-LC3 fusion protein into the cells using transfection reagents, such as PEI, or electroporation method. The level of autophagy in the GFP-LC3 transfected cells can be analyzed by manual counting of GFP-LC3 positive cells on fluorescent images or quantifying the fluorescence intensity of GFP using flow cytometry.

In the current study, we used different kinds of methods to better confirm the induction of autophagy in RPE cells as a result of H_2O_2-treatment. The results of the Western blot

analysis showed that the LC3-II/LC3-I ratio was increased in a time- and concentration-dependent manner, especially upon 2h, 1mM H_2O_2-treatment in all of the three applied RPE cell types. Moreover, in ARPE-19 cells, we could determine significantly decreased level of p62 by Western blot analysis, as well as accumulation of autophagosomes by TEM, increased number of GFP-LC3-positive cells using fluorescent microscopy and higher GFP fluorescence intensity in GFP-LC3 transfected cells by flow cytometry after 2h, 1mM H_2O_2-treatment in the absence of serum, compared to the untreated control cells.

In parallel, we intended to assess the whole dynamic process of autophagy during H_2O_2-exposure (2h, 1mM) in ARPE-19 and hRPE cells. Therefore, we checked the turnover of LC3-II by Western blot analysis in the presence of CQ to evaluate the autophagic flux (Ju et al., 2010; Mizushima et al., 2010). We could determine accumulation of LC3-II - a significantly increased ratio of LC3-II/LC3-I, which proves that autophagic flux was increased upon H_2O_2-administration. Altogether, we can conclude that the autophagy process could be activated by H_2O_2-treatment (2h, 1mM) in RPE cells; in addition, the combination of these approaches resulted in the establishment of an *in vitro* detection model for studying autophagy in RPE cells.

Recent studies indicate that, in certain conditions, autophagy can facilitate cell death, depending on the cellular context and the duration and strength of the death triggering stimulus (Cecconi and Levine, 2008; Kroemer and Levine, 2008). We aimed to study what percentage of the $LC3^+$ RPE cells is $AnxV^+$ as well, and what percentage of the $AnxV^+$ dying RPE cell show concomitant LC3-positivity upon H_2O_2-exposure. Therefore, we simultaneously analysed the LC3-positive AVs via mCherry-LC3 plasmid transfection and the PS-externalization using Annexin V-FITC labelling in H_2O_2-treated (2h, 1mM) ARPE-19 cells in the absence of serum by flow cytometry. We could confirm that autophagy-associated process are triggered in most of the dying ARPE-19 cells as a result of serum deprivation and oxidative stress caused by H_2O_2 (2h, 1mM) treatment.

The continuous clearance of dying cells is crucial for maintaining the retinal homeostasis and for preventing the accumulation of cellular debris in the space between the Bruch's membrane and the RPE layer and the progression of AMD (Kinnunen et al., 2012; Szabo et al., 2014). RPE cells represent non-professional phagocytes, which are responsible for the diurnal removal of the shed tips of the POS, to maintain the normal visual cycle (Bosch et al., 1993; Travis et al., 2007; Young and Bok, 1969). Moreover,

RPE cells play an essential role in the engulfment of dying neighbouring cells in dry AMD, because in this case, professional phagocytes cannot penetrate through the intact BRB. RPE cells are considered as one of the most effective phagocytes in the human body (Bowes Rickman et al., 2013). Wet AMD can be characterized by the breakdown of BRB, neovascularization, retinal edema, highly immunogenic environment, and recruitment and activation of professional phagocytes, such as macrophages or DCs (Klettner et al., 2013). Increasing evidence suggests accumulation of macrophages in the drusen and in the areas of breakdown of the Bruch's membrane and CNVs (Ambati et al., 2013; Kauppinen et al., 2016).

The leakage from CNVs can be transiently decreased and the blood-retinal barrier can be stabilized by TC treatment. This CS has anti-inflammatory, anti-fibrotic and anti-angiogenic effects (Danis et al., 2000; Jonas et al., 2004; Jonas et al., 2003; Lim et al., 2015). Furthermore, it has been described that the TC injections can significantly increase visual acuity (Gopal and Sharma, 2007; Lim et al., 2015).

In our previous *in vitro* study, we have reported that macrophages and non-professional RPE cells are able to engulf more apoptotic or anoikic cells, as well as the clearance of anoikic dying RPEs becomes enhanced as a result of TC treatment (Petrovski et al., 2011b). Moreover, our research group recently showed that the uptake of autophagy-associated dying MCF-7 cells can occur in two ways: either in a PS-dependent manner, which means such "eat-me" signal on the surface of dying cells contributes to the efficient recognition and engulfment by non-professional phagocytes, or in a PS-independent manner, in which the removal can happen by professional phagocytes, such as macrophages (Petrovski et al., 2007b). To our present knowledge, neither the clearance dynamics of autophagy-associated dying RPE cells by non-professional phagocytes, macrophages and DCs, nor the effect of TC-treatment on their phagocytic capacity have been investigated so far. In addition, no data exist about the removal of anoikic dying hRPE and hESC-RPE by macrophages or how efficiently can anoikic dying ARPE-19 be engulfed by DCs.

In the current study, we observed that ARPE-19 cells and macrophages can efficiently and increasingly phagocytose over time autophagy-associated dying ARPE-19, primary hRPE and hESC-RPE cells *in vitro*. Moreover, the enhancing effect of TC pre-treatment on the clearance capacity could also be demonstrated. In parallel with the FACS analysis, we could follow the clearance process of autophagy-associated dying RPEs using time-lapse microscopy. In line with these results, we could show that

macrophages were able to efficiently remove the anoikic dying primary hRPE and hESC-RPE cells; in addition, the phagocytic capacity increased as a result of TC-pre-treatment in both cases.

So far it has been poorly described how effective the DCs are in the clearance of dying cells in case of wet AMD. Interestingly, our *in vitro* data indicate that DCs are able to engulf much more autophagic dying ARPE-19 cells than the non-professional ARPE-19 or the macrophages, while the anoikic dying ARPE-19 cells were taken up less efficiency by the DCs.

Next, we checked how the cell death rate and the clearance of H_2O_2-treated RPE cells by the macrophages changes if we block the formation of autophagosome using PI3K inhibitor 3-MA. First of all, we confirmed that the autophagic process was partially blocked as a result of 3-MA-treatment using Western blot analysis. Parallelly, we observed significantly increased percentage of viable and significantly decreased percentage of $AnxV^+$ and PI^+ H_2O_2-treated ARPE-19 cells upon use of the autophagy inhibitor, which indicated blocking of autophagy-associated cell death in ARPE-19 cells. Finally, when co-incubation of 3-MA pre-treated and H_2O_2-treated APRE-19 cells with the macrophages produced a significantly decreased rate of phagocytosis of these RPE cells. These results are in accordance with our previously reported data in which both autophagic death and clearance could be inhibited by 3-MA in dying MCF-7 cells (Petrovski et al., 2011a; Petrovski et al., 2007a). These findings suggest that autophagy contributes to the specific changes of the cell surface, which are linked with the recognition and engulfment of these dying cells by macrophages.

Next, we aimed to determine more precisely the clearance of autophagy-associated dying ARPE-19 cells from a mixed population of dying cells by the macrophages. A well-established, sensitive, high-throughput flow cytometry technique was applied to sort out the GFP-LC3 positive and negative sub-populations of H_2O_2-treated transfected ARPE-19 cells based on their size, granularity and fluorescence signal; after that, the sorted sub-populations of cells were co-incubated with the macrophages. We found similar phagocytic rate during the engulfment of GFP-LC3 positive RPEs and the non-sorted autophagic dying cells by macrophages, thus verifying their fate in the clearance process. As far as we are aware, this is the first report that demonstrates the phagocytic rate of H_2O_2-treated, GFP-LC3 positive sorted ARPE-19 cells by macrophages using a high-performance cell sorter, as well as the clearance process is visualized by time-lapse microscopy.

The complex, multi-step phagocytic process begins with the recognition of “eat me” signals, such as PS, on the surface of dying cells by specific cell surface receptors on the phagocytic cells (Ravichandran, 2010). One of the well-characterized receptors is the Mertk, which binds to PS indirectly with the help of Gas6 bridging molecule (Penberthy and Ravichandran, 2016; van der Meer et al., 2014). It has been reported that Mertk expression on the surface of non-professional phagocytic RPE cells plays an important role in the regulation of POS clearance (Chaitin and Hall, 1983; D'Cruz et al., 2000). Overall, to date, little is known about the molecular mechanisms and contributors of the phagocytic synapse which regulate the effective dead RPE cells clearance. We aimed to investigate the gene expression pattern changes in TC-treated and untreated macrophages before and during engulfment of anoikic ARPE-19 cells using TLDA.

Specific siRNA transfection method was applied to silence the following genes: ADORA3, THBS1, AXL, MERTK, which were found to be upregulated as a result of TC treatment. The goal was to determine whether such upregulation of apopto-phagocytic genes had a direct impact on the increased clearance efficiency of professional phagocytes. We observed that only silencing of MERTK and AXL could prevent TC-induced enhancement in engulfment of anoikic ARPE-19 cells by macrophages. Parallelly, the pivotal role of MerTk receptor in this clearance process has been further confirmed using blocking antibodies against MerTk. We could prove the role of MerTk receptor in the case of TC-mediated non-professional phagocytosis of anoikic ARPE-19 cells, because the TC-enhanced phagocytosis rate was significantly reduced upon MerTk blocking antibody treatment either on the side of the phagocytes or on the side of anoikic ARPE-19 cells. In addition, the clearance of anoikic dying hRPE cells by TC-treated macrophages was significantly decreased as a result of blocking MerTk receptor. Finally, we found that Gas6 treatment led to considerable increased phagocytic capacity of TC-treated macrophages, which showed concentration dependence. To our present knowledge, this is the first study demonstrating the major role of MerTk in the regulation of TC-enhanced clearance of anoikic dying RPE cells not only by non-professional phagocytes, but also by macrophages. The upregulation of MFG-E8, ITGAV, TYRO3, AXL and THSB-1 genes in the TC-treated macrophages confirms the role of TC in the different stages of phagocytosis.

Under healthy conditions, the BRB contributes to the inhibition of certain substances to enter the “immunologically privileged” retina (Stein-Streilein, 2013). In addition, the activity of immune-competent cells is blocked by immunosuppressive factors within

this tissue under such circumstances (Zhou and Caspi, 2010). Growing evidence suggests that the pathogenesis of AMD is strongly associated with immunological processes, such as the generation of inflammation-related molecules in the Bruch's membrane, recruitment of macrophages, DCs or microglial cells into the subretinal space and activation of the complement system in the macular area (Ambati et al., 2013; Kauppinen et al., 2016). The dual role of macrophages has been detected in AMD. On the one hand, pro-inflammatory M1 macrophages have been shown to contribute towards tissue damage, acting as inflammatory stimulators, while the relatively anti-inflammatory M2 macrophages act as housekeepers and are responsible for the removal of drusen deposits (Bowes Rickman et al., 2013; Ding et al., 2009).

The imbalance between different types of cytokines may also lead to the progression of AMD (Klettner et al., 2013). IL-6 being known to be a multifunctional cytokine, it contributes to the acute phase of the inflammation reaction, wound healing, angiogenesis and fibrogenesis (Barnes et al., 2011). Recent evidence suggests that the levels of IL-6 correlate with the activation of pro-angiogenic growth factors, such as VEGF in neovascular AMD (Klein et al., 2014; Mooijaart et al., 2007; Seddon et al., 2005). In the therapy of wet AMD, IL-6 may provide a possible novel target in the future therapy (Cui et al., 2014). Moreover, the role of IL-8 in angiogenesis, CNV and macular edema has been also reported in AMD patients (Ambreen et al., 2015; Cascella et al., 2014; Ricci et al., 2013).

The inflammatory response of macrophages has been well-studied during the engulfment of apoptotic and necrotic cells. It is well-known that the clearance of apoptotic cells is an immunologically silent process, which can be characterized by the secretion of anti-inflammatory cytokines, such as IL-10 or TGF-β by the phagocytic cells (Gregory and Devitt, 2004; Savill et al., 2002; Savill and Fadok, 2000). In contrast, pro-inflammatory and immunostimulatory effect can be observed as a result of necrotic cells' uptake by macrophages (Fadok et al., 2001; Fadok et al., 1998; Poon et al., 2010). In case the clearance of apoptotic dying cells is not complete, the membrane integrity of the uncleared cells can be abrogated, which eventually can cause secondary necrosis, as well as can trigger inflammatory responses (Fernandez-Boyanapalli et al., 2010; Medina and Ravichandran, 2016; Poon et al., 2014). However, only a few reports to date could show the immunogenic features of phagocytes upon clearance of anoikic or autophagy-associated dying cells (Ayna et al.; Petrovski et al., 2011a).

In this study, we could demonstrate that the concentration of the released IL-6 and IL-8 cytokines increases during the clearance of autophagy-associated dying ARPE-19 or hRPE cells by macrophages; in addition, we could demonstrate a significantly decreased release of interleukins by TC-treated macrophages, as a result of the anti-inflammatory effect of the glucocorticoid TC. In accordance with this finding**,** we detected a similar impact when the macrophages engulfed the autophagy-associated dying hESC-RPE cells. These results suggest that the clearance of autophagy-associated dying RPE cells can trigger a pro-inflammatory response in human macrophages *in vitro*.

Surprisingly, in the case of phagocytosis of anoikic dying hESC-RPE cells by macrophages, high amount of IL-6 and IL-8 production could be detected, which showed decreasing tendency in response to TC treatment. The induction of the sectretion of such pro-inflammatory mediators might be related to the improper clearance of anoikic dying cells. Moreover, the possibility cannot be excluded that a small ratio of secondary necrotic cells, as a result of culturing cells on poly-HEMA-covered dishes over a 24h period, did not contribute to the release of the pro-inflammatory cytokines under such conditions.

7. Summary

The clearance of dying RPE cells is crucial for maintaining retinal homeostasis. Inefficient removal of these cells by phagocytes may result in accumulation of debris and progression of AMD. We hypothesize that not only intracellular protein clearance in RPE cells, but also the clearance of autophagy-associated dying cells by phagocytes are essential in the pathogenesis of AMD. In this work, the engulfment of autophagy-associated and anoikic dying RPE cells by phagocytes is being investigated.

An increasing percentage of PS^+ or dying RPE cells due to serum deprivation and H_2O_2 co-treatment could be observed. The induction of autophagy could be detected within 2h of treatment with 1mM H_2O_2 using TEM, LC3/p62 expression and GFP-LC3 transfection assays, as well as increased autophagic flux could be measured during H_2O_2-exposure under CQ treatment. Autophagy-associated cell death could be induced in ARPE-19, hRPE or hESC-RPE cells. Moreover, the anoikic cell death could be triggered in hESC-RPE cells by ECM detachment.

The *in vitro* phagocytosis assays found that autophagy-associated and anoikic dying RPE cells can be efficiently and increasingly engulfed by macrophages, DCs and living RPE cells in a time-dependent manner. Inhibition of autophagy by 3-MA led to decreased phagocytic capacity of macrophages during the engulfment of autophagy-associated dying cells, while sorting out the GFP-LC3 positive cell population or TC treatment enhanced it. We could demonstrate a phagocytosis-enhancing effect of TC treatment in non-professional and professional phagocytes during the clearance of anoikic dying RPE cells via the MerTk signaling pathway. The key role of MerTK in the macrophages engulfing dying cells could be confirmed using siRNA-based gene silencing or blocking antibodies. The phagocytic efficiency of TC-treated macrophages was remarkably increased upon Gas6 treatment via the MerTK receptor. The clearance of autophagy-associated dying RPE cells by macrophages resulted in a pro-inflammatory response.

Our findings suggest that the phagocytosis of anoikic and autophagy-associated dying RPE cells can be used as models for studying AMD *in vitro*, and for investigating future pharmacological agents for treating AMD. The hESC-RPE cell death models might be appropriate for examining the *in vivo* potential or immunological consequence of using such cells for stem cell therapy. Specific agonists of the MerTK receptors may have a potential role as phagocytosis enhancers in the retina and might serve as future targets for AMD therapy.

8. Összefoglalás

Az elhaló retina pigment epitél (RPE) sejtek eltávolítása elengedhetetlen a retina homeosztázisának fenntartásához. Ezeknek az elhaló sejteknek a fagocitákkal történő nem megfelelő eltávolítása, a törmelékek felhalmozódását és az időskori makula degeneráció (AMD) progresszióját eredményezhetik. Azt feltételezzük, hogy az AMD patomechanizmusában nem csak az RPE sejtek intracelluláris fehérjéinek eltávolítása esszenciális, hanem az autofágia-asszociált elhaló sejtek fagocitákkal történő eltávolítása is. Munkánk során az autofágia-asszociált és az anoikisz módon elhaló RPE sejtek fagociták általi bekebelezését vizsgáltuk.

Szérummegvonás és hidrogén-peroxid (H_2O_2) kettős kezelés hatására növekvő foszfatidil-szerin pozitív (PS^+), elhaló RPE sejt ráta volt megfigyelhető. Autofágia indukciót detektáltunk 2h, 1mM H_2O_2 kezelés után transzmissziós elektron mikroszkópos (TEM), LC3/p62 expresszió és GFP-LC3 transzfekciós vizsgálatokkal, valamint klorokvin (CQ) kezeléssel igazoltuk a H_2O_2-expozíció alatti autofágiás flux növekedését. Autofágia-asszociált sejthalált indukáltunk az ARPE-19, primer humán RPE és a humán embrionális őssejt eredetű (hESC)-RPE sejtekben. Továbbá, anoikisz sejthalált váltottunk ki a hESC-RPE sejtekben extracelluláris mátrixról (ECM) való leválással.

Az *in vitro* fagocitózis vizsgálatok során azt találtuk, hogy az autofágia-asszociált és az anoikisz módon elhaló sejteket időfüggő módon, hatékonyan és növekvő mértékben tudták bekebelezni a makrofágok, a dendritikus sejtek és az élő RPE sejtek. A 3-metiladeninnel (3-MA) történő autofágia gátlás a makrofágok fagocitáló kapacitásának csökkenéséhez vezetett az autofágia-asszociált elhaló sejtek bekebelezésekor, míg az „osztályozott" GFP-LC3 pozitív sejtpopulációk és a triamcinolone (TC) kezelés fokozta azt. A TC-kezelés fagocitózis-fokozó hatását igazolni tudtuk a nem-professzionális és a professzionális fagocitáknál az anoikisz módon elhaló RPE sejtek eltávolításakor a MerTK szignalizációs útvonalon keresztül. Géncsendesítéssel és blokkoló antitestekkel bizonyítottuk, hogy a MerTK kulcsszerepet tölt be a makrofágokban az elhaló sejtek bekebelezésekor. A TC-kezelt makrofágok fagocitáló hatékonysága figyelemreméltó módon növekedett Gas6 kezelés hatására a MerTK receptoron keresztül. Az autofágia-asszociált elhaló RPE sejtek makrofágok általi eltávolítása pro-inflammatórikus választ váltott ki.

Eredményeink azt jelzik, hogy az anoikisz és az autofágia-asszociált elhaló RPE sejtek fagocitózisa modellként felhasználható az AMD *in vitro* tanulmányozására, és az AMD

kezelésére szolgáló jövőbeni farmakológiai szerek vizsgálatára. A hESC-RPE sejthalál modellek alkalmasak lehetnek feltárni ezen sejtek őssejt terápiás felhasználásának *in vivo* potenciálját és immunológiai következményeit. A MerTK receptorok specifikus agonistái fagocitózis-fokozó szerepet tölthetnek be a retinában, és jövőbeni célpontokként szolgálhatnak az AMD-terápiában.

9. Reference

1. Albert, M.L., S.F. Pearce, L.M. Francisco, B. Sauter, P. Roy, R.L. Silverstein, and N. Bhardwaj. 1998. Immature dendritic cells phagocytose apoptotic cells via alphavbeta5 and CD36, and cross-present antigens to cytotoxic T lymphocytes. *The Journal of experimental medicine*. 188:1359-1368.
2. Albert, R., E. Kristof, G. Zahuczky, M. Szatmari-Toth, Z. Vereb, B. Olah, M.C. Moe, A. Facsko, L. Fesus, and G. Petrovski. 2014. Triamcinolone regulated apopto-phagocytic gene expression patterns in the clearance of dying retinal pigment epithelial cells. A key role of Mertk in the enhanced phagocytosis. *Biochim Biophys Acta*. 1850:435-446.
3. Alers, S., A.S. Loffler, S. Wesselborg, and B. Stork. 2012. Role of AMPK-mTOR-Ulk1/2 in the regulation of autophagy: cross talk, shortcuts, and feedbacks. *Mol Cell Biol*. 32:2-11.
4. Ambati, J., J.P. Atkinson, and B.D. Gelfand. 2013. Immunology of age-related macular degeneration. *Nature reviews. Immunology*. 13:438-451.
5. Ambreen, F., M. Ismail, and I.Z. Qureshi. 2015. Association of gene polymorphism with serum levels of inflammatory and angiogenic factors in Pakistani patients with age-related macular degeneration. *Molecular vision*. 21:985-999.
6. Amoaku, W.M., U. Chakravarthy, R. Gale, M. Gavin, F. Ghanchi, J. Gibson, S. Harding, R.L. Johnston, S.P. Kelly, A. Lotery, S. Mahmood, G. Menon, S. Sivaprasad, J. Talks, A. Tufail, and Y. Yang. 2015. Defining response to anti-VEGF therapies in neovascular AMD. *Eye*. 29:721-731.
7. Armstrong, R.A., and M. Mousavi. 2015. Overview of Risk Factors for Age-Related Macular Degeneration (AMD). *J Stem Cells*. 10:171-191.
8. Ashabi, G., A. Ahmadiani, A. Abdi, S.B. Abraki, and F. Khodagholi. 2013. Time course study of Abeta formation and neurite outgrowth disruption in differentiated human neuroblastoma cells exposed to H_2O_2: protective role of autophagy. *Toxicology in vitro : an international journal published in association with BIBRA*. 27:1780-1788.
9. Ayna, G., D.V. Krysko, A. Kaczmarek, G. Petrovski, P. Vandenabeele, and L. Fesus. ATP release from dying autophagic cells and their phagocytosis are crucial for inflammasome activation in macrophages. *PloS one*. 7:e40069.
10. Barnes, T.C., M.E. Anderson, and R.J. Moots. 2011. The many faces of interleukin-6: the role of IL-6 in inflammation, vasculopathy, and fibrosis in systemic sclerosis. *Int J Rheumatol*. 2011:721608.
11. Blasiak, J., G. Petrovski, Z. Vereb, A. Facsko, and K. Kaarniranta. 2014. Oxidative stress, hypoxia, and autophagy in the neovascular processes of age-related macular degeneration. *Biomed Res Int*. 2014:768026.
12. Bosch, E., J. Horwitz, and D. Bok. 1993. Phagocytosis of outer segments by retinal pigment epithelium: phagosome-lysosome interaction. *J Histochem Cytochem*. 41:253-263.

13. Bowes Rickman, C., S. Farsiu, C.A. Toth, and M. Klingeborn. 2013. Dry age-related macular degeneration: mechanisms, therapeutic targets, and imaging. *Investigative ophthalmology & visual science*. 54:ORSF68-80.

14. Burman, C., and N.T. Ktistakis. 2010. Regulation of autophagy by phosphatidylinositol 3-phosphate. *FEBS Lett*. 584:1302-1312.

15. Buschini, E., A.M. Fea, C.A. Lavia, M. Nassisi, G. Pignata, M. Zola, and F.M. Grignolo. 2015. Recent developments in the management of dry age-related macular degeneration. *Clinical ophthalmology*. 9:563-574.

16. Cascella, R., M. Ragazzo, C. Strafella, F. Missiroli, P. Borgiani, F. Angelucci, L.T. Marsella, A. Cusumano, G. Novelli, F. Ricci, and E. Giardina. 2014. Age-related macular degeneration: insights into inflammatory genes. *Journal of ophthalmology*. 2014:582842.

17. Cecconi, F., and B. Levine. 2008. The role of autophagy in mammalian development: cell makeover rather than cell death. *Dev Cell*. 15:344-357.

18. Chaitin, M.H., and M.O. Hall. 1983. Defective ingestion of rod outer segments by cultured dystrophic rat pigment epithelial cells. *Investigative ophthalmology & visual science*. 24:812-820.

19. Chang, C.W., L. Ye, D.M. Defoe, and R.B. Caldwell. 1997. Serum inhibits tight junction formation in cultured pigment epithelial cells. *Investigative ophthalmology & visual science*. 38:1082-1093.

20. Chang, Y.C., M.C. Hsieh, H.J. Wu, W.C. Wu, and Y.H. Kao. 2015. Methylglyoxal, a reactive glucose metabolite, enhances autophagy flux and suppresses proliferation of human retinal pigment epithelial ARPE-19 cells. *Toxicology in vitro : an international journal published in association with BIBRA*. 29:1358-1368.

21. Chen, Y., and D.J. Klionsky. 2011. The regulation of autophagy - unanswered questions. *J Cell Sci*. 124:161-170.

22. Chiras, D., G. Kitsos, M.B. Petersen, I. Skalidakis, and C. Kroupis. 2015. Oxidative stress in dry age-related macular degeneration and exfoliation syndrome. *Critical reviews in clinical laboratory sciences*. 52:12-27.

23. Coyle, C.H., L.J. Martinez, M.C. Coleman, D.R. Spitz, N.L. Weintraub, and K.N. Kader. 2006. Mechanisms of H_2O_2-induced oxidative stress in endothelial cells. *Free radical biology & medicine*. 40:2206-2213.

24. Cui, W., H. Zhang, and Z.L. Liu. 2014. Interleukin-6 receptor blockade suppresses subretinal fibrosis in a mouse model. *Int J Ophthalmol*. 7:194-197.

25. Cunha-Vaz, J., R. Bernardes, and C. Lobo. 2011. Blood-retinal barrier. *European journal of ophthalmology*. 21 Suppl 6:S3-9.

26. D'Cruz, P.M., D. Yasumura, J. Weir, M.T. Matthes, H. Abderrahim, M.M. LaVail, and D. Vollrath. 2000. Mutation of the receptor tyrosine kinase gene Mertk in the retinal dystrophic RCS rat. *Hum Mol Genet*. 9:645-651.

27. Damico, F.M., F. Gasparin, M.R. Scolari, L.S. Pedral, and B.S. Takahashi. 2012. New approaches and potential treatments for dry age-related macular degeneration. *Arq Bras Oftalmol*. 75:71-76.

28. Danis, R.P., D.P. Bingaman, Y. Yang, and B. Ladd. 1996. Inhibition of preretinal and optic nerve head neovascularization in pigs by intravitreal triamcinolone acetonide. *Ophthalmology*. 103:2099-2104.

29. Danis, R.P., T.A. Ciulla, L.M. Pratt, and W. Anliker. 2000. Intravitreal triamcinolone acetonide in exudative age-related macular degeneration. *Retina*. 20:244-250.

30. de Jong, P.T. 2006. Age-related macular degeneration. *N Engl J Med*. 355:1474-1485.

31. Ding, X., M. Patel, and C.C. Chan. 2009. Molecular pathology of age-related macular degeneration. *Progress in retinal and eye research*. 28:1-18.

32. Dunaief, J.L., T. Dentchev, G.S. Ying, and A.H. Milam. 2002. The role of apoptosis in age-related macular degeneration. *Archives of ophthalmology*. 120:1435-1442.

33. Dunn, K.C., A.E. Aotaki-Keen, F.R. Putkey, and L.M. Hjelmeland. 1996. ARPE-19, a human retinal pigment epithelial cell line with differentiated properties. *Exp Eye Res*. 62:155-169.

34. Dunn, K.C., A.D. Marmorstein, V.L. Bonilha, E. Rodriguez-Boulan, F. Giordano, and L.M. Hjelmeland. 1998. Use of the ARPE-19 cell line as a model of RPE polarity: basolateral secretion of FGF5. *Investigative ophthalmology & visual science*. 39:2744-2749.

35. Elliott, M.R., and K.S. Ravichandran. 2010. Clearance of apoptotic cells: implications in health and disease. *The Journal of cell biology*. 189:1059-1070.

36. Erwig, L.P., and P.M. Henson. 2008. Clearance of apoptotic cells by phagocytes. *Cell death and differentiation*. 15:243-250.

37. Eskelinen, E.L., and P. Saftig. 2009. Autophagy: a lysosomal degradation pathway with a central role in health and disease. *Biochim Biophys Acta*. 1793:664-673.

38. Essick, E.E., R.M. Wilson, D.R. Pimentel, M. Shimano, S. Baid, N. Ouchi, and F. Sam. 2013. Adiponectin modulates oxidative stress-induced autophagy in cardiomyocytes. *PloS one*. 8:e68697.

39. Fadok, V.A., D.L. Bratton, L. Guthrie, and P.M. Henson. 2001. Differential effects of apoptotic versus lysed cells on macrophage production of cytokines: role of proteases. *Journal of immunology*. 166:6847-6854.

40. Fadok, V.A., D.L. Bratton, A. Konowal, P.W. Freed, J.Y. Westcott, and P.M. Henson. 1998. Macrophages that have ingested apoptotic cells in vitro inhibit proinflammatory cytokine production through autocrine/paracrine mechanisms involving TGF-beta, PGE2, and PAF. *The Journal of clinical investigation*. 101:890-898.

41. Ferguson, T.A., and G.W. Laurie. 2016. Introduction to Autophagy in the Eye (or "What's Eatin' You?"). *Exp Eye Res*. 144:1-3.

42. Fernandez-Boyanapalli, R., K.A. McPhillips, S.C. Frasch, W.J. Janssen, M.C. Dinauer, D.W. Riches, P.M. Henson, A. Byrne, and D.L. Bratton. 2010. Impaired phagocytosis of apoptotic cells by macrophages in chronic granulomatous disease

is reversed by IFN-gamma in a nitric oxide-dependent manner. *Journal of immunology*. 185:4030-4041.

43. Fernandez-Robredo, P., A. Sancho, S. Johnen, S. Recalde, N. Gama, G. Thumann, J. Groll, and A. Garcia-Layana. 2014. Current treatment limitations in age-related macular degeneration and future approaches based on cell therapy and tissue engineering. *Journal of ophthalmology*. 2014:510285.

44. Finkel, T. 2011. Signal transduction by reactive oxygen species. *The Journal of cell biology*. 194:7-15.

45. Frisch, S.M., and H. Francis. 1994. Disruption of epithelial cell-matrix interactions induces apoptosis. *The Journal of cell biology*. 124:619-626.

46. Frisch, S.M., and R.A. Screaton. 2001. Anoikis mechanisms. *Curr Opin Cell Biol*. 13:555-562.

47. Frisch, S.M., K. Vuori, E. Ruoslahti, and P.Y. Chan-Hui. 1996. Control of adhesion-dependent cell survival by focal adhesion kinase. *The Journal of cell biology*. 134:793-799.

48. Fujimoto, H., K. Kato, and H. Iwata. 2010. Layer-by-layer assembly of small interfering RNA and poly(ethyleneimine) for substrate-mediated electroporation with high efficiency. *Anal Bioanal Chem*. 397:571-578.

49. Fullgrabe, J., D.J. Klionsky, and B. Joseph. 2014. The return of the nucleus: transcriptional and epigenetic control of autophagy. *Nat Rev Mol Cell Biol*. 15:65-74.

50. Galluzzi, L., I. Vitale, J.M. Abrams, E.S. Alnemri, E.H. Baehrecke, M.V. Blagosklonny, T.M. Dawson, V.L. Dawson, W.S. El-Deiry, S. Fulda, E. Gottlieb, D.R. Green, M.O. Hengartner, O. Kepp, R.A. Knight, S. Kumar, S.A. Lipton, X. Lu, F. Madeo, W. Malorni, P. Mehlen, G. Nunez, M.E. Peter, M. Piacentini, D.C. Rubinsztein, Y. Shi, H.U. Simon, P. Vandenabeele, E. White, J. Yuan, B. Zhivotovsky, G. Melino, and G. Kroemer. 2012. Molecular definitions of cell death subroutines: recommendations of the Nomenclature Committee on Cell Death 2012. *Cell death and differentiation*. 19:107-120.

51. Gaynes, B.I., and R.G. Fiscella. 2004. Safety of verteporfin for treatment of subfoveal choroidal neovascular membranes associated with age-related macular degeneration. *Expert Opin Drug Saf*. 3:345-361.

52. Gehrs, K.M., D.H. Anderson, L.V. Johnson, and G.S. Hageman. 2006. Age-related macular degeneration--emerging pathogenetic and therapeutic concepts. *Annals of medicine*. 38:450-471.

53. Gemenetzi, M., and A.J. Lotery. 2016. Complement pathway biomarkers and age-related macular degeneration. *Eye*. 30:1-14.

54. Geng, J., and D.J. Klionsky. 2008. The Atg8 and Atg12 ubiquitin-like conjugation systems in macroautophagy. 'Protein modifications: beyond the usual suspects' review series. *EMBO Rep*. 9:859-864.

55. Giannelli, S.G., G.C. Demontis, G. Pertile, P. Rama, and V. Broccoli. 2011. Adult human Muller glia cells are a highly efficient source of rod photoreceptors. *Stem cells*. 29:344-356.

56. Gilmore, A.P. 2005. Anoikis. *Cell death and differentiation*. 12 Suppl 2:1473-1477.

57. Gopal, L., and T. Sharma. 2007. Use of intravitreal injection of triamcinolone acetonide in the treatment of age-related macular degeneration. *Indian J Ophthalmol*. 55:431-435.

58. Gordois, A., H. Cutler, L. Pezzullo, K. Gordon, A. Cruess, S. Winyard, W. Hamilton, and K. Chua. 2012. An estimation of the worldwide economic and health burden of visual impairment. *Global public health*. 7:465-481.

59. Green, D.R., T.H. Oguin, and J. Martinez. 2016. The clearance of dying cells: table for two. *Cell death and differentiation*. 23:915-926.

60. Gregory, C.D., and A. Devitt. 2004. The macrophage and the apoptotic cell: an innate immune interaction viewed simplistically? *Immunology*. 113:1-14.

61. Grossniklaus, H.E., E.E. Geisert, and J.M. Nickerson. 2015. Introduction to the Retina. *Prog Mol Biol Transl Sci*. 134:383-396.

62. Ha, J.H., H.S. Noh, I.W. Shin, J.R. Hahm, and D.R. Kim. 2012. Mitigation of H2O2-induced autophagic cell death by propofol in H9c2 cardiomyocytes. *Cell biology and toxicology*. 28:19-29.

63. Hageman, G.S., P.J. Luthert, N.H. Victor Chong, L.V. Johnson, D.H. Anderson, and R.F. Mullins. 2001. An integrated hypothesis that considers drusen as biomarkers of immune-mediated processes at the RPE-Bruch's membrane interface in aging and age-related macular degeneration. *Progress in retinal and eye research*. 20:705-732.

64. Hanneken, A., F.F. Lin, J. Johnson, and P. Maher. 2006. Flavonoids protect human retinal pigment epithelial cells from oxidative-stress-induced death. *Investigative ophthalmology & visual science*. 47:3164-3177.

65. Hanus, J., C. Anderson, and S. Wang. 2015. RPE necroptosis in response to oxidative stress and in AMD. *Ageing Res Rev*. 24:286-298.

66. He, C., and D.J. Klionsky. 2009. Regulation mechanisms and signaling pathways of autophagy. *Annu Rev Genet*. 43:67-93.

67. Hernandez, E.V., J.G. Hu, D.A. Frambach, and R.P. Gallemore. 1995. Potassium conductances in cultured bovine and human retinal pigment epithelium. *Investigative ophthalmology & visual science*. 36:113-122.

68. Hoar, R.M. 1982. Embryology of the eye. *Environ Health Perspect*. 44:31-34.

69. Hochreiter-Hufford, A., and K.S. Ravichandran. 2013. Clearing the dead: apoptotic cell sensing, recognition, engulfment, and digestion. *Cold Spring Harb Perspect Biol*. 5:a008748.

70. Hodrea, J., G. Majai, Z. Doro, G. Zahuczky, A. Pap, E. Rajnavolgyi, and L. Fesus. 2012. The glucocorticoid dexamethasone programs human dendritic cells for enhanced phagocytosis of apoptotic neutrophils and inflammatory response. *Journal of leukocyte biology*. 91:127-136.

71. Hoon, M., H. Okawa, L. Della Santina, and R.O. Wong. 2014. Functional architecture of the retina: development and disease. *Progress in retinal and eye research*. 42:44-84.

72. Hornof, M., E. Toropainen, and A. Urtti. 2005. Cell culture models of the ocular barriers. *Eur J Pharm Biopharm*. 60:207-225.

73. Idelson, M., R. Alper, A. Obolensky, E. Ben-Shushan, I. Hemo, N. Yachimovich-Cohen, H. Khaner, Y. Smith, O. Wiser, M. Gropp, M.A. Cohen, S. Even-Ram, Y. Berman-Zaken, L. Matzrafi, G. Rechavi, E. Banin, and B. Reubinoff. 2009. Directed differentiation of human embryonic stem cells into functional retinal pigment epithelium cells. *Cell stem cell*. 5:396-408.

74. Ilmarinen, T., H. Hiidenmaa, P. Koobi, S. Nymark, A. Sorkio, J.H. Wang, B.V. Stanzel, F. Thieltges, P. Alajuuma, O. Oksala, M. Kataja, H. Uusitalo, and H. Skottman. 2015. Ultrathin Polyimide Membrane as Cell Carrier for Subretinal Transplantation of Human Embryonic Stem Cell Derived Retinal Pigment Epithelium. *PloS one*. 10:e0143669.

75. Itakura, E., and N. Mizushima. 2010. Characterization of autophagosome formation site by a hierarchical analysis of mammalian Atg proteins. *Autophagy*. 6:764-776.

76. Johnen, S., Z. Izsvak, M. Stocker, N. Harmening, A.K. Salz, P. Walter, and G. Thumann. 2012. Sleeping Beauty transposon-mediated transfection of retinal and iris pigment epithelial cells. *Investigative ophthalmology & visual science*. 53:4787-4796.

77. Jonas, J.B., I. Kreissig, and R.F. Degenring. 2004. Factors influencing visual acuity after intravitreal triamcinolone acetonide as treatment of exudative age related macular degeneration. *The British journal of ophthalmology*. 88:1557-1562.

78. Jonas, J.B., I. Kreissig, P. Hugger, G. Sauder, S. Panda-Jonas, and R. Degenring. 2003. Intravitreal triamcinolone acetonide for exudative age related macular degeneration. *The British journal of ophthalmology*. 87:462-468.

79. Ju, J.S., A.S. Varadhachary, S.E. Miller, and C.C. Weihl. 2010. Quantitation of "autophagic flux" in mature skeletal muscle. *Autophagy*. 6:929-935.

80. Juuti-Uusitalo, K., H. Vaajasaari, T. Ryhanen, S. Narkilahti, R. Suuronen, E. Mannermaa, K. Kaarniranta, and H. Skottman. 2012. Efflux protein expression in human stem cell-derived retinal pigment epithelial cells. *PloS one*. 7:e30089.

81. Kaarniranta, K., A. Salminen, A. Haapasalo, H. Soininen, and M. Hiltunen. 2011. Age-related macular degeneration (AMD): Alzheimer's disease in the eye? *J Alzheimers Dis*. 24:615-631.

82. Kaarniranta, K., D. Sinha, J. Blasiak, A. Kauppinen, Z. Vereb, A. Salminen, M.E. Boulton, and G. Petrovski. 2013. Autophagy and heterophagy dysregulation leads to retinal pigment epithelium dysfunction and development of age-related macular degeneration. *Autophagy*. 9:973-984.

83. Kabeya, Y., N. Mizushima, T. Ueno, A. Yamamoto, T. Kirisako, T. Noda, E. Kominami, Y. Ohsumi, and T. Yoshimori. 2000. LC3, a mammalian homologue of yeast Apg8p, is localized in autophagosome membranes after processing. *The EMBO journal*. 19:5720-5728.

84. Kamao, H., M. Mandai, S. Okamoto, N. Sakai, A. Suga, S. Sugita, J. Kiryu, and M. Takahashi. 2014. Characterization of human induced pluripotent stem cell-

derived retinal pigment epithelium cell sheets aiming for clinical application. *Stem cell reports*. 2:205-218.

85. Kanuga, N., H.L. Winton, L. Beauchene, A. Koman, A. Zerbib, S. Halford, P.O. Couraud, D. Keegan, P. Coffey, R.D. Lund, P. Adamson, and J. Greenwood. 2002. Characterization of genetically modified human retinal pigment epithelial cells developed for in vitro and transplantation studies. *Investigative ophthalmology & visual science*. 43:546-555.

86. Kauppinen, A., J.J. Paterno, J. Blasiak, A. Salminen, and K. Kaarniranta. 2016. Inflammation and its role in age-related macular degeneration. *Cellular and molecular life sciences : CMLS*. 73:1765-1786.

87. Kimbrel, E.A., and R. Lanza. 2015. Current status of pluripotent stem cells: moving the first therapies to the clinic. *Nat Rev Drug Discov*. 14:681-692.

88. Kinnunen, K., G. Petrovski, M.C. Moe, A. Berta, and K. Kaarniranta. 2012. Molecular mechanisms of retinal pigment epithelium damage and development of age-related macular degeneration. *Acta Ophthalmol*. 90:299-309.

89. Kis-Toth, K., I. Bacskai, P. Gogolak, A. Mazlo, I. Szatmari, and E. Rajnavolgyi. 2013. Monocyte-derived dendritic cell subpopulations use different types of matrix metalloproteinases inhibited by GM6001. *Immunobiology*. 218:1361-1369.

90. Klein, R., and B.E. Klein. 2013. The prevalence of age-related eye diseases and visual impairment in aging: current estimates. *Investigative ophthalmology & visual science*. 54:ORSF5-ORSF13.

91. Klein, R., C.E. Myers, K.J. Cruickshanks, R.E. Gangnon, L.G. Danforth, T.A. Sivakumaran, S.K. Iyengar, M.Y. Tsai, and B.E. Klein. 2014. Markers of inflammation, oxidative stress, and endothelial dysfunction and the 20-year cumulative incidence of early age-related macular degeneration: the Beaver Dam Eye Study. *JAMA Ophthalmol*. 132:446-455.

92. Klettner, A., A. Kauppinen, J. Blasiak, J. Roider, A. Salminen, and K. Kaarniranta. 2013. Cellular and molecular mechanisms of age-related macular degeneration: from impaired autophagy to neovascularization. *Int J Biochem Cell Biol*. 45:1457-1467.

93. Klimanskaya, I., J. Hipp, K.A. Rezai, M. West, A. Atala, and R. Lanza. 2004. Derivation and comparative assessment of retinal pigment epithelium from human embryonic stem cells using transcriptomics. *Cloning and stem cells*. 6:217-245.

94. Klionsky, D.J., K. Abdelmohsen, A. Abe, M.J. Abedin, H. Abeliovich, A. Acevedo Arozena, H. Adachi, C.M. Adams, P.D. Adams, K. Adeli, P.J. Adhihetty, S.G. Adler, G. Agam, R. Agarwal, M.K. Aghi, M. Agnello, P. Agostinis, P.V. Aguilar, J. Aguirre-Ghiso, E.M. Airoldi, S. Ait-Si-Ali, T. Akematsu, E.T. Akporiaye, M. Al-Rubeai, G.M. Albaiceta, C. Albanese, D. Albani, M.L. Albert, J. Aldudo, H. Algul, M. Alirezaei, I. Alloza, A. Almasan, M. Almonte-Beceril, E.S. Alnemri, C. Alonso, N. Altan-Bonnet, D.C. Altieri, S. Alvarez, L. Alvarez-Erviti, S. Alves, G. Amadoro, A. Amano, C. Amantini, S. Ambrosio, I. Amelio, A.O. Amer, M. Amessou, A. Amon, Z. An, F.A. Anania, S.U. Andersen, U.P. Andley, C.K. Andreadi, N. Andrieu-Abadie, A. Anel, D.K. Ann, S. Anoopkumar-Dukie, M. Antonioli, H. Aoki, N. Apostolova, S. Aquila, K. Aquilano, K. Araki, E. Arama, A. Aranda, J. Araya, A. Arcaro, E. Arias, H. Arimoto, A.R. Ariosa, J.L. Armstrong, T. Arnould, I. Arsov, K. Asanuma, V.

Askanas, E. Asselin, R. Atarashi, S.S. Atherton, J.D. Atkin, L.D. Attardi, P. Auberger, G. Auburger, L. Aurelian, R. Autelli, L. Avagliano, M.L. Avantaggiati, L. Avrahami, S. Awale, N. Azad, T. Bachetti, J.M. Backer, D.H. Bae, J.S. Bae, O.N. Bae, S.H. Bae, E.H. Baehrecke, S.H. Baek, S. Baghdiguian, A. Bagniewska-Zadworna, et al. 2016. Guidelines for the use and interpretation of assays for monitoring autophagy (3rd edition). *Autophagy*. 12:1-222.

95. Kohno, H., Y. Chen, B.M. Kevany, E. Pearlman, M. Miyagi, T. Maeda, K. Palczewski, and A. Maeda. 2013. Photoreceptor proteins initiate microglial activation via Toll-like receptor 4 in retinal degeneration mediated by all-trans-retinal. *J Biol Chem*. 288:15326-15341.

96. Kolb, H. 1995. Simple Anatomy of the Retina. *In* Webvision: The Organization of the Retina and Visual System. H. Kolb, E. Fernandez, and R. Nelson, editors, Salt Lake City (UT).

97. Kovala, A.T., K.A. Harvey, P. McGlynn, G. Boguslawski, J.G. Garcia, and D. English. 2000. High-efficiency transient transfection of endothelial cells for functional analysis. *FASEB journal : official publication of the Federation of American Societies for Experimental Biology*. 14:2486-2494.

98. Kristof, E., G. Zahuczky, K. Katona, Z. Doro, E. Nagy, and L. Fesus. 2013. Novel role of ICAM3 and LFA-1 in the clearance of apoptotic neutrophils by human macrophages. *Apoptosis : an international journal on programmed cell death*. 18:1235-1251.

99. Kroemer, G., and B. Levine. 2008. Autophagic cell death: the story of a misnomer. *Nat Rev Mol Cell Biol*. 9:1004-1010.

100. Kulkarni, A.D., and B.D. Kuppermann. 2005. Wet age-related macular degeneration. *Adv Drug Deliv Rev*. 57:1994-2009.

101. Kunchithapautham, K., and B. Rohrer. 2007. Apoptosis and autophagy in photoreceptors exposed to oxidative stress. *Autophagy*. 3:433-441.

102. Kuznetsova, A.V., A.M. Kurinov, and M.A. Aleksandrova. 2014. Cell models to study regulation of cell transformation in pathologies of retinal pigment epithelium. *Journal of ophthalmology*. 2014:801787.

103. Lamb, T.D. 2013. Evolution of phototransduction, vertebrate photoreceptors and retina. *Progress in retinal and eye research*. 36:52-119.

104. Levonen, A.L., B.G. Hill, E. Kansanen, J. Zhang, and V.M. Darley-Usmar. 2014. Redox regulation of antioxidants, autophagy, and the response to stress: implications for electrophile therapeutics. *Free radical biology & medicine*. 71:196-207.

105. Li, W., Q. Yang, and Z. Mao. 2011. Chaperone-mediated autophagy: machinery, regulation and biological consequences. *Cellular and molecular life sciences : CMLS*. 68:749-763.

106. Li, Y., H. Shen, J. Shi, and L. Tang. 2014. The effects of alpha lipoic acid in preventing oxidative stress-induced retinal pigment epithelial cell injury. *Can J Physiol Pharmacol*. 92:765-772.

107. Lim, J.I., M. Niec, and V. Wong. 2015. One year results of a phase 1 study of the safety and tolerability of combination therapy using sustained release intravitreal

triamcinolone acetonide and ranibizumab for subfoveal neovascular AMD. *The British journal of ophthalmology*. 99:618-623.

108. Lippai, M., and P. Low. 2014. The role of the selective adaptor p62 and ubiquitin-like proteins in autophagy. *Biomed Res Int*. 2014:832704.

109. Luo, Y., Y. Zhuo, M. Fukuhara, and L.J. Rizzolo. 2006. Effects of culture conditions on heterogeneity and the apical junctional complex of the ARPE-19 cell line. *Investigative ophthalmology & visual science*. 47:3644-3655.

110. Maenpaa, H., M. Mannerstrom, T. Toimela, L. Salminen, P. Saransaari, and H. Tahti. 2002. Glutamate uptake is inhibited by tamoxifen and toremifene in cultured retinal pigment epithelial cells. *Pharmacol Toxicol*. 91:116-122.

111. Maiuri, M.C., E. Zalckvar, A. Kimchi, and G. Kroemer. 2007. Self-eating and self-killing: crosstalk between autophagy and apoptosis. *Nat Rev Mol Cell Biol*. 8:741-752.

112. Majai, G., P. Gogolak, C. Ambrus, G. Vereb, J. Hodrea, L. Fesus, and E. Rajnavolgyi. 2010. PPARgamma modulated inflammatory response of human dendritic cell subsets to engulfed apoptotic neutrophils. *Journal of leukocyte biology*. 88:981-991.

113. Mao, H., S.J. Seo, M.R. Biswal, H. Li, M. Conners, A. Nandyala, K. Jones, Y.Z. Le, and A.S. Lewin. 2014. Mitochondrial oxidative stress in the retinal pigment epithelium leads to localized retinal degeneration. *Investigative ophthalmology & visual science*. 55:4613-4627.

114. Marmorstein, A.D., S.C. Finnemann, V.L. Bonilha, and E. Rodriguez-Boulan. 1998. Morphogenesis of the retinal pigment epithelium: toward understanding retinal degenerative diseases. *Annals of the New York Academy of Sciences*. 857:1-12.

115. Masland, R.H. 2012a. The neuronal organization of the retina. *Neuron*. 76:266-280.

116. Masland, R.H. 2012b. The tasks of amacrine cells. *Vis Neurosci*. 29:3-9.

117. Medina, C.B., and K.S. Ravichandran. 2016. Do not let death do us part: 'find-me' signals in communication between dying cells and the phagocytes. *Cell death and differentiation*. 23:979-989.

118. Meyer, J.S., R.L. Shearer, E.E. Capowski, L.S. Wright, K.A. Wallace, E.L. McMillan, S.C. Zhang, and D.M. Gamm. 2009. Modeling early retinal development with human embryonic and induced pluripotent stem cells. *Proceedings of the National Academy of Sciences of the United States of America*. 106:16698-16703.

119. Michels, S., F. Hansmann, W. Geitzenauer, and U. Schmidt-Erfurth. 2006. Influence of treatment parameters on selectivity of verteporfin therapy. *Investigative ophthalmology & visual science*. 47:371-376.

120. Mijaljica, D., M. Prescott, and R.J. Devenish. 2011. Microautophagy in mammalian cells: revisiting a 40-year-old conundrum. *Autophagy*. 7:673-682.

121. Miranti, C.K., and J.S. Brugge. 2002. Sensing the environment: a historical perspective on integrin signal transduction. *Nat Cell Biol*. 4:E83-90.

122. Mizushima, N. 2007. Autophagy: process and function. *Genes Dev*. 21:2861-2873.

123. Mizushima, N., and T. Yoshimori. 2007. How to interpret LC3 immunoblotting. *Autophagy*. 3:542-545.

124. Mizushima, N., T. Yoshimori, and B. Levine. 2010. Methods in mammalian autophagy research. *Cell*. 140:313-326.

125. Mizushima, N., T. Yoshimori, and Y. Ohsumi. 2011. The role of Atg proteins in autophagosome formation. *Annu Rev Cell Dev Biol*. 27:107-132.

126. Mooijaart, S.P., K.M. Koeijvoets, E.J. Sijbrands, M.R. Daha, and R.G. Westendorp. 2007. Complement Factor H polymorphism Y402H associates with inflammation, visual acuity, and cardiovascular mortality in the elderly population at large. *Experimental gerontology*. 42:1116-1122.

127. Nagata, S., R. Hanayama, and K. Kawane. 2010. Autoimmunity and the clearance of dead cells. *Cell*. 140:619-630.

128. Nakaya, M., M. Tanaka, Y. Okabe, R. Hanayama, and S. Nagata. 2006. Opposite effects of rho family GTPases on engulfment of apoptotic cells by macrophages. *J Biol Chem*. 281:8836-8842.

129. Nguyen-Ba-Charvet, K.T., and A. Chedotal. 2014. Development of retinal layers. *C R Biol*. 337:153-159.

130. Nowak, J.Z. 2014. AMD--the retinal disease with an unprecised etiopathogenesis: in search of effective therapeutics. *Acta poloniae pharmaceutica*. 71:900-916.

131. Onnela, N., V. Savolainen, K. Juuti-Uusitalo, H. Vaajasaari, H. Skottman, and J. Hyttinen. 2012. Electric impedance of human embryonic stem cell-derived retinal pigment epithelium. *Medical & biological engineering & computing*. 50:107-116.

132. Pankiv, S., T.H. Clausen, T. Lamark, A. Brech, J.A. Bruun, H. Outzen, A. Overvatn, G. Bjorkoy, and T. Johansen. 2007. p62/SQSTM1 binds directly to Atg8/LC3 to facilitate degradation of ubiquitinated protein aggregates by autophagy. *J Biol Chem*. 282:24131-24145.

133. Paoli, P., E. Giannoni, and P. Chiarugi. 2013. Anoikis molecular pathways and its role in cancer progression. *Biochim Biophys Acta*. 1833:3481-3498.

134. Park, S.Y., S.Y. Kim, K.B. Kang, and I.S. Kim. 2010. Adaptor protein GULP is involved in stabilin-1-mediated phagocytosis. *Biochem Biophys Res Commun*. 398:467-472.

135. Parmeggiani, F., M.R. Romano, C. Costagliola, F. Semeraro, C. Incorvaia, S. D'Angelo, P. Perri, P. De Palma, K. De Nadai, and A. Sebastiani. 2012. Mechanism of inflammation in age-related macular degeneration. *Mediators Inflamm*. 2012:546786.

136. Parnaik, R., M.C. Raff, and J. Scholes. 2000. Differences between the clearance of apoptotic cells by professional and non-professional phagocytes. *Curr Biol*. 10:857-860.

137. Parzych, K.R., and D.J. Klionsky. 2014. An overview of autophagy: morphology, mechanism, and regulation. *Antioxidants & redox signaling*. 20:460-473.

138. Penberthy, K.K., and K.S. Ravichandran. 2016. Apoptotic cell recognition receptors and scavenger receptors. *Immunol Rev*. 269:44-59.

139. Petrovski, G., G. Ayna, G. Majai, J. Hodrea, S. Benko, A. Madi, and L. Fesus. 2011a. Phagocytosis of cells dying through autophagy induces inflammasome activation and IL-1beta release in human macrophages. *Autophagy*. 7:321-330.

140. Petrovski, G., E. Berenyi, M.C. Moe, A. Vajas, L. Fesus, A. Berta, and A. Facsko. 2011b. Clearance of dying ARPE-19 cells by professional and nonprofessional phagocytes in vitro- implications for age-related macular degeneration (AMD). *Acta Ophthalmol*. 89:e30-34.

141. Petrovski, G., G. Zahuczky, K. Katona, G. Vereb, W. Martinet, Z. Nemes, W. Bursch, and L. Fesus. 2007a. Clearance of dying autophagic cells of different origin by professional and non-professional phagocytes. *Cell death and differentiation*. 14:1117-1128.

142. Petrovski, G., G. Zahuczky, G. Majai, and L. Fesus. 2007b. Phagocytosis of cells dying through autophagy evokes a pro-inflammatory response in macrophages. *Autophagy*. 3:509-511.

143. Plafker, S.M., G.B. O'Mealey, and L.I. Szweda. 2012. Mechanisms for countering oxidative stress and damage in retinal pigment epithelium. *Int Rev Cell Mol Biol*. 298:135-177.

144. Poon, I.K., M.D. Hulett, and C.R. Parish. 2010. Molecular mechanisms of late apoptotic/necrotic cell clearance. *Cell death and differentiation*. 17:381-397.

145. Poon, I.K., C.D. Lucas, A.G. Rossi, and K.S. Ravichandran. 2014. Apoptotic cell clearance: basic biology and therapeutic potential. *Nature reviews. Immunology*. 14:166-180.

146. Ravichandran, K.S. 2010. Find-me and eat-me signals in apoptotic cell clearance: progress and conundrums. *The Journal of experimental medicine*. 207:1807-1817.

147. Reichhart, N., and O. Strauss. 2014. Ion channels and transporters of the retinal pigment epithelium. *Exp Eye Res*. 126:27-37.

148. Ricci, F., G. Staurenghi, T. Lepre, F. Missiroli, S. Zampatti, R. Cascella, P. Borgiani, L.T. Marsella, C.M. Eandi, A. Cusumano, G. Novelli, and E. Giardina. 2013. Haplotypes in IL-8 Gene Are Associated to Age-Related Macular Degeneration: A Case-Control Study. *PloS one*. 8:e66978.

149. Rizzolo, L.J. 2014. Barrier properties of cultured retinal pigment epithelium. *Exp Eye Res*. 126:16-26.

150. Rose, R.C., S.P. Richer, and A.M. Bode. 1998. Ocular oxidants and antioxidant protection. *Proceedings of the Society for Experimental Biology and Medicine. Society for Experimental Biology and Medicine*. 217:397-407.

151. Ross, R.J., V. Verma, K.I. Rosenberg, C.C. Chan, and J. Tuo. 2007. Genetic markers and biomarkers for age-related macular degeneration. *Expert Rev Ophthalmol*. 2:443-457.

152. Sarvari, A.K., Q.M. Doan-Xuan, Z. Bacso, I. Csomos, Z. Balajthy, and L. Fesus. 2015. Interaction of differentiated human adipocytes with macrophages leads to trogocytosis and selective IL-6 secretion. *Cell death & disease*. 6:e1613.

153. Sato, E., T. Suzuki, N. Hoshi, T. Sugino, and H. Hasegawa. 2008. Sodium azide induces necrotic cell death in rat squamous cell carcinoma SCC131. *Med Mol Morphol*. 41:211-220.

154. Savill, J., I. Dransfield, C. Gregory, and C. Haslett. 2002. A blast from the past: clearance of apoptotic cells regulates immune responses. *Nature reviews. Immunology*. 2:965-975.

155. Savill, J., and V. Fadok. 2000. Corpse clearance defines the meaning of cell death. *Nature*. 407:784-788.

156. Savolainen, V., K. Juuti-Uusitalo, N. Onnela, H. Vaajasaari, S. Narkilahti, R. Suuronen, H. Skottman, and J. Hyttinen. 2011. Impedance spectroscopy in monitoring the maturation of stem cell-derived retinal pigment epithelium. *Annals of biomedical engineering*. 39:3055-3069.

157. Scandalios, J.G. 2005. Oxidative stress: molecular perception and transduction of signals triggering antioxidant gene defenses. *Brazilian journal of medical and biological research = Revista brasileira de pesquisas medicas e biologicas / Sociedade Brasileira de Biofisica ... [et al.]*. 38:995-1014.

158. Schwartz, S.D., J.P. Hubschman, G. Heilwell, V. Franco-Cardenas, C.K. Pan, R.M. Ostrick, E. Mickunas, R. Gay, I. Klimanskaya, and R. Lanza. 2012. Embryonic stem cell trials for macular degeneration: a preliminary report. *Lancet*. 379:713-720.

159. Schwartz, S.D., C.D. Regillo, B.L. Lam, D. Eliott, P.J. Rosenfeld, N.Z. Gregori, J.P. Hubschman, J.L. Davis, G. Heilwell, M. Spirn, J. Maguire, R. Gay, J. Bateman, R.M. Ostrick, D. Morris, M. Vincent, E. Anglade, L.V. Del Priore, and R. Lanza. 2015. Human embryonic stem cell-derived retinal pigment epithelium in patients with age-related macular degeneration and Stargardt's macular dystrophy: follow-up of two open-label phase 1/2 studies. *Lancet*. 385:509-516.

160. Seddon, J.M., S. George, B. Rosner, and N. Rifai. 2005. Progression of age-related macular degeneration: prospective assessment of C-reactive protein, interleukin 6, and other cardiovascular biomarkers. *Archives of ophthalmology*. 123:774-782.

161. Shaw, P.X., T. Stiles, C. Douglas, D. Ho, W. Fan, H. Du, and X. Xiao. 2016. Oxidative stress, innate immunity, and age-related macular degeneration. *AIMS Mol Sci*. 3:196-221.

162. Shiloach, T., C. Berens, C. Danke, O. Waiskopf, R. Perlman, and D. Ben-Yehuda. 2014. tLivin displays flexibility by promoting alternative cell death mechanisms. *PloS one*. 9:e101075.

163. Simo, R., M. Villarroel, L. Corraliza, C. Hernandez, and M. Garcia-Ramirez. 2010. The retinal pigment epithelium: something more than a constituent of the blood-retinal barrier--implications for the pathogenesis of diabetic retinopathy. *J Biomed Biotechnol*. 2010:190724.

164. Skottman, H. 2010. Derivation and characterization of three new human embryonic stem cell lines in Finland. *In vitro cellular & developmental biology. Animal*. 46:206-209.

165. Smith, A.G., and P.K. Kaiser. 2014. Emerging treatments for wet age-related macular degeneration. *Expert Opin Emerg Drugs*. 19:157-164.

166. Stanton, C.M., and A.F. Wright. 2014. Inflammatory biomarkers for AMD. *Advances in experimental medicine and biology*. 801:251-257.

167. Stanzel, B.V., E.M. Espana, M. Grueterich, T. Kawakita, J.M. Parel, S.C. Tseng, and S. Binder. 2005. Amniotic membrane maintains the phenotype of rabbit retinal pigment epithelial cells in culture. *Exp Eye Res*. 80:103-112.

168. Stein-Streilein, J. 2013. Mechanisms of immune privilege in the posterior eye. *Int Rev Immunol*. 32:42-56.

169. Stern, J., and S. Temple. 2015. Retinal pigment epithelial cell proliferation. *Experimental biology and medicine*. 240:1079-1086.

170. Strauss, O. 2005. The retinal pigment epithelium in visual function. *Physiological reviews*. 85:845-881.

171. Szabo, D.J., M. Szatmari-Toth, Z. Doro, R. Nagymihaly, N. Josifovska, A. Facsko, and G. Petrovski. 2014. Cell death, clearance and inflammation: molecular crossroads and gene polymorphisms in the pathogenesis of age-related macular degeneration. *J of Biochemical and Pharmacological Research*. 2:132-143.

172. Taddei, M.L., E. Giannoni, T. Fiaschi, and P. Chiarugi. 2012. Anoikis: an emerging hallmark in health and diseases. *J Pathol*. 226:380-393.

173. Takahashi, K., K. Tanabe, M. Ohnuki, M. Narita, T. Ichisaka, K. Tomoda, and S. Yamanaka. 2007. Induction of pluripotent stem cells from adult human fibroblasts by defined factors. *Cell*. 131:861-872.

174. Tanida, I., T. Ueno, and E. Kominami. 2004. LC3 conjugation system in mammalian autophagy. *Int J Biochem Cell Biol*. 36:2503-2518.

175. Travis, G.H., M. Golczak, A.R. Moise, and K. Palczewski. 2007. Diseases caused by defects in the visual cycle: retinoids as potential therapeutic agents. *Annu Rev Pharmacol Toxicol*. 47:469-512.

176. Turowski, P., P. Adamson, J. Sathia, J.J. Zhang, S.E. Moss, G.W. Aylward, M.J. Hayes, N. Kanuga, and J. Greenwood. 2004. Basement membrane-dependent modification of phenotype and gene expression in human retinal pigment epithelial ARPE-19 cells. *Investigative ophthalmology & visual science*. 45:2786-2794.

177. Vaajasaari, H., T. Ilmarinen, K. Juuti-Uusitalo, K. Rajala, N. Onnela, S. Narkilahti, R. Suuronen, J. Hyttinen, H. Uusitalo, and H. Skottman. 2011. Toward the defined and xeno-free differentiation of functional human pluripotent stem cell-derived retinal pigment epithelial cells. *Molecular vision*. 17:558-575.

178. van der Meer, J.H., T. van der Poll, and C. van 't Veer. 2014. TAM receptors, Gas6, and protein S: roles in inflammation and hemostasis. *Blood*. 123:2460-2469.

179. Vermes, I., C. Haanen, H. Steffens-Nakken, and C. Reutelingsperger. 1995. A novel assay for apoptosis. Flow cytometric detection of phosphatidylserine expression on early apoptotic cells using fluorescein labelled Annexin V. *Journal of immunological methods*. 184:39-51.

180. Vugler, A., A.J. Carr, J. Lawrence, L.L. Chen, K. Burrell, A. Wright, P. Lundh, M. Semo, A. Ahmado, C. Gias, L. da Cruz, H. Moore, P. Andrews, J. Walsh, and

P. Coffey. 2008. Elucidating the phenomenon of HESC-derived RPE: anatomy of cell genesis, expansion and retinal transplantation. *Experimental neurology*. 214:347-361.

181. Wada, M., C.M. Gelfman, H. Matsunaga, M. Alizadeh, L. Morse, J.T. Handa, and L.M. Hjelmeland. 2001. Density-dependent expression of FGF-2 in response to oxidative stress in RPE cells in vitro. *Curr Eye Res*. 23:226-231.

182. Wang, A.L., T.J. Lukas, M. Yuan, N. Du, M.O. Tso, and A.H. Neufeld. 2009. Autophagy and exosomes in the aged retinal pigment epithelium: possible relevance to drusen formation and age-related macular degeneration. *PloS one*. 4:e4160.

183. Wang, S., K.M. Koster, Y. He, and Q. Zhou. 2012. miRNAs as potential therapeutic targets for age-related macular degeneration. *Future medicinal chemistry*. 4:277-287.

184. Winkler, B.S., M.E. Boulton, J.D. Gottsch, and P. Sternberg. 1999. Oxidative damage and age-related macular degeneration. *Molecular vision*. 5:32.

185. Yang, Y.H., B. Li, X.F. Zheng, J.W. Chen, K. Chen, S.D. Jiang, and L.S. Jiang. 2014. Oxidative damage to osteoblasts can be alleviated by early autophagy through the endoplasmic reticulum stress pathway--implications for the treatment of osteoporosis. *Free radical biology & medicine*. 77:10-20.

186. Yang, Y.P., L.F. Hu, H.F. Zheng, C.J. Mao, W.D. Hu, K.P. Xiong, F. Wang, and C.F. Liu. 2013. Application and interpretation of current autophagy inhibitors and activators. *Acta Pharmacol Sin*. 34:625-635.

187. Yonekawa, Y., J.W. Miller, and I.K. Kim. 2015. Age-Related Macular Degeneration: Advances in Management and Diagnosis. *J Clin Med*. 4:343-359.

188. Young, R.W., and D. Bok. 1969. Participation of the retinal pigment epithelium in the rod outer segment renewal process. *The Journal of cell biology*. 42:392-403.

189. Yu, J., M.A. Vodyanik, K. Smuga-Otto, J. Antosiewicz-Bourget, J.L. Frane, S. Tian, J. Nie, G.A. Jonsdottir, V. Ruotti, R. Stewart, Slukvin, II, and J.A. Thomson. 2007. Induced pluripotent stem cell lines derived from human somatic cells. *Science*. 318:1917-1920.

190. Zahuczky, G., E. Kristof, G. Majai, and L. Fesus. 2011. Differentiation and glucocorticoid regulated apopto-phagocytic gene expression patterns in human macrophages. Role of Mertk in enhanced phagocytosis. *PloS one*. 6:e21349.

191. Zarbin, M. 2016. Cell-Based Therapy for Degenerative Retinal Disease. *Trends Mol Med*. 22:115-134.

192. Zhan, M., H. Zhao, and Z.C. Han. 2004. Signalling mechanisms of anoikis. *Histol Histopathol*. 19:973-983.

193. Zhang, X.J., S. Chen, K.X. Huang, and W.D. Le. 2013. Why should autophagic flux be assessed? *Acta Pharmacol Sin*. 34:595-599.

194. Zhou, R., and R.R. Caspi. 2010. Ocular immune privilege. *F1000 biology reports*. 2.

195. Zhou, Z., and X. Yu. 2008. Phagosome maturation during the removal of apoptotic cells: receptors lead the way. *Trends in cell biology*. 18:474-485.

10. Publications

UNIVERSITY OF DEBRECEN
UNIVERSITY AND NATIONAL LIBRARY

Registry number: DEENK/210/2016.PL
Subject: PhD Publikációs Lista

Candidate: Mária Szatmári-Tóth
Neptun ID: BNF50W
Doctoral School: Doctoral School of Molecular Cellular and Immune Biology

List of publications related to the dissertation

1. **Szatmári-Tóth, M.**, Kristóf, E., Veréb, Z., Akhtar, S., Facskó, A., Fésüs, L., Kauppinen, A., Kaarniranta, K., Petrovski, G.: Clearance of autophagy-associated dying retinal pigment epithelial cells - a possible source for inflammation in age-related macular degeneration. *Cell Death Dis. [Accepted by Publisher]*, 2016.
   IF: 5.378 (2015)
2. Albert, R., Kristóf, E., Zahuczky, G., **Szatmári-Tóth, M.**, Veréb, Z., Oláh, B., Moe, M. C., Facskó, A., Fésüs, L., Petrovski, G.: Triamcinolone regulated apopto-phagocytic gene expression patterns in the clearance of dying retinal pigment epithelial cells. A key role of Mertk in the enhanced phagocytosis.
   Biochim. Biophys. Acta-Gen. Subj. 1850 (2), 435-446, 2015.
   DOI: http://dx.doi.org/10.1016/j.bbagen.2014.10.026
   IF: 5.083

Address: 1 Egyetem tér, Debrecen 4032, Hungary Postal address: Pf. 39. Debrecen 4010, Hungary
Tel.: +36 52 410 443 Fax: +36 52 512 900/63847 E-mail: publikaciok@lib.unideb.hu, ¤ Web: www.lib.unideb.hu

List of other publications

3. Szabó, D. J., **Szatmári-Tóth, M.**, Doró, Z., Nagymihály, R., Josifovska, N., Facskó, A., Petrovski, G.: Cell death, clearance and inflammation: molecular crossroads and gene polymorphisms in the pathogenesis of age-related macular degeneration.
J. Biochem. Pharmacol. Res. 2 (3), 132-143, 2014.

Total IF of journals (all publications): 10,461
Total IF of journals (publications related to the dissertation): 10,461

The Candidate's publication data submitted to the iDEa Tudóstér have been validated by DEENK on the basis of Web of Science, Scopus and Journal Citation Report (Impact Factor) databases.

08 August, 2016

Address: 1 Egyetem tér, Debrecen 4032, Hungary Postal address: Pf. 39. Debrecen 4010, Hungary
Tel.: +36 52 410 443 Fax: +36 52 512 900/63847 E-mail: publikaciok@lib.unideb.hu, ¤ Web: www.lib.unideb.hu

11. Keywords

age-related macular degeneration, anoikis, autophagy, AXL, inflammation, macrophage, MERTK, phagocytosis, RPE, triamcinolone

Tárgyszavak

anoikisz; autofágia; AXL; fagocitózis; gyulladás; időskori makula degeneráció; makrofág; MERTK; RPE; triamcinolone

12. Acknowledgements

First of all, I would like to express my sincere gratitude to my supervisor, Prof. Dr. Goran Petrovski, for the excellent training, continuous support and motivation, and the scientific discussions during my Ph.D. candidacy period. I am thankful that he gave me the opportunity to learn and work in his research group.

I am especially grateful to Prof. Dr. László Fésüs, former Head of the Department of Biochemistry and Molecular Biology for his valuable suggestions, constructive advices, and for letting me work in the department in an excellent research atmosphere.

I am also thankful to Prof. Dr. József Tőzsér, Head of the Department of Biochemistry and Molecular Biology for the opportunity to work in a well-equipped institute.

Much obliged I am to our collaborators: Prof. Dr. Kai Kaarniranta, Dr. Anu Kauppinen, Dr. Heli Skottman, Dr. Tanja Ilmarinen, Dr. Alexandra Mikhailova and Prof. Saeed Akhtar, for their excellent help and valuable suggestions.

Many thanks to all the past and present member of the Stem Cell and Eye Research Laboratory for the friendly working atmosphere. Special thanks to Dr. Zoltán Veréb, Dr. Réka Albert, Zoltán Doró and Brigitta Oláh for their help and sharing their knowledge and experience with me. I also would like to thank Irén Mező for her excellent technical assistance.

Furthermore, I would like to thank all my colleagues from the Apoptosis Research Group. I am especially thankful to Dr. Endre Kristóf for helping me with his constructive advices and scientific discussions and to Dr. Máté Demény for his nice ideas and suggestions for writing my papers.

I wish to express my deepest gratitude to my colleagues and dear friends Dr. Dóra Szabó, Dr. Luna Djirackor, Pál Botó, Emília Simó, Ágnes Klusóczki, Károly Jambrovics, Éva Sivadó for their kindness and great emotional support.

Most importantly and dearly, I would like to thank my beloved family and to all of my dear friends helping me get through the difficult times, and for their continuous encouragement.

All my love and deepest gratitude I wish to express to my husband László Szatmári who supports me in each situation with his endless love, understanding and patience.